Technical University of Denmark

DTU

# Hybridized reactive iron-containing nano-materials for water purification

**Mines, Paul D.; Andersen, Henrik Rasmus; Yavuz, Cafer T.; Hwang, Yuhoon; Jakobsen, Mogens Havsteen**

*Publication date:*
2016

*Document Version*
Publisher's PDF, also known as Version of record

[Link back to DTU Orbit](#)

**DTU Library**
Technical Information Center of Denmark

# Hybridized reactive iron-containing nano-materials for water purification

Paul D. Mines

PhD Thesis
October 2016

DTU Environment
Department of Environmental Engineering
Technical University of Denmark

**Hybridized reactive iron-containing nano-materials for water treatment**

**Paul D. Mines**

PhD Thesis, October 2016

The synopsis part of this thesis is available as a pdf-file for download from the DTU research database ORBIT: http://www.orbit.dtu.dk.

# Preface

This dissertation is submitted in partial fulfilment of the requirements for the Degree of Doctor of Philosophy at the Department of Environmental Engineering at the Technical University of Denmark (DTU). The research for the entitled thesis "Reactive nanomaterials for water treatment" was conducted at the Department of Environmental Engineering at the Technical University of Denmark, the Department of Micro- and Nanotechnology at the Technical University of Denmark, and at the Graduate School of EEWS at the Korea Advanced Institute of Science and Technology (KAIST) in the period of December 2012 – September 2016, under the supervision of Associate Professor Henrik R. Andersen at DTU Environment, and co – supervision from Associate Professor Cafer T. Yavuz at the Graduate School of EEWS at the Korea Advanced Institute of Science and Technology, Assistant Professor Yuhoon Hwang at the Department of Environmental Engineering at Seoul National University of Science and Technology, and Associate Professor Mogens H. Jakobsen at DTU Nanotech. The project was funded by the KAIST-DTU Signature Project on Integrated Water Technology.

Ten scientific papers constitute the PhD work presented herein. The papers are outlined below and will be referred to in the text by their paper number written with the Roman numerals **I-X**. Papers **I – III** and **V** are currently published, Papers **IX** and **X** are submitted and under review, and Papers **IV, VII,** and **VIII** are attached as manuscripts.

**I**    Hwang Y., Lee Y.-C., **Mines P.D.**, Huh Y.S., Andersen H.R. (2014). Nanoscale zero-valent iron (nZVI) synthesis in a Mg-aminoclay solution exhibits increased stability and reactivity for reductive decontamination. *Applied Catalysis B: Environmental,* 147:748-755.

**II**   **Mines P.D.**, Byun J., Hwang Y., Patel H.A., Andersen H.R., Yavuz C.T. (2016). Nanoporous networks as effective stabilization matrices for nanoscale zero-valent iron and groundwater pollutant removal. *Journal of Materials Chemistry A,* 4:632-639.

**III**  Hwang Y., Lee Y.-C., **Mines P.D.**, Oh Y.-K., Seok Choi J., Andersen H.R. (2014). Investigation of washing and storage strategy on aging of

Mg-aminoclay (MgAC) coated nanoscale zero-valent iron (nZVI) particles. *Chemical Engineering Science*, 119:310-317.

IV  Uthuppu B., **Mines P.D.**, Fjordbøge A.S., Broholm M.M., Jakobsen M.H., Andersen H.R., Hwang Y. (2016). Appropriate washing and storage strategy to prolong life-time of nanoscale zero-valent iron using sodium borohydride solution. *Manuscript.*

V  Hwang Y., **Mines P.D.**, Jakobsen M.H., Andersen H.R. (2015), Simple colorimetric assay for dehalogenation reactivity of nanoscale zero-valent iron using 4-chlorophenol. *Applied Catalysis B: Environmental,* 166:18-24.

VI  Hwang Y., Salatas A., **Mines P.D.**, Jakobsen M.H., Andersen H.R. (2016), Graduated characterization method using a multi-well microplate for reducing reactivity of nanoscale zero valent iron materials. *Applied Catalysis B: Environmental,* 181:314-320.

VII  **Mines P.D.**, Hansen K.M.S., Droumpali A., Lee W., Andersen H.R., Hwang Y. (2016). Trichloroethylene dehalogenation comparison with 4-chlorophenol reduction color assay by bimetallic zero-valent Fe/Ni particles. *Manuscript.*

VIII **Mines P.D.**, Andersen H.R., Hwang Y. (2016). One-pot synthesis of nanoscale zero-valent iron immobilized granular activated carbon (GAC/nZVI) and appropriate methods for characterizing reducing reactivity. *Manuscript.*

IX  **Mines P.D.**, Thirion D., Uthuppu B., Hwang Y., Jakobsen M.H., Andersen H.R., Yavuz C.T. (2016). Covalent organic polymer functionalization of activated carbon surfaces through acyl chloride for environmental clean-up. *Under Review – Chemical Engineering Journal.*

X  **Mines P.D.**, Uthuppu B., Thirion D., Jakobsen M.H., Yavuz C.T., Andersen H.R., Hwang Y. (2016). Granular activated carbon with grafted nanoporous polymer enhances nanoscale zero-valent iron impregnation and water contaminant removal. *Submitted – Journal of Hazardous Materials.*

# Acknowledgements

First and foremost, I would like to thank my supervisor, Dr. Henrik Andersen. His guidance and trust in me and my work has made the experience and productivity all the more worthwhile during my time spend here as a PhD student at DTU Environment. I must also thank my co-supervisor and main point-of-contact during my PhD, Dr. Yuhoon Hwang. Without his advice and guidance on a daily basis, my work would not have been so fruitful or rewarding, and it was an honor to grow academically with his support. Additionally, thank you to the combined research time at the Korea Advanced Institute of Science and Technology and DTU, including Drs. Cafer Yavuz, Damien Thirion, Hasmukh Patel, Jeehye Byun, Mogens Jakobsen, and Basil Uthuppu, as well as fellow PhD student Dong Ah Ko.

I would also like to thank a couple important people from my past that encouraged my academic growth and brought me to where I am right now, Dr. Tzahi Cath at the Colorado School of Mines and Dr. Larry Besaw at Michigan State University. Moreover, a special thanks to Dr. Eric Dickenson, who brought me in to the Colorado School of Mines family and set me on the path that has brought me to where I am today.

My time here the last three and a half years have been some of the most rewarding years of my life, affirming how wonderful of an opportunity and decision it has been to come to Denmark for my PhD studies. This includes the relationships made with people in the department here, including Anne Harsting, Jens Schaarup Sørensen, Dr. Hans-Jørgen Albrechtsen, and many others.

Finally, I want to thank my friends here that have made my time here so special, including Carson, Florian, Aiga, Uli, Denisa, and Pedram. And, last but not least, my family for their support throughout my life; in particular, my sister Elizabeth for being my best friend and always being there when I need someone.

# Summary

Groundwater is an important source for drinking water in all corners of the globe, and in places like Denmark, it is the primary source for drinking water. Climate change and population growth will only lead to further dependence on groundwater as the supply for drinking water. However, the expanding population and industrialization of human civilization also leads to environmental consequences affecting groundwater sources. Storm-water and agricultural runoff, industrial spillage and dumping, acid mine drainage, and leakage from landfills are a few prime examples of routes of contamination for pollutants to enter groundwater systems. In order to make these contaminated water sources viable for human consumption, the use of reactive iron (i.e. $Fe^0$ or zero-valent iron), and in particular nanoscale zero-valent iron (nZVI), is being employed to reductively degrade and/or adsorb many of these pollutants. However, the use of nZVI, as it currently stands, has its limitations. These limitations are primarily rapid oxidation and aggregation, resulting in loss of reactivity and applicability. Therefore, development of new materials incorporating nZVI and improving synthesis strategies to increase the applicability of nZVI is paramount to its future success as a remediation technique. This PhD project has investigated various materials aimed at solving the reactivity loss of reactive iron to create a robust treatment system capable of treating polluted waters. This PhD project also investigated and developed a procedure to appropriately measure the reactivity of reactive iron for a universal testing method.

Coating of nZVI is a common solution to combatting the limitations of the material, in that the coating can surround the nZVI particle and prevent it from interacting with other particles while still allowing for interaction with the aqueous pollutant. This study employed a synthetic organo-functionalized magnesium-based aminoclay (MgAC) for this exact purpose. By varying the ratio of MgAC to nZVI and monitoring the change in physical characteristics and reactivity, a composite material was formed that improved the overall functionality of nZVI. It was determined that the reactive iron (vs. oxidized iron) content, colloidal stability, particle size, and nitrate degradation could all be best enhanced at a weight ratio of 7.5:1 of MgAC:Fe. Another solution, although less common, to combatting the limitations, is to entrap or impregnate a porous material with nZVI. This way acts in a similar

manner, except that the nZVI is bound within a complex matrix rather than coated with a protective barrier. A variety of porous polymeric networks, termed covalent organic polymers (COPs), were impregnated with nZVI and evaluated similarly as with the MgAC. All COPs exhibited high uptake of nZVI, approximately 10% by mass. Reactivity quantification proved to be difficult when degrading an azo dye, due to the very high propensity of the COPs to adsorb both the dye and its degradation products. However, these COPs acted as extremely efficient carriers of nZVI for maintaining colloidal stability. In one case, the COP used (COP-19) increased the colloidal stability of nZVI by two orders of magnitude. Building on the application of these composite materials, investigating how best to handle the synthesized materials can prolong their lifetime. To do this, three washing and storage strategies of the MgAC coated nZVI were investigated. They were: washing the particles immediately after synthesis with a $NaHCO_3$ buffer, washing the particles after storing with a $NaHCO_3$ buffer, and washing the particles immediately after synthesis with a MgAC solution. For all the particle reactivity tests done, it was apparent that washing the particles after storing was detrimental to the material. The colloidal stability, reactive iron, and reactivity towards nitrate dropped rapidly through one week of storage. The other strategies, where washing was done immediately was able to preserve the three aforementioned properties much more efficiently though one week of storage, with MgAC washed particles faring better of the two. This pre-washing technique removes residual reactants in the synthesis mixture that can corrode the iron, and furthermore, pre-washing with MgAC adds more of the stabilizer to the material that protects the nZVI even more. Moreover, by looking deeper into the characteristics of uncoated nZVI, depending on the washing method, allowed for more insight to the nature of the mechanisms taking place during storage. It was observed that washing nZVI with MilliQ water after synthesis created an environment where the particles were slightly more oxidized from the start, which led to an increased formation of an iron-hydroxide shell during storage. Not washing nZVI or washing with the reductant $NaBH_4$ prohibited initial oxidation, leading to subsequent iron-oxide formation during storage. This is important, because the hydroxide shell promotes more electron transfer, whereas the oxide shell acts as a depassivation layer. The increased electron transfer then allowed for higher reactivity during storage, up to one week.

To make comparison and quantification for researchers, a simple and effective method to assess the reactivity of nZVI is extremely important. And, as it is now, most of the reactivity characterization methods are often analytically intensive, requiring expensive equipment, and often don't respond uniformly to different nZVI-based materials. This study sought to solve this problem, by developing a simple colorimetric assay that is capable to taking a degradation product produced by nZVI reacting with a compound, and creating a color reaction detectable with a simple spectrophotometer. This was done by utilizing the indophenol reaction, which uses phenol and selected other reagents to produce a blue color. Phenol can be produced from the dehalogenation of 4-chlorophenol by nZVI, and to a greater extent by bimetallic nickel-nZVI. That simple method was then optimized to reduce reagent volumes, nickel concentration, and to broaden the range of detectable compounds. These compounds capable of being used in the color assay with the same set of reagents were ultimately aniline, ammonium, and phenol; all of which can be produced by the degradation reaction from nZVI. Finally, to compare the applicability of the colorimetric assay to common halogenated groundwater contaminants; it was compared to the dehalogenation of TCE, TCA, and atrazine. The colorimetric assay performed similarly to the degradation of those chlorinated compounds; meaning the assay can be a simple tool to assess the reactivity of any nZVI when ultimately targeting more difficult to analyze compounds in real-world sources.

Ultimately, the primary goal of this PhD study was to develop a robust nanocomposite material containing nZVI for water treatment systems. Taking the lessons learned from initial composite work using MgAC and COPs, the final material combined granular activated carbon with COP and nZVI. After a lengthy process in developing a method to chemically graft COP material to the surface of activated carbon, it was possible to impregnate that composite material with nZVI. Because of the activated carbon backbone, the final material proved to be an extremely robust material with the structural integrity to be used in a packed-bed column that is common when treating high volumes of water. Although, continued optimization of the material is necessary, preliminary results when adsorbing and degrading contaminants were very promising, outperforming activated carbon alone and just the carbon impregnated with nZVI. Also, a bonus effect was achieved in the process. In that the entire composite material, in particular the COP attached to the sur-

face of the carbon, acted as a protective barrier from the effects of oxidation. The carbon-COP-nZVI composites exhibited nearly 100% reactive iron content upon synthesis, compared to much lower amounts in other reported nZVI composites or the carbon-nZVI produced in this study having only 80% reactive iron content.

The results of this PhD concluded in various advances in the application and assessment of nZVI and nZVI composite materials. Various composite materials provided increased colloidal stability and reactivity for nZVI. Various washing and storage strategies elucidated better methods for delivering nZVI to a water contaminant and the underlying mechanisms taking place in the nZVI corrosion process. Finally, novel materials combining three different technologies were developed to eventually lead to a robust water treatment system capable of degrading typically hard to remediate water pollutants.

# Dansk sammenfatning

Grundvand er en vigtig kilde til drikkevand alle steder på Jorden, og steder som Danmark er det dén primære kilde til drikkevand. Klimaændringer og befolkningstilvækst vil kun betyde en større afhængighed af grundvand som kilde til drikkevand. Men den voksende befolkning og industrialisering af jordens befolkede arealer har miljømæssige konsekvenser for de naturlige grundvandsressourcer. Stormvand og afstrømning fra landbrug, spild og dumping fra industrien, syreholdig afstrømning fra minebrug og perkolat fra lossepladser er primære eksempler på måder hvordan forurenende stoffer trænger ned i grundvandet. For at gøre dette forurenede vand brugbart til menneskeligt indtag benytter man reaktivt jern og i særdeleshed nano-zero-valent jern (nZVI) for at nedbryde og/eller absorbere mange af disse forurenende stoffer. Imidlertid har den nuværende anvendelse af nZVI begrænsninger. Disse begrænsninger er primært hurtig oxidering og aggregering, der medfører nedsat reaktivitet og anvendelighed. Derfor er udviklingen af nye materialer med inkorporeret nZVI og forbedring af strategien for syntese for at forbedre anvendeligheden af nZVI afgørende for den fremtidige succes for brug af nZVI som rensningsteknik. Dette ph.d.-studie har undersøgt forskellige materialer hvis formål er at løse tabet af reaktivitet af nZVI for dermed at skabe et robust behandlingssystem der er i stand til at håndtere det forurenede vand. Dette ph.d.-studie har også undersøgt og udviklet en fremgangsmåde til hensigtsmæssigt at måle reaktiviteten af det reaktive jern som en universel testmetode.

Overflademodifikation af nZVI er en almindelig løsning til at modvirke begrænsningen af materialet, da overflademodifikationen kan indfatte nZVI-partiklen og forhindre den i at interagere med andre partikler men stadigt tillade partiklen at interagere med den vandopløste forurening. I denne undersøgelse anvendtes en syntetisk fremstillet organo-funktionaliseret magnesiumbaseret aminoler (MgAC) til netop dette formål. Ved at variere forholdet af MgAC til nZVI og overvåge forandringen af den fysiske fremtræden og reaktivitet, blev der fremstillet et komposit materiale, der forbedrede den generelle virkning af nZVI. Det blev fastslået, at det reaktive jern indhold, dets kolloide stabilitet, partikelstørrelse og evne til at reducere nitrat (i modsætning til det oxiderede jern) var optimalt ved en støkiometrisk ratio på 7½:1 af MgAC:Fe. En alternativ, men mindre anvendt løsning, er at indbygge eller imprægnere et porøst materiale med nZVI. Denne metode fungerer på tilsva-

rende måde, med undtagelse af, at nZVI er fanget i en kompleks indlejrings-masse i modsætning til at være belagt med en beskyttende barriere. Forskellige porøse polymerer, samlet betegnet som kovalente organiske polymere (COP), blev imprægneret med nZVI og undersøgt på samme måde som MgAC. Alle COP udviste et højt optag af nZVI på omtrent 10 % på vægtbasis. Kvantificering af reaktiviteten viste sig at være vanskelig i forbindelse med nedbrydning af et azo-farvestof pga. COP materialernes meget høje tilbøjelighed til at adsorbere både farvestoffet og dets nedbrydningsprodukt. Imidlertid var disse COP ekstremt effektive bærere af nZVI med henblik på at opretholde kolloid stabilitet. I et tilfælde fordoblede den anvendte COP (COP-19) den kolloide stabilitet. For at udvide anvendelsesmulighederne for disse komposit materialer, kan en undersøgelse af hvordan man optimalt håndterer disse syntetiske materialer bruges til at forlænge deres levetid. For at gøre dette blev tre vaske- og opbevaringsmetoder for nZVI belagt med MgAC undersøgt. Metoderne var: Vask af partiklerne umiddelbart efter syntese med en $NaHCO_3$-opløsning, vask af partiklerne med en $NaHCO_3$-opløsning efter opbevaring og vask af partiklerne umiddelbart efter syntese med en MgAC-opløsning. Det var tydeligt ved alle reaktivitetstestene af partiklerne, at vask af partiklerne efter opbevaring var ødelæggende for materialet. Kolloidstabilitet, indhold af reaktivt jern og aktiviteten overfor nitrat faldt hurtigt i løbet af en uges opbevaring. De andre metoder hvor vask af partikler skete umiddelbart efter brug, evnede at fastholde de tre førnævnte egenskaber langt mere effektivt ved en uges opbevaring, og partiklerne vasket med MgAC-opløsningen klarede sig bedst i forhold til $NaHCO_3$ opløsningen. Denne præ-opbevaring-vask-teknik fjernede tilbageblevne reaktanter i syntese-blandingen som kan korrodere jernet, og ydermere tilfører præ-opbevaring-vask med MgAC endnu mere stabilitet til materialet, der beskytter nZVI'en. Herudover, var det muligt at undersøge karakteristikken af den ikke-overflademodificerede nZVI og dermed at få en større indsigt i de ændringer, der opstår ved opbevaring af stoffet. Det blev observeret at ved at vaske nZVI med MilliQ vand efter syntese blev der skabt et miljø, hvor partiklerne var en smule mere oxiderede fra begyndelsen, hvilket betød en forøget dannelse af en jern-hydroxid skal ved opbevaring. Ved ikke at vaske nZVI sammenlignet med vask med reduktionsmidlet $NaBH_4$ forhindredes en initial oxidering, der medfører en efterfølgende jernoxid dannelse ved opbevaring. Dette har betydning da hydroxidskallen fremmer en større elektron-overførsel, hvorimod den oxiderede skal fungerer som et passiverende lag.

Den forhøjede elektron-overførsel medførte en højere reaktivitet i op til en uge ved opbevaring.

Til brug for sammenligning og kvantificering for forskere er det utroligt vigtigt med en simpel og effektiv metode til at vurdere nZVI's reaktivitet. Nu er de fleste metoder til at karaktisere reaktiviteten af nZVI ofte analytiske tunge, kræver dyrt udstyr og mangler en standardiseret måde at udføre behandlingen på. Dette studie har forsøgt at løse denne problemstilling ved at udvikle en simpel kolorimetrisk karakteriseringsmetode, der gør det muligt at detektere et nedbrydelsesprodukt produceret af nZVI og ved at tilsætte en kemisk forbindelse skabe en farve-reaktion, der er mulig at aflæse med et simpelt spektrofotometer. Dette blev opnået ved at anvende indophenol-reaktionen, der benytter fenol og andre udvalgte reagenser til at skabe en blå farve. Fenol kan produceres ved dehalogenering af 4-chlorphenol med nZVI, og endnu lettere ved reaktion med bi-metallisk nikkel-nZVI. Denne simple metode blev herefter optimeret for at reducere reagent voluminerne og nikkelkoncentrationen og for at udvide rækken af detekterede reduktionsreaktionsprodukter. De forbindelser, der kunne anvendes i farve-analysen med de samme reagenter var sluttelig anilin, ammonium og fenol, som alle kan blive produceret ved reduktiv nedbrydning af passende reagenser med nZVI. Til sidst, for at sammenligne anvendeligheden af den kolorimetriske analyse med almindelige halogenerede grundvandsforureningsstoffer, blev resultatet sammenlignet med dehalogenering af TCE, TCA og atrazin. Den kolorimetriske analyse fungerede også i forhold til nedbrydningen af disse klor-forbindelser, hvilket betyder at analysemetoden kan fungere som et simpelt værktøj til at måle reaktiviteten af al slags nZVI, når det endelige behandlingsmål er vanskeligt analyserbare forbindelser i reelle vandmatricer.

I den sidste ende var det primære mål for dette ph.d.-projekt at udvikle et robust nano-komposit materiale indeholdende nZVI til brug i vandbehandlingssystemer. Belært af de tidlige erfaringer med komposit materialet, hvor MgAC og COP blev anvendt, blev slutresultatet en kombination af granulært aktivt kul, COP og nZVI. Efter en længere proces for at udvikle en metode til kemisk at binde COP-materialet til overfladen af aktivt kul, blev det muligt at imprægnere komposit materialet med nZVI. På grund af hovedbestanddelen af aktivt kul i det endelige materiale, viste det sig at være ekstremt robust med en strukturel som kunne anvendes i et gennemstrømningsfilter som er det almindelige, når man behandler store mængder af vand. Selvom en fortsat

optimering af materialet er nødvendig, viser de første resultater for adsorbering og nedbrydning af forureningen meget lovende resultater, langt bedre end aktivt kul alene og også bedre end kul imprægneret med nZVI. Endvidere medførte processen en uventet bonus, da det kompositte materiale, og i særdeleshed når kullet blev imprægneret med COP, fungerede som en beskyttende barriere mod effekterne af oxidering. Kompositionen af aktivt kul-COP-nZVI udviste tæt på 100 % reaktivt jern efter syntesen, sammenlignet med meget lavere mængder i andre kendte nZVI-kompositter eller aktiv kul-nZVI-kompositionen anvendt i dette forsøg, hvor der kun var 80 % reaktivt jern indhold.

Resultaterne af dette ph.d.-projekt konkluderer i forskellige fremskridt i anvendelsen og analysen af nZVI og nZVI-kompositte materialer. Forskellige kompositte materialer udviste forhøjet kolloid stabilitet og reagerede på nZVI. Forskellige vaske- og opbevaringsteknikker belyste bedre metoder for at anvende nZVI til vandforureningen og de underliggende (sekundære) mekanismer, der opstår i korrosionen af nZVI. Slutteligt, så blev der ved at kombinere tre forskellige teknologier udviklet nye materialer, der med tiden kan føre til et mere robust vandbehandlingssystem i stand til at nedbryde typiske problematiske forureningsstoffer i vand.

# Table of contents

# Abbreviations

|  |  |
|---|---|
| AC | Activated carbon |
| AC-COP | Activated carbon – covalent organic polymer |
| AC-Mel | Activated carbon – melamine grafted |
| AC-Ox | Activated carbon – oxidized |
| BET | Brunauer-Emmett-Teller method |
| CNT | Carbon nanotube |
| COF | Covalent organic framework |
| COP | Covalent organic polymer |
| DLS | Dynamic light scattering |
| FTIR | Fourier transform infrared spectroscopy |
| GAC | Granular activated carbon |
| GAC-COP-Fe | GAC – COP – iron impregnated |
| GC | Gas chromatography |
| GC-MS | Gas chromatography – mass spectrometry |
| HPLC | High performance liquid chromatography |
| IC | Ion chromatography |
| ICP-MS | Inductively coupled plasma – mass spectrometry |
| LOD | Limit of detection |
| LOQ | Limit of quantification |
| MgAC | Magnesium-aminoclay |
| NP | Nanoparticle |
| nZVI | Nanoscale zero-valent iron |
| PRB | Permeable reactive barrier |
| SEM | Scanning electron microscopy |
| TCA | 1,1,1-trichloroethane |
| TCE | Trichloroethylene |
| TGA | Thermogravimetric analysis |
| TEM | Transmission electron microscopy |
| UV-Vis | Ultraviolet-visible spectroscopy |
| XPS | X-ray photoelectron spectroscopy |
| XRD | X-ray diffraction |
| ZVI | Zero-valent iron |
| 2D-NLDFT | 2-dimensional non-local density functional theory |

# 1 Introduction

Reactive iron-containing materials are at the forefront of researched materials being applied towards water treatment, and more specifically contaminant degradation in the water treatment process. Although they are frequently used in field application and in lab-scale research, much optimization and insight remains needed before the use of these materials becomes a mainstream means for degrading typically difficult to remediate compounds found in various water sources. By exploring novel advanced materials that can mitigate some of the inherent problems with reactive iron application, the possibility for field advancement is promising. Additionally, advancement of these technologies not only mandates exploring alternative materials for composite fabrication; it also mandates exploring new analytical techniques for measuring the success of existing and future reactive iron-containing materials towards their application in water treatment. Outlined in Figure 1, this PhD project focuses on those two necessary routes in the eventual proliferation of these materials. First, the combination of different technologies with different individual advantages to create unique hybridized composite materials. And, second, the development of appropriate, efficient, and user-friendly methods for standardizing the efficacy of current and new materials.
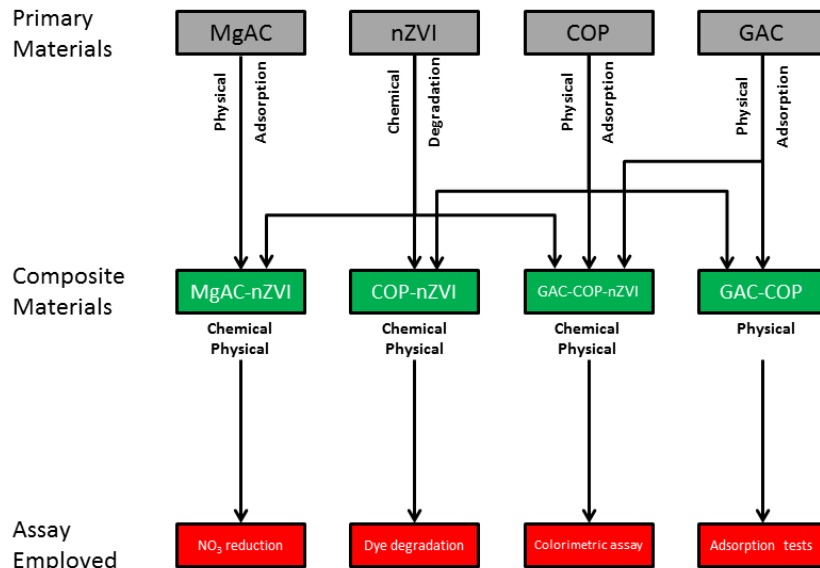


**Figure 1.** Flow diagram summarizing the evolution of produced nano-composite materials and the subsequent assay used to evaluate applicability comprising the basic work structure of the PhD project.

## 1.1  Research objectives and aim

This PhD project has focused on the use of reactive iron, specifically nanoscale zero-valent iron (nZVI), as a means for water treatment. In particular, developing advanced and novel materials containing nZVI for more effective and robust treatment operation; as well as developing an adequate method to assess nZVI material reactivity.

The primary objectives and aims of the research were:

- Development and employment of innovative materials that can result in an increased colloidal stability of nZVI, while preserving or increasing reductive decontamination reactivity (Paper **I** and Paper **II**); and, investigation into new methods during nZVI synthesis and storage that can preserve or prolong the reactivity of nZVI for more efficient pollutant remediation (Paper **III** and Paper **IV**)

- Establishing a new technique or assay that can quantify and standardize the reactivity of a given nZVI material in a simple and user-friendly manner (Paper **V**, Paper **VI**, and Paper **VII**)

- Fabrication of a new hybridized class of nZVI-containing materials that combine different technologies for a more robust and efficient treatment system (Paper **VIII**, Paper **IX**, and Paper **X**)

## 1.2  Thesis structure

Chapter 2 "Background" introduces the general motivation for advancing the global landscape of water treatment, and more specifically the use of nanotechnology and nanomaterials for various water treatment operations. This also includes more insight to the use of reactive iron for water treatment, more specifically the advantages, associated drawbacks, and proposed solutions for combatting those problems.

Chapter 3 "Maintaining and increasing the reactivity of nZVI" details the first work package of the thesis that explores combining nZVI with advanced materials to optimize the reactivity, as well as formulating new methods to prolong the lifetime and reactivity of nZVI long enough to successfully deliver it to various contaminants. This chapter contains work detailed in full in Papers **I – IV**.

Chapter 4 "Assay for reactivity quantification and real-world application" details the second work package of the thesis that develops a novel colorimetric assay to quantify and standardize reactivity for nZVI particles, including comparing the assay to dehalogenation of halogenated organics to prove real-world applicability. This chapter contains work detailed in full in Papers **V – VII**.

Chapter 5 "Hybridized materials for robust water treatment operation" details work from the third and final work package of the thesis that fabricates a new class of materials containing multiple components operating synergistically with different functionalities for an optimized and robust water treatment system. This chapter contains work detailed in full in Papers **VIII – X**.

Finally, there is a brief recap, summary of findings, and future outlook presented in Chapter 6. Note: other than some specific overlaps of methods and/or data, each sub-chapter refers to a particular paper or manuscript.

# 2 Background

The global human population is a dynamic and constantly changing system, which has seen a world with only a few million inhabitants approximately 10,000 years ago expand ever-faster to an estimated 7+ billion today, and expected to meteorically rise to potentially at least 8 billion by the year 2024 [1]. This, in turn, has a direct effect on the available water for human consumption, whether it be for drinking water, agriculture, industry, etc. Consequently, water scarcity is becoming an ever-increasing problem as aquifers are depleted, ground and surface waters are contaminated, and populations move to arid climates not sustainable for long-term human inhabitation. As this problem deepens, water treatment becomes an increasingly crucial issue for the health and development of societies [2]. This, in turn, creates a need for new, effective, and affordable solutions that can address the need for clean water throughout the globe. Therefore, accessing groundwater sources that are currently unused due to various contamination issues is a necessary evolution in the water treatment sector, which includes a plethora of sources that are, or will be, contaminated from various environmental pollutants. To put this in perspective, a recent estimate has determined that there at least 20,000 contaminated groundwater sites in Europe alone, and possibly up to 350,000 sites that remain unidentified [3].

There are many different types of water sources that require various treatment goals, such as groundwater, drinking water, industrial process water, and wastewater. These goals can include the removal of nutrients, undesirable substances, or disinfection, and many different approaches have been taken to address these concerns. With approaches being packed-bed filters of sand or porous carbon, membranes, biological degradation, chemical oxidation, or UV-irradiation, to name a few. Recent advances in the world of nanotechnology and nanomaterials have resulted in the subsequent application in the field of water treatment. To date, nanotechnology for water or wastewater treatment has been applied in one of three ways. First, adsorption/filtration, where the materials are selectively targeting and up-taking pollutants to physically remove them from the bulk solution of water being treated. Second, disinfection, where the materials can physically or chemically attack a water-born pathogen and either cause cell lysis or render it inactive to the extent where it is no longer an anthropological threat. And third, by chemical or photocatalytic degradation, where the nanomaterials are capable to degrading

a specific pollutant into subsequent tertiary compounds that are more benign in nature.

## 2.1 Overview of nanotechnologies for water treatment

There are three main categories for the treatment of water: groundwater treatment, industrial and/or wastewater treatment, and drinking water treatment. Although many of the treatment targets overlap in all three of these categories, each category tends to have its own problems that need to be solved. Groundwater is nearly free of pathogenic contamination, so disinfection of groundwater is irrelevant; treatment of groundwater focuses primarily on heavy metals and possible industrial source pollution, such as halogenated organics, dyes, or pesticides. Treatment of groundwater may be carried out for environmental purposes or for purification prior to use for drinking or for sensitive industrial applications. Industrial/wastewater treatment is similar to that of groundwater treatment in terms of compounds to treat, except that in industrial/wastewater, the compounds usually occur in much higher concentrations, as would be the case in smelting or electroplating operations, for example. Drinking water treatment focuses much more on disinfection, and on some of the same industrial compounds at much lower concentrations. However, drinking water operations need to be fit for human consumption. For example, the Danish Ministry of the Environment has set drinking water limits at the tap at 10, 20, and 10 µg/L for bromate, nickel, and arsenic, respectively (BEK no 292). It is apparent that these various treatment targets can overlap when employing nanomaterials for treatment. So, it is possible to organize these technologies with respect to the method of treatment, which is one of three methods: pollutant removal by adsorption, disinfection of water, and pollutant degradation by chemical reduction or photocatalysis. Certain nanoproducts can be applied in more than one category, as is the case with $TiO_2$, which is effective at both disinfection and photocatalytic degradation of contaminants. The more prolific types of nanomaterials, in terms of application and research include, but aren't limited to: chitosan, zeolites, activated carbon and carbon nanotubes (CNTs), silver and gold nanoparticles, metal oxides of titanium, magnesium, and zinc, as well as iron oxides and zero valent iron.

*Chitosan*

Chitosan is a polysaccharide compound derived from naturally occurring peptides called chitin, which is very similar to cellulose and the next most abundant naturally occurring fiber after cellulose. It comes from a wide range of sources in the environment, most notably the shells of crustaceans, insects, and mushrooms. Being that it can be made cheaply from already naturally occurring sources, chitosan has an advantage that it can be operated at low costs in a low-tech manner. This ability also draws the appeal of chitosan towards rural areas and developing countries.

In addition to being an appealing bio-sorbent, chitosan also displays antimicrobial properties. The particular antimicrobial mechanism is the formation of tight nanoscale pathways that allow for molecular transport across cell membranes, which ultimately can lead to the collapse of a cell [4]. It is also for this reason that nanoscale chitosan is so widely used in the biomedical and drug delivery markets. More specific to water disinfection, however, this process can lead to cell membrane damage as well as chelation of trace metals within the cell that are necessary for life. Given this phenomenon, it was made possible to custom-make these nano-structures for specific applications, whether that be for removal bacteria, viruses, or fungi [4].

Chitosan, due to its high hydrophilicity, presence of surface functional groups, and flexible nature, is also used as a bio-sorbent for many different contaminants, namely heavy metals, dyes, phenols, and certain anions [5]. Some of the adsorption rates for various compounds include numbers in the range of hundreds of mg of dye for each gram of chitosan and reaching as high as 1000 mg dye per gram chitosan, 100 – 200 mg of phenol per gram chitosan, or as much as 100 mg of nitrate per gram chitosan [5]. The unique nature of these particles gives chitosan the ability to be used in applications like flocculation in water and wastewater treatment as well as the disinfection of drinking water. Use of nanoscale chitosan for disinfection remains slightly elusive for large-scale operations, unless incorporated into a membrane; however, its use in coagulation and flocculation operations is increasing and appears to be the most promising use for it. It is promising because it is extremely efficient at coagulating organic and inorganic compounds and chelating highly toxic heavy metals; and in the process, the particles grow in size to a point where the unknown risks coming from their nano-size become irrelevant.

*Zeolites*

Natural zeolites are found in regions all over the world, coming primarily from minerals in volcanogenic sedimentary rock. Zeolites, which can be generally defined as highly crystalline and highly porous inorganic materials, are comprised primarily of silicon and aluminum and oxygen, for example $Na_6Al_6Si_{10}O_{32}$ [6]. There are at least 50 natural zeolites and there are well over 150 synthetic versions of zeolites being produced for various purposes.

Natural zeolites and conventionally synthesized zeolites typically range from 1-10 μm; however, zeolites can be synthesized on the nanoscale, from 5-100 nm [7], most often by grinding e.g. using a ball-milling procedure in a wet environment. When synthesized in this and other similar manners, these nanoscale zeolites can have targeted and uniform crystal structures, depending on the application. These nanoscale versions of zeolites have substantially higher surface areas and smaller diffusion path lengths than non-nano zeolites [8,9]. It is their robustness towards mechanical and chemical stresses that gives zeolites such proliferation in the catalysis, separation, and ion-exchange markets [10]. Specifically, what makes zeolites so great for sorption and ion exchange is the high density of ion exchange sites (e.g. $Na^+$) and porosity. Due to this phenomenon, nanoscale zeolites have been given much attention to their incorporation into various types of membranes to aid in the desalination process of seawater and brackish water sources within the past decade.

For example, this ion exchange mechanism was applied towards heavy metal removal in acid mine drainage [11] and electroplating wastewaters [12]. Furthermore, it has been established that nanoscale zeolites are also capable of removing radioactive elements from liquid nuclear waste streams, providing an extremely cheap alternative to current treatment practices [13]. Recent large-scale applications incorporating the use of zeolites include operations targeting the removal of inorganic ions such as ammonium, heavy metals, organic pollutants, dyes, humic substances, and radioactive elements. However, outside of the use in membrane technologies, in particular those designated "mixed-matrix membranes," introduction of nanoscale zeolites into these operations are still in its infancy.

*Activated carbon and carbon nanotubes*

Activated carbon has been applied for decades as a sorbent material to clean drinking water, as well as wastewaters of industrial, petrochemical, residential, and commercial operations. This usage occurs primarily because it is

extremely cheap, contains a wide variety of various surface functional groups (including carboxyl, quinone, phenol, and lactone), and has a high surface area for adsorption (up to 2000 m²/g), stemming from the nano-porous nature of the material itself, with pores as small as $2 - 50$ nm.

Activated carbon systems are usually made in the form of cartridges or columns where water is passed through via gravity or a pressure-driven method. As the water flows through the carbon, contaminants found in the water come into contact with the carbon and are adsorbed by the carbon material. Furthermore, this carbon can be regenerated simply by repeating the original production process, where the heat and oxidizing gas drive off any sorbed contaminant. However, the further development of carbon into carbon nanotubes (CNTs), whose usage has exploded onto the market in the past two decades [14], with the promise that they can eventually lead to at least partial substitution of activated carbon in the marketplace.

Studies have already proven that CNTs can vastly outperform typical activated carbon with the adsorption of various organic pollutants, as much as 99% greater in certain cases [15], and 3-4 times higher for heavy metals, such as $Pb^{2+}$, $Cu^{2+}$, and $Cd^{2+}$ [16]. Furthermore, CNTs provide a sustainable approach, in that as the metals sorb to the surface functional groups found on the carbon, the metals can subsequently be released and collected simply by adjusting the pH of the solution [17]. In short, these CNTs consist of graphitic cylinders made up of networks of hexagonal carbon linkages that can be as small as 2 nm in diameter [18], and in spite of their small diameter, CNTs can have extremely high length/diameter ratios. The advantage that CNTs possess over traditional activated carbon is that while retaining their high surface area, the structure is easily controllable and well-defined, offering fine-tuning of the compound for application purposes. It is these abilities to control size and length of the CNT, to open/close the ends of the CNT, and to functionalize the surface of the CNT with various metals, functional groups (e.g. alcohol, carboxylic, or carbonyl groups) that provide for extremely effective adsorption properties.

Hence, water treatment with CNTs can be very effective and is used primarily as an adsorbent material, applied to a wide range of compounds such as various heavy metals (As, Cd, Pb, etc.), organic pollutants (benzene, toluene, halogenated solvents, herbicides, etc.), and inorganic contaminants, as well as chlorinated organics like 1,2-dichlorobenzene and trichloroethylene, polycyclic aromatic hydrocarbons, phenolic compounds, surfactants, herbicides like

atrazine, antibiotics like tetracycline, and many others [19]. However, being that CNTs are to date quite expensive, effective use of this technology has been limited to the adsorption of more complex molecules (e.g. polar aromatics, pharmaceuticals, and pesticides) that are not as readily adsorbed using traditional methods. Regardless, the market is seeing a shift into CNT-based water treatment technologies. Foremost is their incorporation into membrane materials, not only to adsorb contaminants, but also to provide mechanical strength. Current research has also seen a shift into using CNT-incorporated membranes for lower-cost seawater desalination purposes; however, realization of this remains yet to be determined. Some companies have also introduced prototype portable water filters containing CNT meshes or sheets in to the market, capable of treating polluted water sources. These portable water CNT water filters have been targeted mainly for military use, disaster relief, remote-area travelling, and also as an attachment at the tap for residential use.

*Silver and gold nanoparticles*

Silver (Ag) has been used to improve human health and conditions for centuries and its toxicity towards various microorganisms has been extensively studied since the 1970's [20], resulting in the use of silver antimicrobials in many bio-medical applications [21]. This notion led the United States National Aeronautics and Space Administration (NASA) to develop a light-weight device that released silver ions in the water supply of a spacecraft that would keep the drinking water bacteria-free, thus eliminating the need for chlorine. Building on this technology, many companies later used similar methods to deliver silver ions into swimming pool waters, keeping them free of bacteria. Such devices are now frequently used in private pools all over Denmark and the rest of the world.

This history has led to the development of silver being engineered as nanoparticles, and is currently the most utilized nanomaterial for disinfection and anti-microbial applications. Most notably available on the commercial market is the use of silver nanoparticles (AgNPs) for small-scale personal water purifiers, the type typically used by hikers and backpackers in the wilderness. Using AgNPs this way (usually as part of a membrane system in combination with activated carbon) eliminates the need for more toxic and foul-tasting disinfection methods like iodine tablets. The idea driving the use of (AgNPs) is that there is a release of biocidal silver ions ($Ag^+$) that attach to and alter the membrane permeability of a cellular organism, which can subsequently

9

attack the thiol groups in proteins or the phosphates in DNA [22]. In this process, these AgNPs then break down the respiratory chain and cell division, which eventually leads to the death of the cell [23].
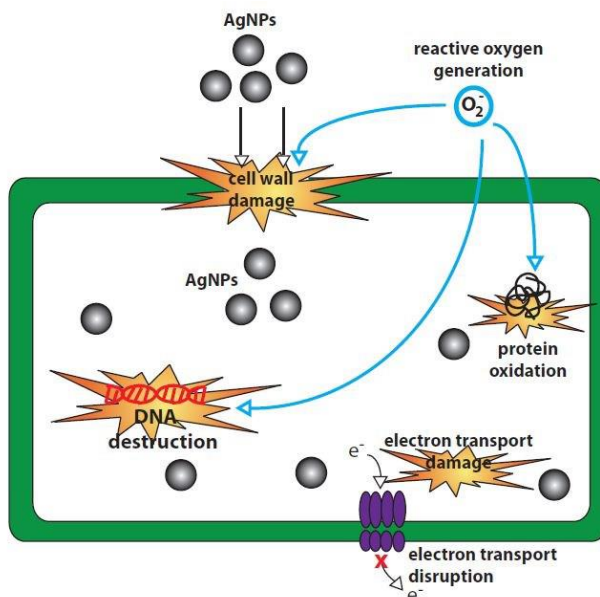


**Figure 2.** Various antimicrobial activities using silver nanoparticles.

In this context, AgNPs have been used as a disinfectant for Gram-negative organisms (e.g. E. coli, V. cholerae, Salmonella), Gram-positive organisms (e.g. Staphylococcus), and many other pathogens in drinking water and wastewater treatment [10,24,25]. Furthermore, the versatility of AgNPs comes with their ability to be incorporated into a plethora of different materials. These materials include zeolites, dendrimers, and membranes, among others, which are then incorporated into disinfection treatment systems as particles in bulk solution or as a means of filtering.

Even though AgNPs are very effective and can be sufficiently immobilized in many materials, the problem of re-dissolution of the particles remains, and consequently that of silver release control and further replenishment of AgNPs. This last statement is important in the further implementation of silver for water treatment purposes, as it is that the Danish Ministry of the Environment has set a limit of only 10 μg/L of silver at the tap (BEK no 292). However, even if silver is released into the water treatment and distribution network from any of these sources, it is usually effectively removed during the municipal wastewater treatment process as silver can be readily transformed into non-dissolvable silver sulfide ($Ag_2S$).

Although the current price of gold makes the notion of using gold nano-particles (AuNPs) for water treatment purposes seem daunting at first, the unique properties that gold exhibits on the nanoscale make the idea more plausible, although the economics may make the use of gold AuNPs unrealistic in the long run. Even so, given that AuNPs have the ability to remove such extremely harmful compounds like mercury or trichloroethylene (TCE), they may be economically justified. For example, when combining AuNPs with a simple citrate molecule, it is possible to adsorb and remove mercury from contaminated river water [26]. This works in a multi-step process where citrate reduces the AuNPs, which then acts as a catalyst to reduce mercury and allow for it to be trapped by other metals (e.g. copper or iron) in solution. Moreover, when combined with another noble metal, such as palladium, AuNPs exhibit extremely high catalytic reduction capacity towards some hazardous compounds, such as TCE [27] and nitrite [28]. Various other operations employing AuNPs are proving effective for removal of certain halocarbons, BTEX compounds, and sulfur-containing organic contaminants (i.e. pesticides). However, as with AgNPs, the problem of cost remains present with AuNPs. Addition of catalytic noble metals and/or a stabilizing agent into which to incorporate the gold remains the only current method to ensure AuNPs can be used at an appropriate cost level.

*Metal oxides of titanium, magnesium, and zinc*

Of all the metal oxides, titanium dioxide ($TiO_2$) is perhaps the most versatile, and possibly the most widely used for various forms of water treatment. $TiO_2$, by means of photocatalysis, is capable of adsorbing metals, organic contaminants, and various other compounds, disinfecting water contaminated with a wide range of bacteria, and degrading certain pollutants. An ideal example of how $TiO_2$ can adsorb metals is in the treatment of arsenic (As) by Pena *et al*. [29]. They demonstrated how it is possible to oxidize, and subsequently adsorb, As(III) to As(V) with $TiO_2$ acting as a photocatalyst by producing various reactive oxygen species such as the $H^+$ ion, hydroxyl radical ($OH^-$), superoxide ($O_2^-$), and hydrogen peroxide in the presence of UV-light. Going even further, single crystal nano $TiO_2$ particles have been developed to a point where nearly the entire face of the particle has a reactive surface, enabling one of the most efficient treatment mechanisms in the nanoproduct market [30].

Moreover, when targeting disinfection purposes, $TiO_2$ is also extremely effective, whether it be in the form of thin films [31], as $TiO_2$ nanorods [32],

doped with ferric iron [33], or combined with silver nanoparticles [34]. These and many other studies report a killing efficiency of $TiO_2$ of at least 50%, but most often upwards of 80-90%, meaning that this may not be capable of being the final disinfection agent for drinking water treatment purposes. However, if it were coupled with other treatment steps (i.e. advanced oxidation processes, membranes, etc.), it could act as an efficient cost-reducing measure to reduce chemical addition and inhibit biofouling of a membrane system.

Zinc oxide (ZnO) nanoparticles, although not nearly as widely applied as $TiO_2$, are known to act as a disinfectant in water treatment. With their main advantage being their use as an antimicrobial agent against a wide range of bacteria, which has been proven in many situations [35,36]. One of the suggested mechanisms has been that since ZnO is known to have a high affinity for absorbing UV-radiation, this will lead to a photocatalytic production of hydrogen peroxide ($H_2O_2$), a well-known molecule capable of microorganism destruction [35]. Another suggested mechanism for the antimicrobial power of ZnO is that ZnNPs are capable of penetrating the cell and consequently causing the unravelling of the cell membrane [37,38]. Ultimately, though, zinc in significant concentrations can be toxic to humans and aquatic life, making large-scale use troublesome. The Danish Ministry of the Environment recommends no more than 3-5 mg-Zn/L in drinking water at the tap (BEK no 292).

Magnesium based nanoparticles (MgNPs) are primarily used in the disinfection of water. For example, Stoimenov *et al.* (2002) demonstrated that magnesium oxide (MgO) can be extremely effective for treatment against various bacteria (e.g. *E. coli* and *B. megaterium*) [39]. This ability as a biocide comes from an unusually high surface area of MgO in nano-form and a unique crystalized structure that allows for many reactive surface sites [40]. In addition to the very structure of the NPs themselves, these MgNPs also possess a unique ability to uptake high amounts of halogens, and in particular chlorine gas ($Cl_2$), which further contributes to the biocidal activity [41]. However, this poses a problem, as the halogen needs to be introduced to the particle; although, there remains much interest in MgO as an antimicrobial agent in water, even if future progress appears limited.

*Iron oxides and zero-valent iron*

Iron, and iron based particles, are by far the most prolific nanoparticles used in the field of water treatment due to iron being ubiquitous in the earth's

crust, cheap to manufacture, environmentally safe, and also a very effective contaminant reductant when converted to its zero-valent form ($Fe^0$). Hence, the uses of iron-based nanoparticles cover various sorption applications and reductive decontamination applications. Sorption of contaminants stems from the complexation of the dispersed metals and the oxygen in the corresponding metal oxides [42]. Furthermore, as the particle size of these iron-based particles is reduced, the adsorption capacity has the potential to drastically increase. To date, applications involving the use of (nano) iron oxides for the adsorption and subsequent magnetic removal of pollutants include removal of bacteria, arsenic, and organic contaminants, among others [43,44]. Perhaps most notably, drinking water treatment by use of magnetic iron oxide nanoparticles to adsorb arsenic and subsequently be removed by a simple magnet was named one of Forbes Magazine's "Top Five Nanotech Breakthroughs of 2006." This could prove to be one of the cheapest and most effective techniques to remove arsenic from drinking water, which could drastically improve the quality of life for tens of millions of people around the world that suffer from arsenic-laden water, in places like India and Bangladesh, for example.

Iron, in addition to being an extremely successful adsorbent material, becomes highly reactive when converting it into $Fe^0$. The basic mechanism is that as the $Fe^0$ particle oxidizes from an iron-oxide shell, electrons are released and water is broken down into hydroxyl radicals and protons, which in turn creates an environment capable of degrading many pollutants (Figure 3). Consequently, increasing the amount of $Fe^0$ also increases the amount of electron transfer that can take place, which then increases the higher reductive capacity of the $Fe^0$ particle.
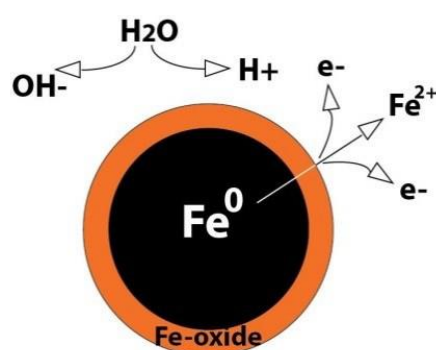


**Figure 3.** Basic reaction mechanism of nZVI particles in water to form pollutant reducing conditions.
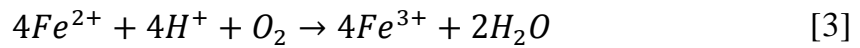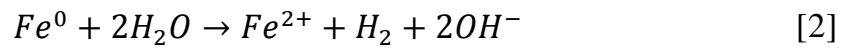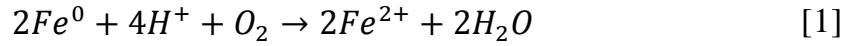
Therefore, nano-Fe$^0$ (nZVI) technologies must take great care in that the reactivity of the particles is not lost before the particles themselves are oxidized and more or less inert. Nonetheless, in 2014, papers dealing with nZVI accounted for 15.8% of all the papers mentioning ZVI [45]. Although the bulk of work performed has to deal with the use of in situ applications of nZVI in the form of soil and groundwater remediation, there are plenty of applications in industrial wastewater, drinking water, or "pump-and-treat" operations for groundwater. For example, when combing nZVI onto a kaolin support, these particles were able to remove 98.8% of Pb$^{2+}$ and 99.8% of total chromium in electroplating wastewater streams [46].

Moreover, there are many companies on the market, which make nZVI powders and slurries that are designed to not only be injected into the ground for soil remediation, but also for the pump-and-treat applications and treating industrial sewage loaded with dyes and various other contaminants. Therefore, although not totally commercial at this point, the future nZVI for pump-and-treat operations lies in one of two forms, that involve attaching the nZVI to some other base material. The first is maintaining nZVI in the form of a slurry and adding that to an already existing treatment operation. The second is by attaching nZVI to a larger particle or granule (e.g. kaolin or activated carbon) and forcing contaminated water through a column as a flow-through system.
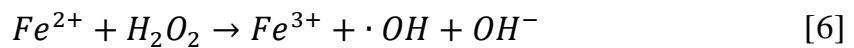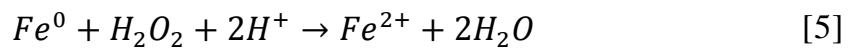
## 2.2 Overview of nZVI for water treatment

Research and application of methods for treating groundwater contamination are continually increasing on a yearly basis, as more and more hazardous compounds in more and more locations are being identified in source waters across the globe. And, one of the most prolific materials for treatment of many of these compounds is zero-valent iron (ZVI). Much of the initial research and most of the current application of ZVI is in the form of *in situ* treatment using permeable reactive barriers (PRBs) [47]; where ZVI in slurry form is injected downstream from a subsurface contaminant zone so that the plume will flow through the injected material, thereby passively degrading the pollutant so that the water comes through treated on the other side [48,49]. This method has its drawbacks though, as subsurface flow modelling is inherently susceptible to a plethora of variables and that after injection the slurry is at the mercy of the environment and all the factors that can lead to particle oxidation and deactivation. On the other hand, albeit more a more

active and costly process, is *ex situ* treatment, where contaminated water is extracted via pump-and-treat methods. In the manner, the treatment material and system can be properly controlled and effluent water quality can be monitored. As briefly mentioned before, ZVI is an ideal material for groundwater treatment due to being ubiquitous in the earth's crust, cheap to manufacture, environmentally safe, and an effective reductant ($E^0$ = -0.44 V). application of ZVI has been studied towards a long list of pollutants, including but not limited to antibiotics, azo dyes, chlorinated solvents, chlorinated pesticides, organophosphates, nitroamines, *p*-chlorophenol, polychlorinated biphenyls, inorganic ions, alkaline earth, transition, and post-transition metals, metalloids, and actinides [50]. The oxidation of ZVI is very well studied, as it will easily oxidize in the presence of water and the dissolved oxygen in water (Eqs. 1-3) [51–54].

$$2Fe^0 + 4H^+ + O_2 \rightarrow 2Fe^{2+} + 2H_2O \qquad [1]$$

$$Fe^0 + 2H_2O \rightarrow Fe^{2+} + H_2 + 2OH^- \qquad [2]$$

$$4Fe^{2+} + 4H^+ + O_2 \rightarrow 4Fe^{3+} + 2H_2O \qquad [3]$$

Moreover, while in the presence of dissolved oxygen in water, ZVI can be extremely effective at degrading a wide variety of organic pollutants [45]. This mechanism consists of $Fe^0$ reacting with $O_2$ to form $H_2O_2$ and $Fe^{2+}$, $Fe^0$ reacting with the produced $H_2O_2$ to produce $Fe^{2+}$, and finally resulting in a Fenton-type reaction that produces the extremely potent hydroxyl radicals for oxidation (Eqs. 4-6) [45].

$$Fe^0 + O_2 + 2H^+ \rightarrow Fe^{2+} + H_2O_2 \qquad [4]$$

$$Fe^0 + H_2O_2 + 2H^+ \rightarrow Fe^{2+} + 2H_2O \qquad [5]$$

$$Fe^{2+} + H_2O_2 \rightarrow Fe^{3+} + \cdot OH + OH^- \qquad [6]$$
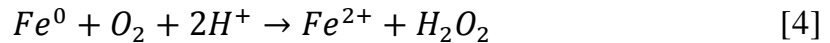
Furthermore, synthesizing ZVI on the nano-scale (nZVI) has proven to increase the effectiveness of the material substantially, as the reactive surface area is dramatically improved; increasing from 0.9 $m^2$/g in commercially available micron-sized ZVI to as much as 33.5 $m^2$/g in nZVI [55]. Although, this increased reactivity also has its detriments, as the reactivity loss also increases due to various interactions with the surrounding environment from constituents like dissolved oxygen and ionic species present. For *in situ* treatment, this correlates to practical problems in application like limited transport and flow in a porous medium [56,57], but also can translate into related issues with *ex situ* treatment when nZVI aggregates into larger particles and reduces treatment capacity. Much of the driving force behind this

aggregation stems from the inherent van der Waals forces and magnetic attraction between particles [56,58]. Because of this problem when dealing with nZVI, many attempts have been made to stabilize the particles from acting against themselves. Often this has been done by attaching some form of coating or various other stabilizing agents [59], with the aim to generate a stable and dispersive material or slurry that does not compromise reactivity or particle surface area.

# 3 Maintaining and increasing the reactivity of nZVI

The first work package of this PhD project consisted of two primary goals involving advancing and expanding the use of nanoscale zero-valent iron (nZVI). This chapter also refers to the work contained in Paper **I**, Paper **II**, Paper **III**, and Paper **IV**. The first part sought to explore different materials that could increase the colloidal stability of nZVI while maintaining or, preferably, increasing the reactivity. The second part delved into techniques that could prolong and preserve the lifetime and reactivity of nZVI long enough for efficient delivery to contaminants. Alone, nZVI can exhibit some remarkable reactivity properties towards a wide variety of contaminants and has been quite extensively studied towards these compounds [50], however its use is limited unless a stabilizing agent is incorporated to maintain the reactivity of nZVI until it can come in contact with the compound to be degraded. With this in mind, many different stabilizing agents have been investigated, in order to attach to the nZVI or act as a coating. These agents include materials such as anionic and nonionic surfactants [60,61], sodium carboxymethyl cellulose [62,63], starch [58,64], and guar gum [65], with the idea that they can provide an environment that will combat the attractive forces between nZVI or other metallic particles.

## 3.1 Mg-aminoclay (MgAC) coating of nZVI

In this PhD project, Paper **I** details the preliminary attempt at stabilization of nZVI was done using synthetic clay-like substance, termed magnesium-aminoclay (MgAC), which has a 2:1 trioctahedral smectite-like structure, but covalently linked with an approximate composition of $R_8Si_8Mg_6O_{16}(OH)_4$, where $R = CH_2CH_2NH_2$ [66,67]. These synthetic organo-functionalized clays, with a Mg-occupied octahedral sheet sandwiched between two tetrahedral silica layers, have been applied in self-assembled bio-nanocomposites [68–71], microalgae-based biorefineries [72–75], and environmental remediation [76–78]. The basic structure of the MgAC is presented in Figure 4.
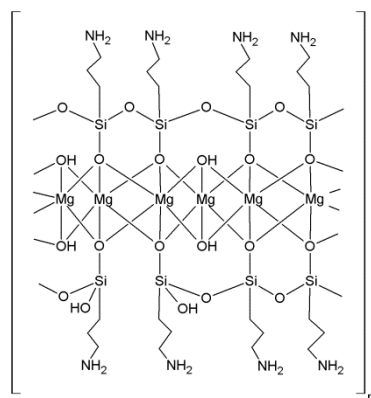
**Figure 4.** Molecular structure of the MgAC used to stabilize nZVI (adapted from Chaturbedy et a. (2010) [67].

The most important facet of the composition of MgAC being the $-NH_2$ groups, as it is known that iron and other metal ions are well complexed with amine containing compounds [79]. Based on this, the precursory $Fe^{2+}$ is expected to bind on the surface of the MgAC, where it can then chelate with the amine groups. Here, various suspensions of MgAC with different weight ratios (i.e., wt:wt, MgAC:Fe), ranging from 0:1 and 1:0 to 20:1 were prepared. This variation in ratios allowed for a determination of an ideal mixture of MgAC and nZVI that allowed for the optimal amount of both particle stability and contaminant degradation. Briefly, this was done mixing the as-prepared MgAC with ferrous iron ($Fe^{2+}$) in a closed system with an inert $N_2$ atmosphere to prevent oxidation, followed by reduction of the $Fe^{2+}$ ions to $Fe^0$ by via the mild chemical reduction of the metal salt using sodium borohydride ($NaBH_4$) [80]:

$$2Fe^{2+} + BH_4^- + 3H_2O \rightarrow 2Fe^0 + H_2BO_3^- + 4H^+ + 2H_2 \qquad [7]$$
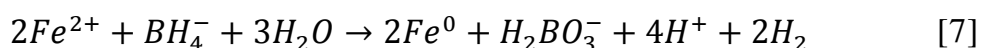
Following particle purification, samples were immediately characterized and tested for both their stability and their reactivity.

## 3.1.1 Properties of MgAC coated nZVI

Nanoparticles of MgAC coated nZVI were prepared in MgAC:Fe (wt:wt) ratios of 0:1, 1:1, 5:1, 7.5:1, 10:1, and 20:1. And, in order to properly characterize them, transmission electron microscopy (TEM) was carried out to observe the morphological change and X-ray diffraction (XRD) was carried out to assess the iron crystallinity and verify the presence of $Fe^0$ and any other iron oxide species present. Figure 5 presents TEM images of uncoated nZVI and MgAC coated nZVI with the various wt:wt ratios. As observed in Figure

5A, the bare nZVI exhibited the typical chain-linked and amorphous structure that nZVI most typically as iron nanoclusters often do, ranging anywhere from approximately 30 nm to 100 nm in particle diameter [81–85]. Subsequent addition of MgAC coating did not alter the nZVI structure at low loading (wt:wt, 1:1), however, as the loading increased the isolation of nZVI became apparent as more spherical like particles emerged with increasingly larger shells of MgAC coating. This is most likely due to the weaker attractive interactions between the individual nZVI particles due to van der Waals and magnetic forces [56], allowing for more uniform and separate coated particles to exist. This in turn increased the individual particle size and also resulted in larger aggregate clusters; which is primarily due to the electrostatic attraction between the positively charged MgAC by the protonated amine groups (pH: 2.0 − 12.0) [67] and the negatively charged zeta potential of the nZVI (pH: >8.1) [86], as it was that the particle synthesis was conducted at a pH of 9.6, due to the pKa of 10.6 for the MgAC [76].
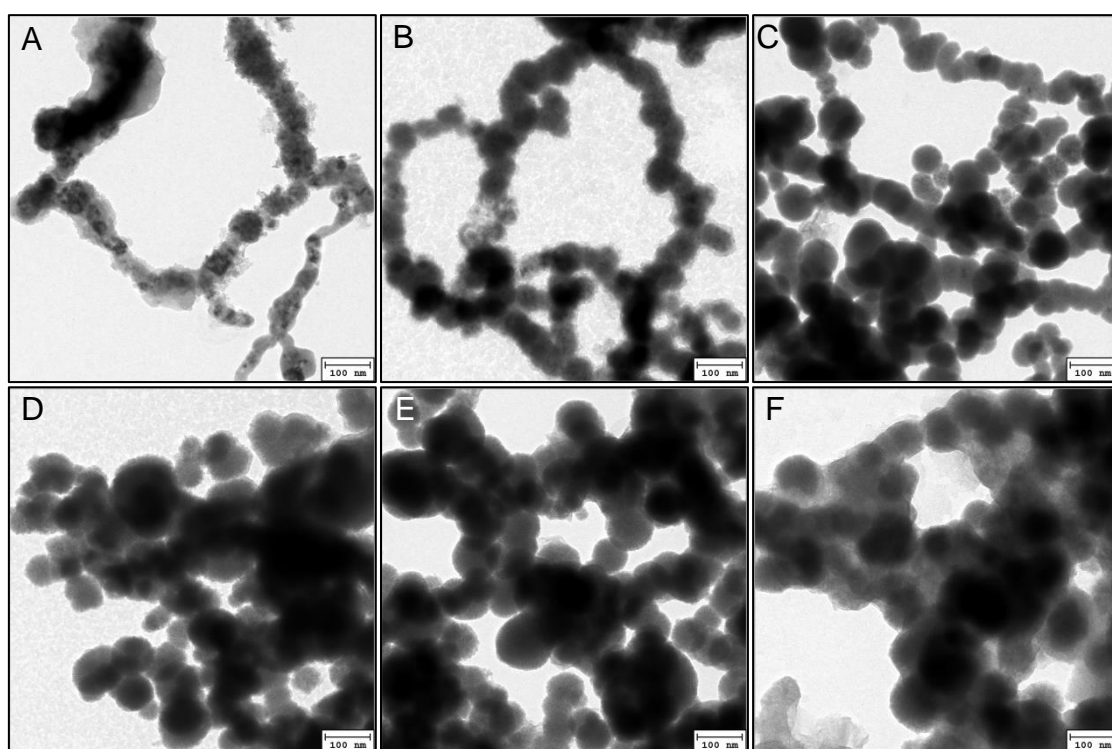


**Figure 5.** Transmission electron microscopy (TEM) images of MgAC coated nZVI with various MgAC:Fe (wt:wt) ratios: A) 0:1, B) 1:1, C) 5:1, D) 7.5:1, E) 10:1, and F) 20:1. Paper **I**.

The morphological observations need to be followed up with determination of the exact iron species and crystallinity present, which was done using XRD. The results of which are plotted in Figure 6. The bare nZVI, as ex-

pected, exhibits an apparent core-shell matrix, given by the small $Fe^0$ peak characteristically found at 44.9° 2θ and a series of peaks related to γ-$Fe_2O_3$ [83,84,87]. With the addition of more and more MgAC, no significant crystallinity was detected until the ratio of 7.5:1 was achieved, upon which a significant peak appeared at 44.9° 2θ. This drastic change in the properties of the iron species is further corroborated when the particles are evaluated for their stability and reactivity. Therefore, it can be assumed that initial analysis with XRD can be an effective screening method for estimating the effectiveness that MgAC coating has on nZVI applicability.
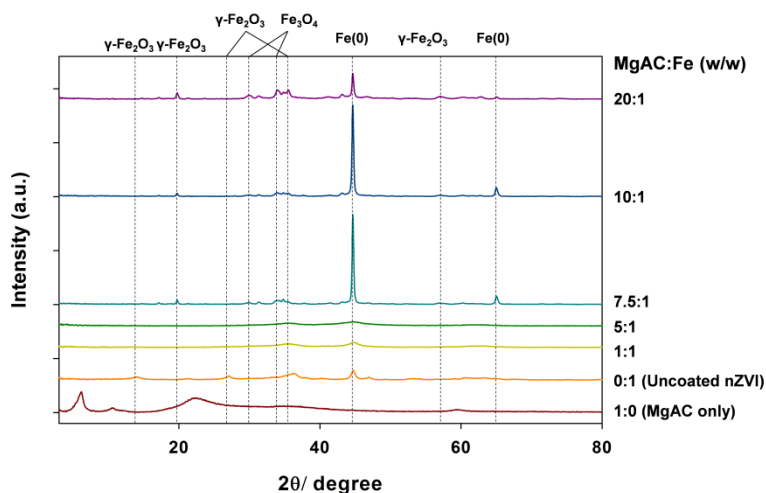


**Figure 6.** X-ray diffraction (XRD) patterns of MgAC, uncoated nZVI, and MgAC coated nZVI with various MgAC:Fe weight ratios; of particular interest is the strong presence of the characteristic $Fe^0$ peak at 44.9° 2θ appearing at the 7.5:1 ratio. Paper **I**.

## 3.1.2 Effect of MgAC on nZVI colloidal stability

In order to determine colloidal stability of nZVI or nZVI immobilized particles in solution, it has been determined that the most accurate measure is to suspend the particles in water and measure the absorbance of the mixture at 508 nm over time [60], and quantify the rate at which particles aggregate and sediment out of solution. Where the less the relative change to the initial absorbance, the more the particles stay suspended and the more stable the particles are determined to be. The MgAC coated nZVIs were measured and compared with bare nZVI, with the results plotted in Figure 7.
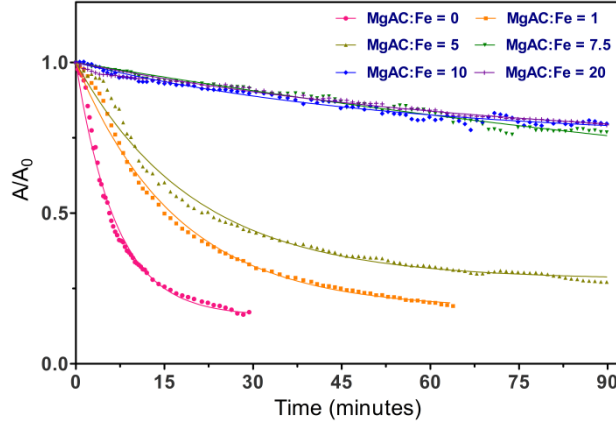
**Figure 7.** Sedimentation patterns of as-prepared MgAC coated nZVI with various MgAC:Fe weight ratios; plotted in terms of optical absorbance at 508 nm, relative to the initial absorbance. Paper **I**.

Based on the sedimentation curves obtained in Figure 7, it is apparent that the ratio of MgAC to Fe has a significant effect on the behavior of nZVI. Most importantly that increasing amounts of MgAC increases the general stability of the particles, up to a point. There is a steady increase in colloidal stability up to a MgAC:Fe ratio of 5:1, and then a jump and plateau effect once a ratio of 7.5:1 is presented. Using the following modified Stoke's equation from Phenrat *et al.*, a characteristic time, or pseudo "half-life" can be determined:

$$A_t = A_0 \times e^{-t/\tau} \qquad [8]$$

Where, $A_t$ is the absorbance at time $t$, $A_0$ is the initial absorbance, and $\tau$ is the characteristic time of sedimentation for the particles in solution. Calculating this, the characteristic time increased from 6.71 minutes in bare nZVI to 83.8 minutes with the highest ratio of MgAC; with a major increase from corresponding to the gap between the 5:1 and 7.5:1 weight ratios (Figure 8A). The characteristic time can be further related directly to the hydrodynamic radius of the particle(s) using Stoke's law:

$$\tau = \frac{9\eta(\beta - p_f)}{2g^2(\rho_s - \rho_L)^2 R_H^2} \qquad [9]$$

Where, η is the solvent viscosity, β is a function of the permeability of the fractal aggregate, $p_f$ is the fluid pressure, $\rho_s$ and $\rho_L$ are the densities of the solid and liquid, $g$ is the gravitational acceleration, and $R_H$ is the hydrodynamic radius.

21
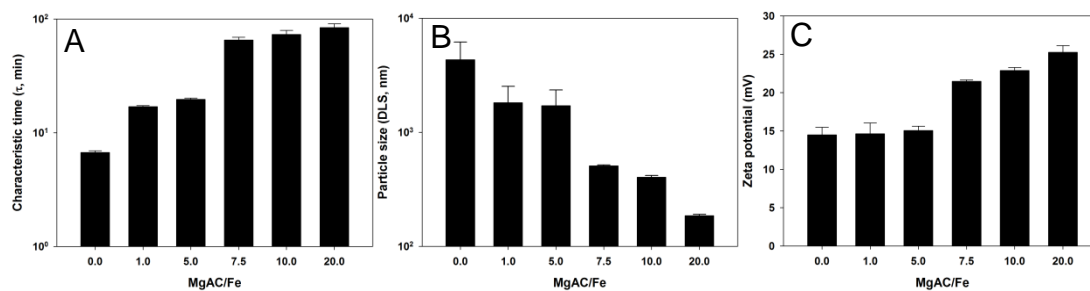
**Figure 8.** Properties of MgAC coated nZVI with different MgAC:Fe weight ratios. Calculated characteristic times (Eq. 2) from the sedimentation test (A); particle size (diameter) from DLS analysis (B); and the zeta potential from DLS analysis (C). Paper **I**.

Using the technique known as dynamic light scattering (DLS) that beams monochromatic light into a solution with spherical (assumed) particles in Brownian motion to measure the Doppler shift when light hits a moving particle, it is possible to obtain an estimated particle size (i.e. diameter). With this technique, the particle size decreased from 5132 nm in bare nZVI to 186 nm in 20:1 MgAC:Fe particles (Figure 8B). Again, a major change occurred in the gap between the ratios of 5:1 to 7.5:1. While using the DLS technique, it is also possible to measure the zeta potential of particles in solution, which is a measure of the electro-kinetic relationship a particle has with its surrounding medium. Basically, the greater the absolute difference in charge, the more stable an individual particle or colloid is from aggregation. Here, the zeta potential increased from +14.5 mV in bare nZVI to +25.3 mV in 20:1 MgAC:Fe particles (Figure 8C). Once more, there was a noticeable change between the ratios of 5:1 and 7.5:1. This significant decrease in particle size and increase in zeta potential beginning at the 7.5:1 ratio, with limited benefits thereafter is important; as this ratio follows the optimal colloidal stability ratio determined per solution optical density (Figure 7).

### 3.1.3 Effect of MgAC on nZVI reactivity

Although the evaluation and increase of colloidal stability for nZVI particles is an important step in the effective application of nZVI and addressing the concerns regarding mobility and protection from oxidation, the ultimate goal remains to be efficient environmental remediation via contaminant degradation. As it is that although an effective technique can be introduced to stabilize nZVI, often times this can also fail to alter the reactivity or in some cases decrease the reactivity. That decrease can come from a variety of mechanisms, such as the blocking of active reactive sites by the coating that inhibits

the diffusion of an aqueous phase contaminant to be transported to the surface of the nZVI. For this work, the matter of reactivity was addressed using a model contamination compound, in the form of nitrate ($NO_3^-$), added as $NaNO_3$. Nitrate was chosen as it has long been recognized as a common groundwater pollutant [88] and that previous reports have used nZVI to degrade nitrate to ammonium [89]. Specifically, nZVI reactivity was assessed by nitrate reduction in an iron-limited environment, with a theoretical nitrate reduction by nZVI as follows [90]:

$$4Fe^0 + NO_3^- + 10H^+ \rightarrow 4Fe^{2+} + NH_4^+ + 3H_2O \qquad [10]$$
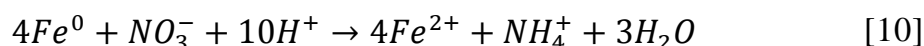
Given this yield and stoichiometry, iron-limiting conditions were controlled so that nitrate reduction and kinetics could be evaluated. And, by performing batch mixing tests for a period of 90 minutes, then measuring the nitrate concentration remaining in solution using ion chromatography (IC); the kinetics were established and plotted in Figure 9, given as the ratio of nitrate concentration (C) at a given sample time during the reaction with respect to the initial nitrate concentration ($C_0$).
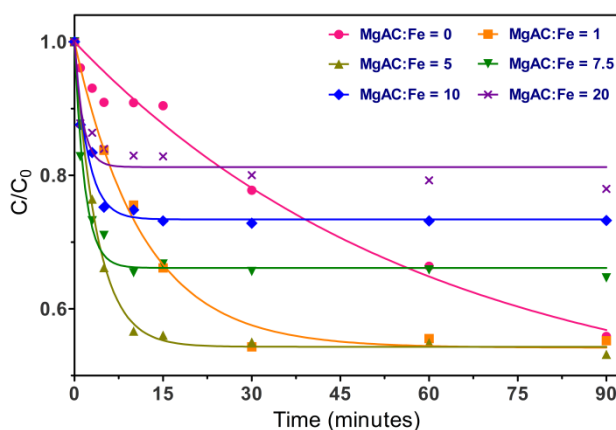


**Figure 9.** Nitrate reduction profiles, as measured by IC, with various MgAC:Fe weight ratios. Paper **I**.

Not surprisingly, the bare nZVI had a very low reaction rate, due to the rapid aggregation of particles not only during the reaction test, but also during the synthesis and washing steps. All of this affects the general structure of the particles and the access of nitrate to the reactive surface area of the particle. Equivalently, another study investigated the effect of sonication of nZVI on the resulting relationship to nitrate reduction and determined a positive correlation between aggregate destruction by sonication and nitrate reduction [91].
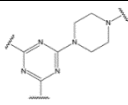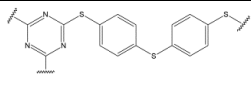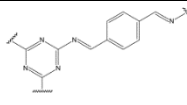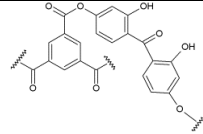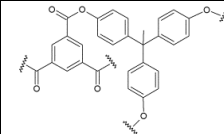
23

In summary, the use of MgAC as a coating for improving the applicability of nZVI was an effective first attempt at using alternative materials in conjunction with nZVI. Characterization and reactivity analyses coincided very well with each other when determining not only that MgAC is a suitable coating material, but also when determining the ideal MgAC loading ratio. These analyses included morphological observations with TEM, $Fe^0$ content with XRD, colloidal stability using solution optical density and DLS, and reactivity analysis determined by nitrate reduction to ammonium.

## 3.2 Covalent organic polymer (COP) impregnated with nZVI

Exploring the use of magnesium-aminoclay (MgAC) was the first material studied, with the work taking place solely at DTU Environment. The second material(s) explored were a class of porous polymers, termed covalent organic polymers (COPs); which were developed at KAIST, and therefore the bulk of this work was conducted in the lab facilities there. Based on the work done here, a manuscript, Paper **II,** was published and the work is discussed here. Following the successful utilization of the MgAC to increase the stability and reactivity of nZVI, new advanced porous organic materials were explored to further increase the stability of nZVI and protect the particles from oxidation before delivery to the contaminated water source. Over the past decade, a widespread interest has developed in the development of compounds termed covalent organic frameworks (COFs) [92], and have delivered some very propitious initial results in the field of carbon dioxide gas capture [93]. Although, further development and later studies have ultimately fallen short of the initially presented promise for environmental applications [94–96]. For example, the issue of stability of COFs in water has been recognized as a major problem, unless extreme measures are taken, such as alkylating the pores and preventing subsequent hydrolysis [97]. This, obviously, is a major drawback when using in environmental applications. Therefore, focus was directed to a different class of porous organic materials, namely, covalent organic polymers (COPs). These COPs have already been established to be suitable candidates for environmental applications such as gas capture [98–100] and solvent uptake from water streams [101]; and, for example are stable enough to withstand boiling water for at least a week at a time [98]. This stability in aqueous environments, along with their unique nanoporous nature with extremely high surface areas of $>600$ $m^2/g$ in some cases [102,103].

With this in mind, we selected five different COPs, with different surface areas and functionalities (amine, imine, thiol, and ester) in order to immobilize nZVI by physically caging it within the porous matrix of the polymer; as opposed to more traditionally nZVI stabilization methods that act as a coating. Table 1 outlines the polymer structure of each polymer used.

**Table 1.** Chemical structure of each COP tested for nZVI stability. COP-1 is the polymerization of triazine trichloride with piperazine; COP-6 is the polymerization of triazine trichloride with 4,4'-thiobisbenzenethiol; COP-19 is the polymerization of melamine with terephthaldehyde; COP-60 is the polymerization of trimesoyl chloride with 2,2',4,4'-tetrahydroxybenzophenone; and COP-61 is the polymerization of trimesoyl chloride with 1,1,1-tris(4-hydroxyphenyl)-ethane. Paper **II**.

| COP-1 | COP-6 | COP-19 | COP-60 | COP-61 |
|---|---|---|---|---|
|  |  |  |  |  |

These COPs are unique compared to typical macromolecular chain structures, in that no post-processing or cross-linking is necessary to create the porosity inherent in their structure. Synthesizing these polymers in a one-pot method allows for an easily reproducible reaction using nucleophilic substitution of one monomer onto the leaving group of another monomer either gradually over time at high temperatures (i.e. COP-19 [102,103]) or by gradually increasing the temperature over time (i.e. COP-1 and COP-6 [98,99]). For example, with COP-1, triazine trichloride has three leaving groups (i.e. chloride) that will preferentially be substituted with the secondary amine nucleophile (i.e. R-NH-R') found in piperazine based on temperature. The first nucleophilic addition at cold temperature (i.e. 0 °C), the second at room temperature (i.e. 25 °C), and the third at high temperature (i.e. >60 °C).

## 3.2.1 Properties of COP-nZVI composites

Each of the COPs used was synthesized fresh, following established methods [98,99,102–104] (note: COPs 60 and 61 were first published in this work as supporting information [104]) for each particular test employing nZVI for stability and reactivity analysis. Before testing, confirmation of successful polymerization of each COP was done using Fourier transform infrared spectroscopy (FTIR) to confirm the desired functional groups were present in

each polymer. The total Brunauer-Emmett-Teller (BET) surface area was measured for each polymer and was 168, 600, 332, 9.1, and 8.8 m$^2$/g for COPs 1, 6, 19, 60, and 61, respectively (Figure 10A, black bars).
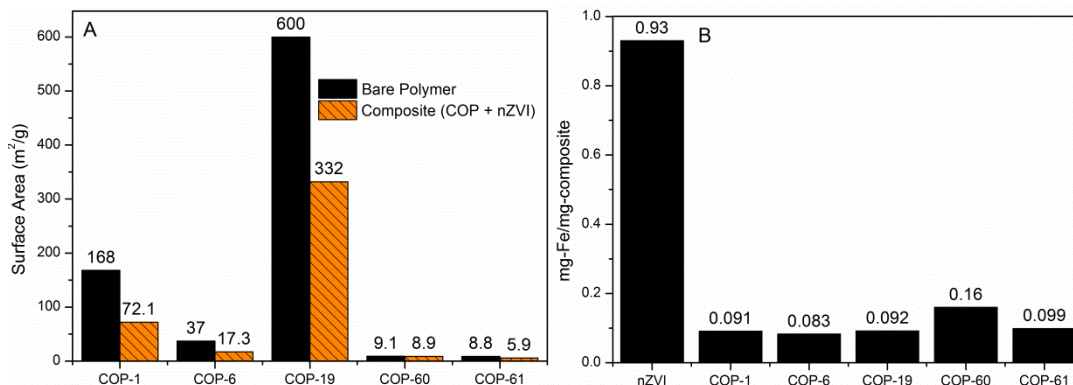


**Figure 10.** BET surface area comparison of the bare COP (black bars) vs. the COP-nZVI composite (orange bars) (A); and, the total iron content contained in each composite after acid digestion and measured by ICP-MS (B). Paper **II**.

For more insight into the composite material, the morphology was observed using TEM, where a stark contrast was observed with respect to the MgAC coated nZVI. Where the MgAC coated particles maintained an overall spherical shape aggregated into clusters, the presence of COP was apparent with impregnated nZVI within the inner matrix of the polymer (Figure 11). The total BET surface area was again measured after nZVI impregnation, and each composite's surface area decreased, to 72.1, 17.3, 332, 8.9, and 5.9 m$^2$/g for COPs 1, 6, 19, 60, and 61, respectively (Figure 10A, orange bars).
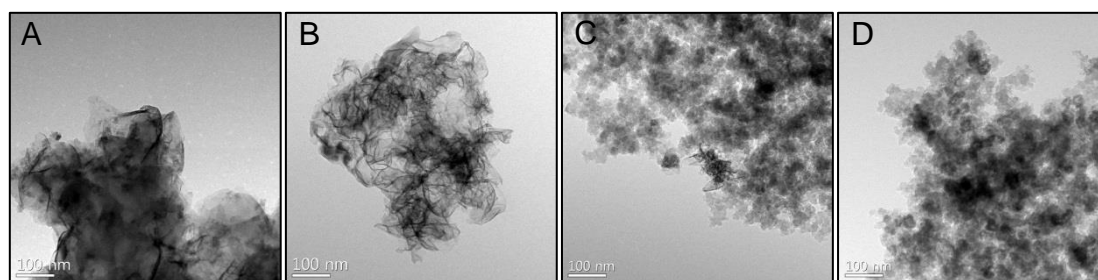


**Figure 11.** TEM images demonstrating the COP/nZVI composite morphology of COP-1 (A); COP-6 (B); COP-19 (C); and COP-60 (D). Paper **II**.

This indicates that the nZVI was loaded into the polymer pores, similar to the effect observed when loading nZVI into the pores of activated carbon [105]. The pore size was also measured concurrently with the BET analysis, and found that the pore size for each COP increased when loaded with nZVI, indicating that free-standing particles of nZVI were formed in and around the COPs, creating additional pores by the self-stacking of nZVI particles [106].

Iron was then confirmed to be a part of the composite matrix by first digesting the samples [43], then analyzing with inductively coupled plasma – mass spectrometry (ICP-MS). Mass values were 9.1, 8.3, 9.2, 16.3, and 9.9 %-Fe for COPs 1, 6, 19, 60, and 61, respectively (Figure 10B). XRD was also performed on each composite to verify the crystallinity of the iron and that $Fe^0$ was present, which was true for all samples, except for the COP-6 composite.

## 3.2.2 Effect of COP on nZVI colloidal stability

Following the same method mentioned for measuring colloidal stability in Section 3.1.2, the composites were tested and compared with bare nZVI, with the results plotted in Figure 12A. As expected, bare nZVI exhibits extremely poor colloidal stability, as the absorbance decreases quickly, meaning fast aggregation and heavier particles sedimenting out of solution. The various COP composites had mixed results, however, all performed far better than bare nZVI. Not only were the kinetics much slower, but the final absorbance values remained higher compared to nZVI, and still higher than a commercial product stabilizing nZVI with a surfactant [107]. Characteristic times were 14, 52, 49, 1340, 93, and 52 minutes for bare nZVI and COP composites of COPs 1, 6, 19, 60, and 61, respectively. However, most notably, the composite with COP-19 performed extremely well, only losing 3.9% of its original absorbance. This was a major achievement in the stabilization of nZVI, as values as high as this had not been observed after performing an extensive literature search. Also, when compared to stabilization with the MgAC coated nZVI that had a maximum characteristic time of 83.8 minutes, the values are comparable. Except for COP-19, which was two orders of magnitude higher.
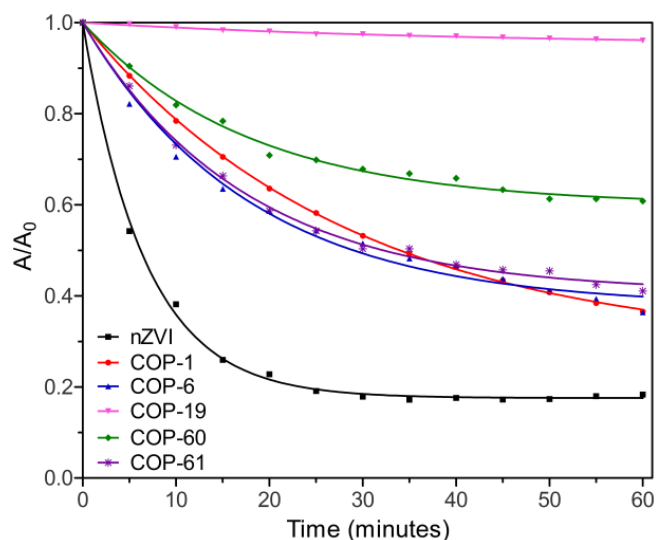
**Figure 12.** Sedimentation profiles of nZVI and COP-nZVI composites, measured by the absorbance at 508 nm, in terms of absorbance relative to the initial absorbance, monitored over time. Paper **II**.

### 3.2.3 Effect of COP on nZVI reactivity

Although successful stabilization of nZVI was achieved by impregnating the nZVI into the pores of the COP materials, especially with COP-19, further testing needs to be done with respect to maintaining the overall reactivity. To do this, a model compound was chosen that would be easy to assess in the laboratory. This was done to increase the range of reactivity tests available for assessing nZVI reactivity. In Paper **I**, reactivity was evaluated by way of nitrate reduction, which requires the use of advanced analytical equipment like IC. A simpler method requiring only a spectrophotometer was chosen. And, as it has been documented that granular ZVI is capable of breaking the azo (R-N=N-R') bond in a variety of azo dyes to decolorize them; the azo dye naphthol blue black (NBB) was chosen to for an ideal compound, as it has a higher peak absorbance ($\lambda_{max}$ = 618 nm) that won't have any absorbance interference from $Fe^{2+}$ or $Fe^{3+}$ ions. As illustrated in Scheme 1, the theoretical mechanism of the decolorization of NBB by nZVI produces three tertiary compounds, with the dominant species being aniline.
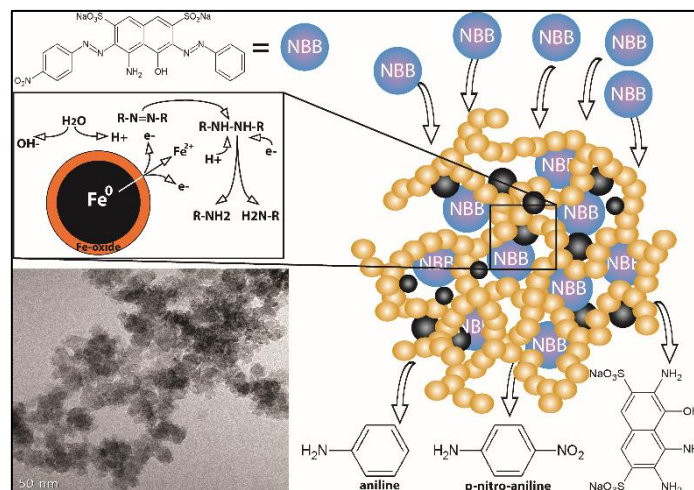
**Scheme 1.** Mechanism of the reductive degradation of naphthol blue black in the presence of nZVI. COP chain drawn as yellow spheres and nZVI drawn as black spheres. Paper **II**.

The various COP-nZVI composites exhibited vastly different results when the dye decolorization test was performed, ranging from nearly no dye removal from the COP-60 and COP-61 composites to nearly complete removal from the COP-1 and -19 composites. This was determined by plotting the measured absorbance of the peak wavelength of NBB over the 30 minute reaction period (Figure 13).
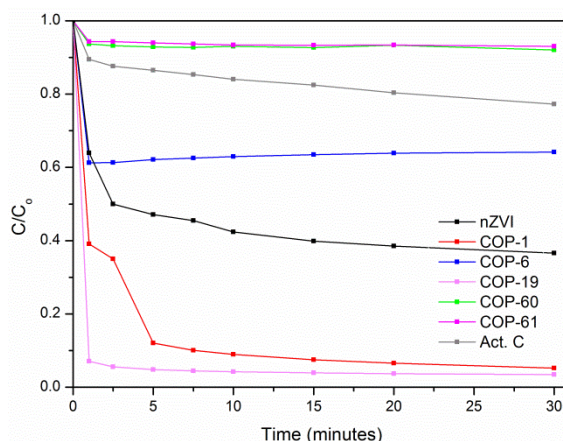


**Figure 13.** Naphthol blue black decolorization over time by the COP-nZVI composites, bare nZVI, and activated carbon. Paper **II**.

Looking at the peak wavelength absorbance, however, is only a fraction of the answer to determining whether or not there is degradation occurring. It is obvious that there is a removal of dye, but dye adsorption must be distinguished from dye degradation. For that, looking at the whole UV-Vis spectra during analysis is necessary (Figure 14). For this, it is important to look at two phenomena that have been observed before when degrading NBB with

ZVI [108] or other compounds[109,110], the peak absorbance shift from 618 nm to 588 nm caused by the subsequent produced chromophore via azo bond reduction and the diminishing of the peak at 310 nm, indicative of the oxidation of naphthalene groups via the Fenton reaction.
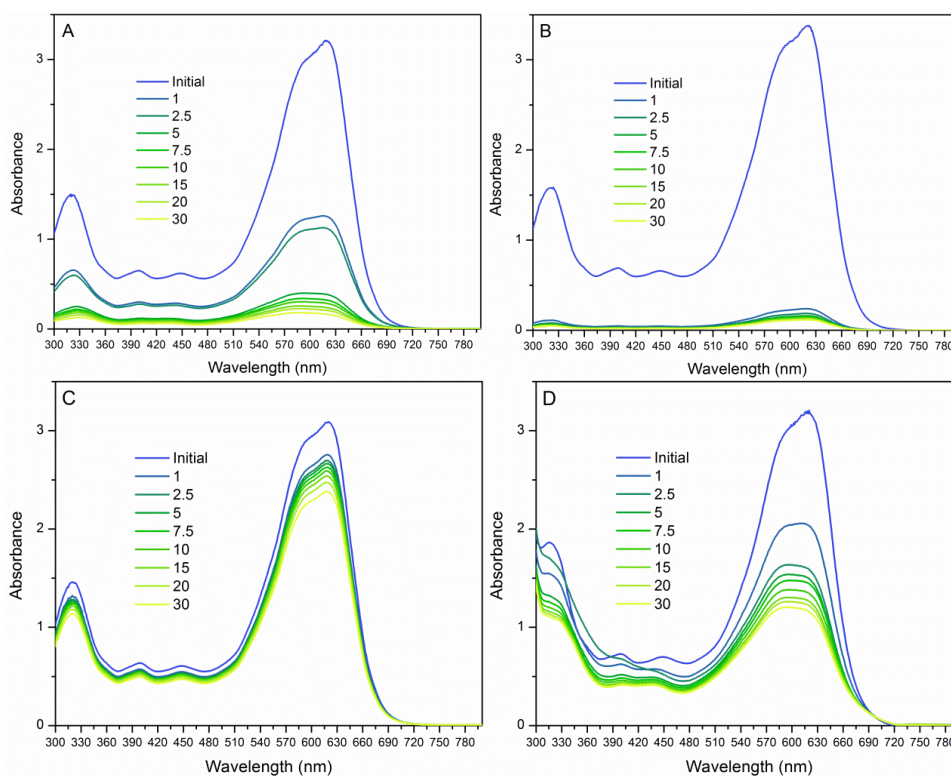


**Figure 14.** UV-Vis absorbance spectra for COP-1 (A); COP-19 (B); activated carbon (C); and bare nZVI (D). Paper **II**.

In a final attempt to verify the degradation of NBB by the composite materials, the primary degradation product [111], aniline, was analyzed for in the samples from the most promising candidates (COP-1 and COP-19) using high performance liquid chromatography (HPLC). However, this proved to be a very difficult task, with only approximately 2.5 % of the total possible yield detected. Although the UV-Vis data was convincing for positive degradation results, the HPLC did not effectively confirm this notion; but, the somewhat controversial explanation [112] of pi-pi stacking between the different aromatic compounds of the aniline and the polymer could possibly explain the lack of aniline detection; as this has been observed before in similar systems [113–115].

In summary, the various COP materials employed for combination with nZVI proved that their porous nature was highly suited for the impregnation of iron, and that they were very capable of protecting the colloidal stability of

nZVI. However, reactivity assessment proved to be difficult for the composite materials, as the unique adsorption traits led to difficulty in analytics. Lessons learned from using COPs are that if they can be better optimized into a matrix, their iron trapping and colloidal stabilizing traits can provide an effective platform for eventual use into a water treatment system. Furthermore, the use of decolorizing a dye by nZVI is an ideal solution on paper; although practical issues with matrix interference yield the notion for the development of a better assay to adequately determine reactivity of nZVI materials.

## 3.3 Washing and storage of MgAC-nZVI to increase reactivity

After exploring two novel types of materials in the initial part of the first work package, work shifted back to DTU Environment for Paper **III**, which studied the effects of washing and storage on MgAC. Significant achievements were produced towards increasing the stability and reactivity of nZVI by the use of two different stabilization agents, a synthetic MgAC and various porous COPs. However, this is only a preliminary step for the eventual proliferation of nZVI use in the field. Application of reactive iron mandates that the materials be exposed to aqueous environments for long periods of time, all the while yielding the potential for oxidation by oxygen in the air or in the dissolved form and by the water itself. Thus, hindering these oxidation effects is necessary so that the materials can be delivered to the contaminants in a near-pristine form [116]. This can be partially controlled by optimizing the aging of the particles during synthesis, which has already been performed on uncoated nZVI [117,118]. Based on the previous success using MgAC as a stabilizing agent for nZVI (Section 3.1), and that MgAC has been reported to have positive effects on preventing the oxidation of copper nanoparticles [119], it was determined to investigate the synthesis of MgAC coated nZVI further. Except, also investigating the washing procedure along with the aging procedure, being that a small amount of stabilizer is inherently lost during this step. For this, we applied three different washing and aging (storage) strategies: Treatment 1, pre-storage washing with 1 mM $NaHCO_3$ buffer immediately after synthesis and stored in water; Treatment 2, post-storage washing with 1 mM $NaHCO_3$ after storing in water; and Treatment 3, pre-storage washing with 3.75 g/L MgAC immediately after synthesis and stored in water.
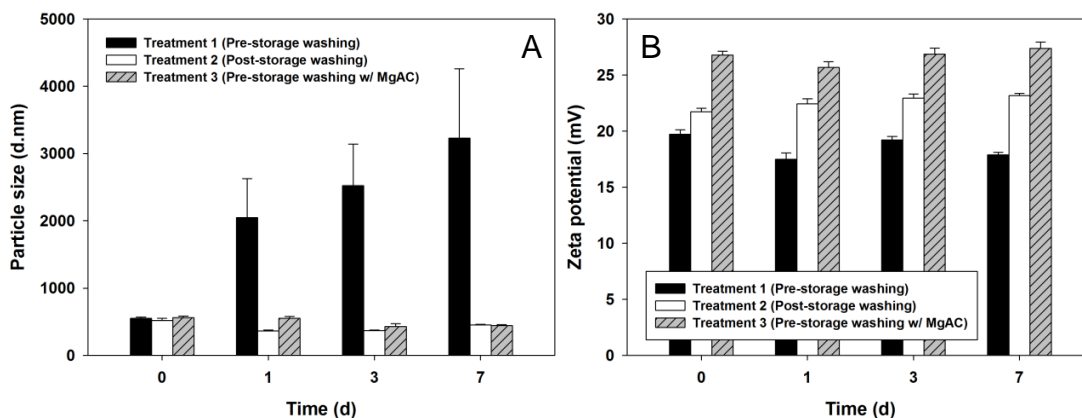
### 3.3.1 Properties of MgAC coated nZVI

Based on the findings from Paper **I**, where the optimal MgAC:Fe ratio was 7.5:1, the same conditions were employed for the investigation into the washing and aging of the particles. Therefore, the measured properties were near identical to those previously stated in Section 3.1 for the particles with said ratio.

### 3.3.2 Effect of washing strategies on nZVI colloidal stability

Three treatment strategies were employed, as previously stated, and each aged for up to seven days. Initial particle sizes, measured by DLS, for all three treatments were nearly identical, at 544 ± 17 nm, and those values remained relatively stable throughout the aging test for both Treatment 2 and 3. However, a significant increase occurred with Treatment 1, where the particle size gradually grew to 3228 ± 1031 nm (Figure 15A). With this method, excess MgAC was removed at the start of the aging process, and therefore much of the protective coating was missing to prevent particle aggregation throughout the aging process. Both of the other treatments retained their residual MgAC coating to maintain that protection from aggregation. The effect that the MgAC has on stability was further confirmed using DLS to measure the zeta potential (Figure 15B). Although, little change was observed for each treatment throughout the aging process, there was however, an obvious trend between each treatment. Treatment 1, with less remaining MgAC had the lowest overall zeta potential at +17.5 to +19.7 mV, with Treatment 2 at +21.7 to +23.2 mV, and Treatment 3 at +25.7 to +27.4 mV. Treatment 2 did not wash off the residual MgAC until after again to maintain a higher value, and Treatment 3 (washed with MgAC) most likely added more MgAC to further increase the zeta potential. This correlation between particle stability and stabilizer present with respect to washing was similarly observed before when using polymer coatings [63].

**Figure 15.** Stability properties of MgAC coated nZVI throughout the aging process, in terms of particle size (A) and zeta potential (B). Paper **III**.

The notion of the effect that MgAC has on the properties and stability of nZVI brought about by the data obtained from DLS was subsequently eluci-dated by morphological observation using TEM (Figure 16). Pre-storage washed particles wish $NaHCO_3$ (Treatment 1, Figure 16A) and MgAC (Treatment 3, Figure 16B) initially do not appear much different, other than the appearance of excess MgAC in proximity to the nZVI itself. On the other hand, after just one day of aging, Treatment 1 particles clearly have much more of a sheet-like structure, where Treatments 2 and 3 particles have re-tained their spherical morphology (Figure 16C,D,E).
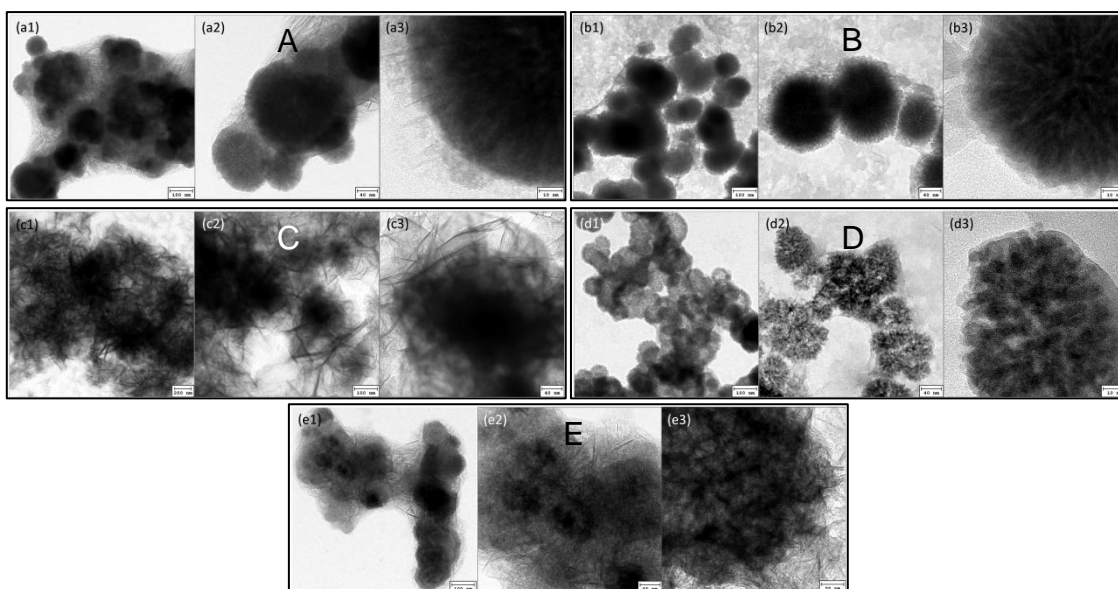


**Figure 16.** TEM images demonstrating MgAC coated nZVI morphology of as-prepared fresh Treatment 1 (A); as-prepared fresh Treatment 3 (B); 1 day aged Treatment 1 (C); 1 day aged Treatment 2 (D); and 1 day aged Treatment 3 (E). Paper **III**.

### 3.3.3 Effect of washing strategies on nZVI reactivity

Two different analyses were undertaken to assess the reactivity of the different washing and storage strategies, and compared with the stabilization/optical absorption test described in Section 3.1.2. The first analysis was a measurement of reactive iron by $H_2$ gas production by acid digestion [120]. In the sample matrix, $Fe^0$ is the only component present capable of producing $H_2$ in the presence of a strong acid [121].

$$2Fe^0 + 6H^+ \rightarrow 2Fe^{3+} + 3H_2 \uparrow \qquad [11]$$
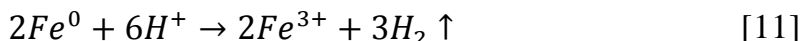
The second analysis was the measurement of nitrate reduction capacity as described in Section 3.1.3.

For each treatment method, all three of these parameters decreased over time, up to one week of aging; upon which the reactivity and measured data had begun to reach steady-state (Figure 17). Although, the reactivity of Treatment 2 dropped substantially, after just one day losing 58% of optical absorbance, 90% reactive iron content, and 70% of nitrate reduction capacity. The other two treatments (both pre-storage washing) both exhibited much slower losses in each of the categories, therefore exhibiting greater resistance to oxidation of nZVI than the post-storage washing.
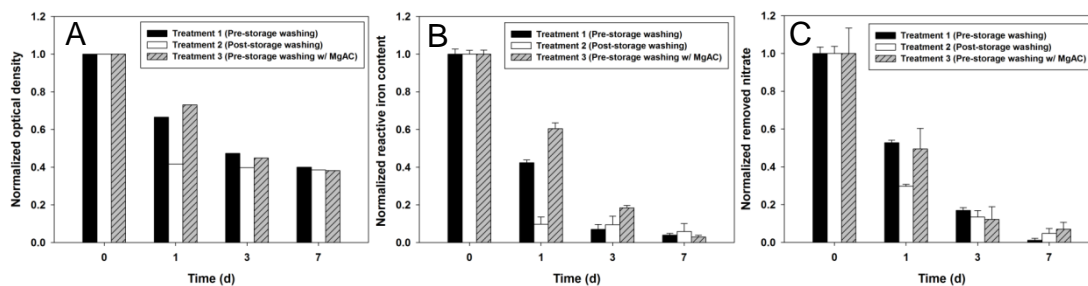


**Figure 17.** Normalized properties for the reactivity of MgAC coated nZVI throughout the aging process, in terms of stability/optical absorption (A); reactive iron content (B); and nitrate reduction capacity (C). Paper **III**.

## 3.4 Effect of washing and storage strategies on nZVI

Paper **III** (Section 3.3) deduced a more appropriate strategy for synthesizing and storing MgAC coated nZVI that kept the particle sizes low, the zeta potentials high, and delayed reactivity loss. Paper **IV** reverted back to working with bare uncoated nZVI and applied different washing and storage strategies to assess the effects they would have on the core-shell structure and reactivity

of nZVI. Efficient and effective formation of ZVI is the most important factor in the process of making and applying nZVI, however, the post-synthesis conditions are also crucial facets for the reactivity and longevity of nZVI particles. Oxidation and surface passivation of nZVI is impossible to avoid, as it is an inherent effect of the interaction between the iron and air or the aqueous media in which it is stored. However, mitigation strategies can be employed throughout the synthesis, separation and drying (if in powder form), and storage phases. For example, washing of nZVI with certain agents such as that in Paper **III** discussed in the previous section can remove excess reagents and residuals formed during the synthesis that can passivate the surface. As it is that $NaBH_4$ is the means by which the nZVI is originally created, the idea is to investigate how it can affect the properties and reactivity of nZVI during the post-synthesis, pre-application phase. Paper **IV** investigated the effects of washing nZVI with MilliQ water and $NaBH_4$ solution would have on various properties of the material, with the goal to gain a better insight into the mechanisms taking place after nZVI synthesis. For this, three treatment schemes were applied to nZVI in post-synthesis: Treatment 1, leaving nZVI as is and un-washed; Treatment 2, washing with MilliQ water; and Treatment 3, washing with $NaBH_4$ solution.

### 3.4.1 Dynamics of nZVI core-shell structure

The primary tool used to monitor the change in core-shell structure was X-ray photoelectron spectroscopy (XPS), so that the elemental composition could be monitored over time during the storage process. More specifically, the iron and oxygen speciation was investigated. Immediately after synthesis, surface iron content was 13.3, 14.9, and 18.3% for Treatment 1, 2, and 3, respectively. Concurrently, the surface oxygen content was 52.1, 57.1, and 51.3% for Treatment 1, 2, and 3, respectively. In this light, it appears that the effect of $NaBH_4$ is that the reducing environment is sustained and that a higher $Fe^0$ content can remain. At the same time, the extra washing with water adds more oxidant to the sample, increasing oxidation on the surface. Furthermore, when looking at the oxide shell during the storage process, valuable insight can be gained by deducing the variation in oxide species, specifically the ratio between $OH^-$ and $O_2^-$ species (Figure 18A). The $OH^-$ fraction increased substantially in Treatment 2 after one day of storage, but then slowly decreased for the remainder of storage time. While the other two treatments had relatively stable ratios throughout. This layer of hydroxides developing is most likely due to a complex layer-forming mechanism of oxida-

tion, re-crystallization, and precipitation [122]. The other treatments maintained a much higher oxide ratio, most likely due to the dominance of a passivation layer build-up more consistent with a simple oxidation mechanism (Eqs. 1,3).
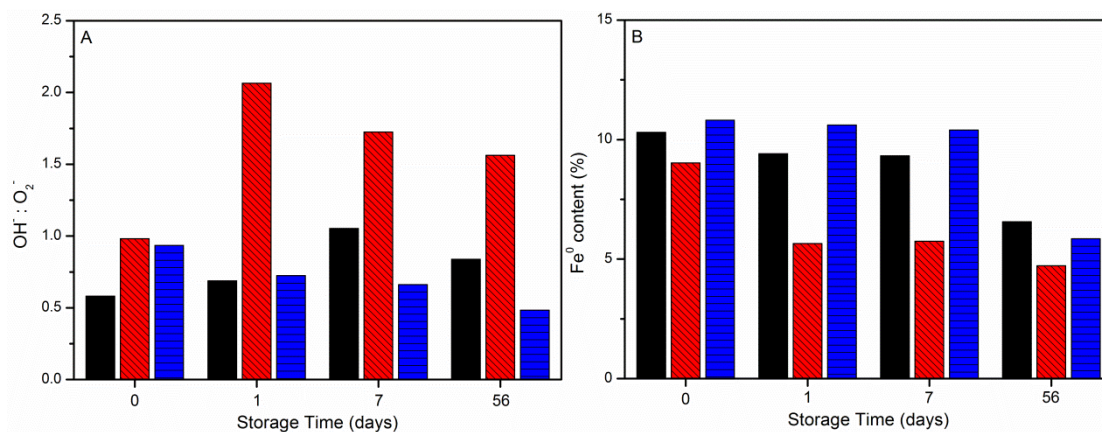


**Figure 18.** Core-shell structure evolution throughout the storage time. Ratio of $OH^-$ to $O_2^-$ on the nZVI surface (A) and $Fe^0$ content on the nZVI surface, for Treatment 1 (solid black bars), Treatment 2 (diagonal-striped red bars), and Treatment 3 (striped blue bars). Paper **IV**.

While the iron hydroxide/oxide layer is important to investigate, it is only half the equation in the core-shell structure, the other half being the $Fe^0$ content found on the surface (Figure 18B). Treatments 1 and 3 do not yield any significant change throughout the first week of storage, while the $Fe^0$ content decreases significantly by the first day, a clear indication of oxidation. The main difference between these two patterns is that in Treatment 1 and 3, the $NaBH_4$ reductant remains in solution with the nZVI. Moreover, Treatment 3 maintains a higher $Fe^0$ content compared to Treatment 1, indicating added protection of the $Fe^0$ by the presence of $NaBH_4$.

## 3.4.2 Dynamics of nZVI reactivity

Elucidation of the physical nature of the core-shell structure during storage is valuable, but how it relates to the produced reactivity is necessary for eventual application. Reactivity was assessed following the dye decolorization method (Paper **II**) in Section 3.2.3. However, the focus of the analysis was applied to the reduction product of aniline, rather than the removal of the dye itself. Figure 19 illustrates the change in reactivity of each treatment scheme over the course of the storage time.
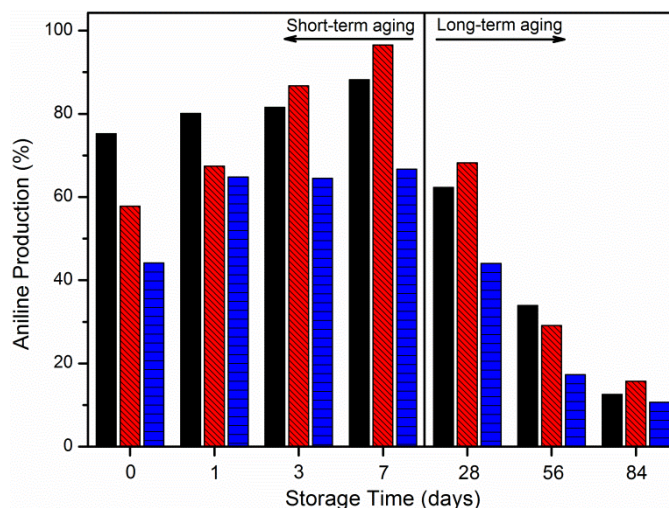
**Figure 19.** Aniline production as a result of azo dye degradation by nZVI throughout the storage period for Treatment 1 (black), Treatment 2 (red), and Treatment 3 (blue).

Somewhat unexpectedly, Treatments 1 and 2 exhibited higher reactivity than Treatment 3, meaning that the role of $NaBH_4$ in the storage process towards reactivity was not as drastic as originally thought. Interestingly, there was an increase in reactivity during the first seven days of storage. This is most likely explained by the depassivation of the formed oxide layer, which includes the breakdown of the iron oxide shell. Also, it is clear that this shell breakdown process is very prominent in the water-washed sample (Treatment 2), and not so with the other two treatments. When compared with the $Fe^0$ surface content (Figure 18B), it is evident that this depassivation is associated with the consumption of the $Fe^0$ core and the formation of a dynamic oxide layer, equating to higher reactivity. Adding these phenomena together, it appears that a higher reactivity of nZVI is not entirely dependent on a higher content of $Fe^0$, but rather a different mechanism involving the nature of the core-shell structure. Presumably, based on a simultaneous look at Figures 18 and 19, the reactivity is highly dependent on the hydroxide content found in the particle shell. This dependence on hydroxide content can be ratiocinated by the fact that hydroxides can have a higher capacity for electron transfer. Previous work postulated that the formation of iron oxides on the surface of nZVI act as a passivating layer, while iron hydroxide formation will act as a non-passivating layer [122].

One final test was done during the storage period, and that was a re-washing of the particles after one week with water. And, although much of the reactivity was lost during the storage process, nearly all of the initial reactivity could be recovered with Treatments 1 and 3 when re-washing after one week

37

with water. Similarly, when re-washing with water after 84 days of storage, some of the reactivity was recovered in Treatments 1 and 3, but not a significant portion. No reactivity was recovered with re-washing samples of Treatment 2.

In summary, it appears that the characteristics of the core-shell structure are extremely important for the reactivity of the nZVI particle. In particular, the presence of hydroxide groups compared to oxide groups in the shell structure, which is more important than the total $Fe^0$ content. This translated well to the reactivity of the particles when degrading the azo dye. Additionally, although the reactivity of Treatment 2 (washing with MilliQ water) was the highest during the short-term storage process, the reactivity was not able to be recovered when re-washing. The best strategy appears to be storing the nZVI unwashed or washed with $NaBH_4$ for up to one week, followed by a re-washing step just before application.

# 4 Assay for reactivity quantification and real-world application

Work package one in Chapter 3 consisted of an in-depth look into using new materials to stabilize nZVI colloids and improve their reactivity, as well as investigating better ways of post-synthesis handling of nZVI for application. Various analytics were also employed to assess the reactivity of nZVI during the first work package, including monitoring nitrate decrease with IC, measuring $H_2$ gas production with GC, and monitoring azo dye decolorization with UV-Vis combined with aniline production with HPLC. All of these techniques have particular limitations when quantifying nZVI reactivity, and none address the ability of nZVI to dehalogenate a halogenated organic compound. It was in the second work package, detailed here in Chapter 4 with Paper **V**, Paper **VI**, and Paper **VII**, that a new means for assessing nZVI was explored. As nZVI grows in popularity in both commercial production and as the focus of research in academia, the types of nZVI in terms of production method (i.e. chemical reduction, ball-milling, etc.), size, stabilizing agent, etc. have resulted and will result in more and more versions available. And, to date, there is not an adequate method to directly compare two or more of these nZVIs, so, an ideal solution would be to establish a universal testing procedure [50]. Several options have been put forward in the past, including measuring the oxidation/reduction potential [123] or measuring the evolution of $H_2$ gas production by the hydrolysis of water during corrosion [124–128] or measuring the parent compound and subsequent degradation product [121,129]. However, all the options to date don't offer a simple, quick, and user-friendly test to measure the reactivity of nZVI. Because of this, the second work package of this PhD project aimed to establish a simple method to universally assess nZVI reactivity by way of a colorimetric assay, needing only a limited supply of chemicals and a standard spectrophotometer.

## 4.1 Simple colorimetric assay for dehalogenation by nZVI

One of the more recalcitrant and difficult to remediate classes of water contaminants is that of halogenated organics, such as trichloroethylene (TCE), polychlorinated biphenyls (PCBs), and chlorophenols. And, research focus of late has seen a lot of attention applied to the reduction of chlorophenols by

ZVI [120,130–133], as it is that chlorophenols can be reduced to simply phenol. Additionally, the reaction of phenol and monochloramine, with a suitable catalyst, to produce a blue color, is well understood and known quite plainly as the indophenol reaction [134]. This indophenol reaction is summarized below in Scheme 2 [135], where each step is reacted to completion by ensuring excess reagents of $NH_3$, $NH_2Cl$, and phenolate for the first, second, and third step, respectively.
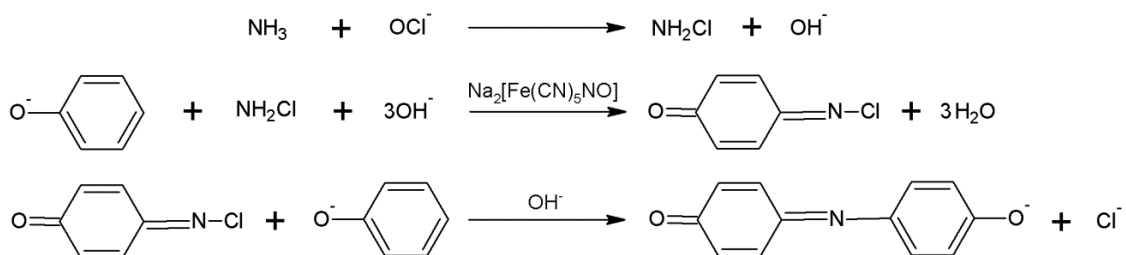


**Scheme 2.** Simplified reaction scheme of the modified indophenol reaction (adapted from Harfmann *et al.* (1989) [135].

For this reason, it was decided to use the dehalogenation of 4-chlorophenol to phenol by nZVI to create the indophenol reaction and produce a colorimetric assay for nZVI reactivity standardization.

## 4.1.1 Sensitivity and selectivity of color assay for phenol detection

In order to confirm the validity of the colorimetric reaction, the assay was tested for detection of both 4-chlorophenol and phenol, in order to make sure that there was not any interference from the primary reactant with nZVI (i.e. 4-chlorophenol). As expected, there was only minimal color produced in the indophenol reaction when 4-chlorophenol was substituted for phenol (Figure 20A). On the contrary, a clear spectral pattern was produced when using phenol for the indophenol reaction (Figure 20B).
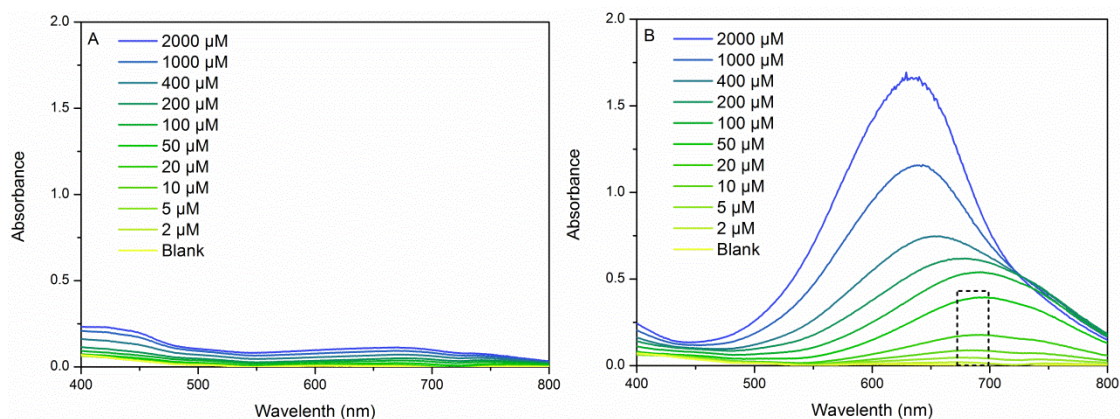
**Figure 20.** Spectra evolution using different concentrations of 4-chlorophenol (A) and phenol (B), after the indophenol reaction with $NH_2Cl$. Paper **V**.

At lower phenol concentrations of <100 µM, the peak absorbance was consistent at $680 \pm 7$ nm, but as the concentration was increased from 100 – 400 µM, the peak absorbance gradually shifted to shorter wavelengths, until it stabilized at $640 \pm 2$ nm at concentrations above 400 µM. As a result of this phenomenon, the ideal concentration range for phenol analysis was determined to be 0 – 50 µM.

Further analysis of the selectivity of the assay towards phenol over 4-chlorophenol was evaluated by mixing equal concentrations (0, 5, 10, 25, and 50 µM) of phenol and 4-chlorophenol and monitoring the difference in color produced (i.e. absorbance) from the indophenol reaction at 680 nm. With a full factorial design, the addition of 4-chlorophenol to phenol did not result in positive correlation towards color production. The net result being that the suggested colorimetric reaction does, in fact, establish selectivity towards phenol over 4-chlorophenol.

## 4.1.2 Reducing reactivity of nZVI for reduction of 4-chlorophenol

For this color assay to work, the nZVI must be able to react sufficiently enough with 4-chlorophenol to produce phenol. Initially, bare nZVI was tested under varying conditions, in buffered and un-buffered conditions, and in varying pH conditions of 3, 5, and 7. However, none of these situations produced a detectable amount of phenol. This gave rise to the notion of incorporating a secondary metal to form a bimetallic nZVI particle, as it has been reported in the past that bimetallic nZVI particles have much increased reactivity towards 4-chlorophenol [130]. Secondary metals used to create bimetallic particles with nZVI have been those commonly referred to as "noble metals," such as copper, nickel, silver, palladium, or platinum [136]. These metals enhance the dehalogenation activity through a combination of galvanic and catalytic effects to increase the rate of reduction. Bimetallic particles of Pd-nZVI have, for example, been documented to enhance the reactivity towards dehalogenation of organic contaminants by way of catalytic hydrogenation [137]. At the same time, nickel has also been documented to have a catalytic effect towards 1,1,1-trichloroethane reduction [137]. However, the price of palladium and platinum can be two or three orders of magnitude higher than less precious metals like copper or nickel; and, the goal of this assay is to not only be simple, but also relatively inexpensive. Therefore,

41

nickel and copper were chosen to assess the dehalogenation reactivity. The results of 4-chlorophenol reduction to phenol are summarized in Figure 21A.
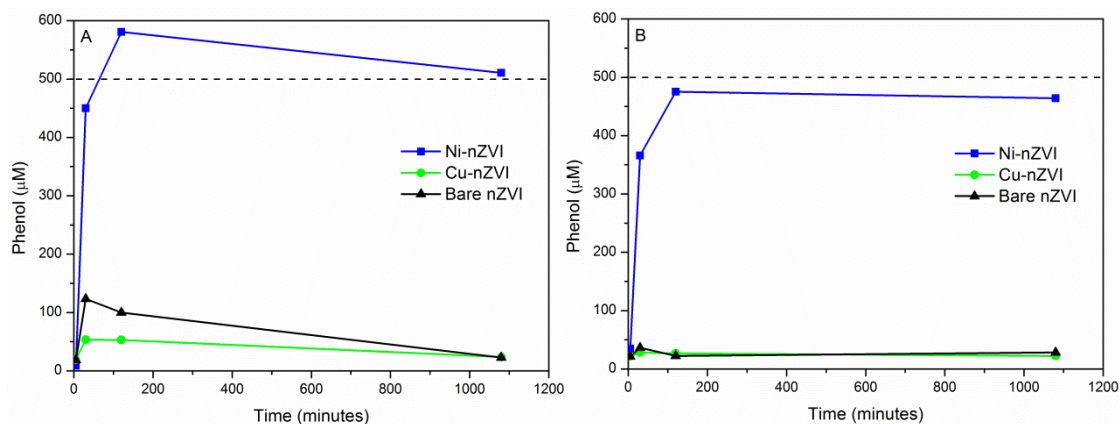


**Figure 21.** Secondary metal effect on the reduction of 4-chlorophenol by bare and bimetallic nZVI without sample pre-treatment (A) and with sample pre-treatment (B), (dotted line indicates the theoretical yield). Paper **V**.

Adding copper to the nZVI had a negligible effect on the reduction capacity of the bimetallic particle; however, adding nickel resulted in the capacity of the bimetallic particle to reduce 4-chlorophenol. Although, the detected phenol concentrations were above the theoretical maximum, which was determined to be interference from a combination of pH variance [133], precipitate formation, and the appearance of a strong yellow color upon addition of the reagents. Consequently, further optimization was needed for the assay to not give false positives.

## 4.1.3 Establishment of a sample pre-treatment regime

Further investigation was conducted, to determine the exact cause and to then avoid the false positives from the interference of possible pH variance and residual ions (described in Section 4.1.2). When conducted under different pH conditions (2.3 – 11), the color development was extremely stable. So, as long as there is enough alkali in the system, the pH effect is minimal; additionally, Searle (1984) reported that the optimum pH range for the indophenol reaction was 10.4 – 13.1 [132]. So, the greatest cause for error proved to be the effect of residual ions in solution, and in particular ferric ($Fe^{3+}$) iron ions. When measuring the absorbance and adding various concentrations of iron in solution, the peak absorbance at 680 nm was stable. However, after adding 100 mg/L of iron, the interference in spectra drastically increased; which correlates to related work investigating the interference of metals on the indo-

42

phenol reaction [138]. This effect was combatted by the addition of $Na_2CO_3$ as a pre-treatment technique. The addition of carbonate solution changed the color of the solution from a slightly yellow-green color to a dark green-blue color, indicating that an iron carbonate precipitate had formed, which subsequently falls out of solution, leaving a clear supernatant for use in the assay.

# 4.2 Colorimetric assay optimization

Building on the first part of the work package, Paper **V**, the second phase in Paper **VI** aimed to improve the developed color assay by targeting a wider range of contaminants and miniaturizing the assay into a multi-well microplate system. Extending applicability outside of solely 4-chlorophenol creates an assay that is more robust and diverse in nature. Miniaturization of the assay into a 96-well microplate allows for analysis of several compounds with several replicates in the same batch, reducing sample preparation time and delays in results collection. It is believed that the reduction kinetics and capacity is unique to individual substrates in this reaction, based on the involved redox reaction and particular chemical bond. All-in-all, this aims to provide for a graduated characterization method for reducing activity by nZVI particles.

## 4.2.1 Miniaturization and target compound expansion

An extended range of target compounds was investigated with the same regime of reagents, to branch out from just 4-chlorophenol to also include nitrate, nitrobenzene, and two other halophenols, 4-bromophenol and 4-iodophenol. During the reaction with nZVI, it is expected that nitrate will reduce to ammonium (Eq. 10), nitrobenzene will reduce to aniline (Eq. 12), and the p-halophenols will all dehalogenate to phenol.

$$C_6H_5NO_2 + 3Fe^0 + 6H^+ \rightarrow C_6H_5NH_2 + 3Fe^{2+} + 2H_2O \qquad [12]$$
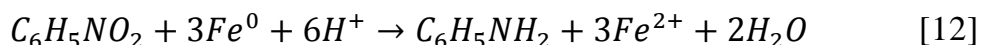
In this manner, the reactivity and effectiveness of the color assay can be further elucidated. The indophenol reaction is highly dependent on ammonium (Scheme 2), and nZVI is well known to reduce nitrate to ammonium (Eq. 4) [90,139], making nitrate an ideal contaminant for the color assay. Additionally, for the chromophore in the indophenol reaction to appear, aniline will act with the same mechanism as phenol. Therefore, by altering the limiting

reactant (Scheme 2) between ammonium, phenol, and aniline, the color assay can be adapted for a wider range of compounds.

Miniaturization of the assay into a 96-well microplate offers the ability to get rapid results from a wide range of samples and standards, avoiding lengthy analysis procedures and analytics. By simply minimizing the reagent volume by an order of magnitude, so that the reaction could take place in the available well volume of 400 µL, assay miniaturization was easily achieved.

Reaction conditions that produce the strongest color are the most ideal for any colorimetric reaction, that way assay set-up and reagent concentrations can be optimized and applied. Optimization consisted of varying the active chlorine concentration, ammonium concentration, and reaction time for both phenol and aniline assays; measuring the peak absorbance (Paper **V**) at 680 nm. Note: ammonium assay optimization was not considered, as it is standardized per American Water Works Association standard 4500-$NH_3$-D. Calibrations included identifying the limit of detection (LOD) and limit of quantification (LOQ). Final summarized values are outlined in Table 2.

**Table 2.** Summary of analytical methods using a 96-well microplate for reaction product determination after optimization. Note, ammonium: 0-143 µM = 0-2 mg-$NH_4^+$-N/L; Reagent A = NaOCl + NaOH; Reagent B = phenol + sodium nitroprusside; Reagent C = $NH_4Cl$ + sodium nitroprusside. Paper **VI**.

| | Ammonium | Phenol | Aniline |
|---|---|---|---|
| Sample volume (µL) | 230 | 230 | 230 |
| Reagents | A + B | A + C | A + C |
| Concentration range for analysis (µM) | 0 – 143 | 0 – 50 | 0 – 75 |
| LOD (µM) | 2.9 | 0.3 | 0.5 |
| LOQ (µM) | 9.6 | 1.0 | 1.7 |
| Reaction time (hours) | 2.0 | 2.0 | 2.0 |

Optimization of the phenol analysis gave a greatest absorbance ($\lambda_{max}$ = 680 nm) using 0.02 % active chlorine in Reagent A and 100 mg-$NH_4^+$-N/L in Reagent C (Figure 22A), yielding nominal concentrations in the sample mixture of 9.3 mg/L of active chlorine and 4 mg-$NH_4^+$-N/L. It is evident that excess NaOCl will decrease the absorbance and that more ammonium is needed to reach maximum absorbance with increasing NaOCl; color development is highly dependent on the stoichiometry. Optimization of the aniline analysis gave a greatest absorbance ($\lambda_{max}$ = 680 nm) using the same concentrations of Reagents A and C (Figure 22B) as with the phenol analysis. (Note: a parallel

experiment was conducted with nitrobenzene present, and absorbances at 680 nm were unchanged, regardless of nitrobenzene). When measured over time, phenol values increased up to 2 hours and were stable until 4 hours; aniline values increased up to 1 hour and remained stable. Therefore, 2 hours was chosen as the standard time for the assay, having the advantage that phenol and aniline can be measured simultaneously.
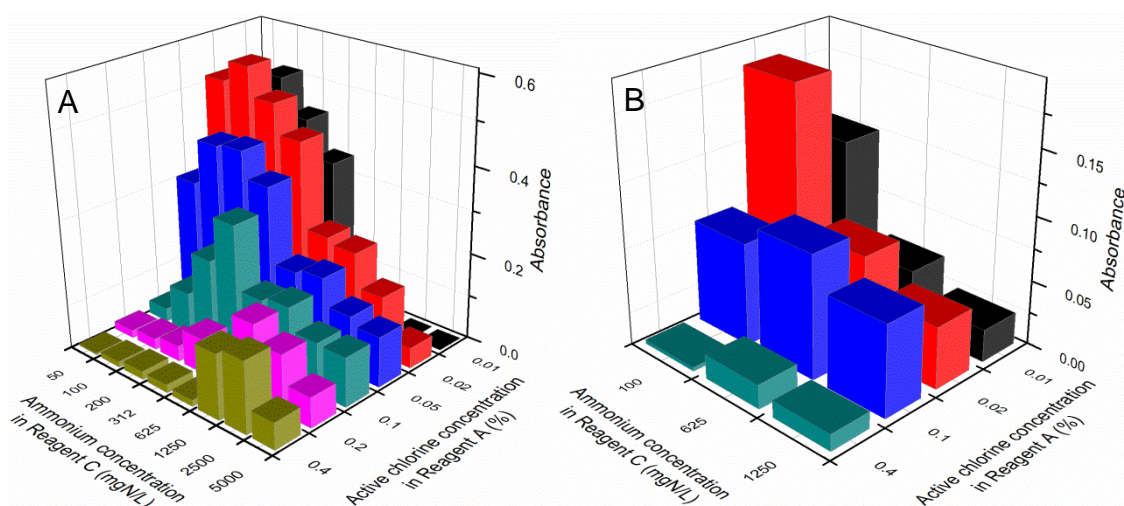


**Figure 22.** Optimization of reagent concentration on color development for phenol (A) and aniline (B). Note that 50 μM of each product was applied and the absorbance was measured after 2 hours of reaction time. Paper **VI.**

### 4.2.2 Graduated characterization of reducing activity

Following optimization of the color assay for the detection of ammonium, phenol, and aniline; a range of reducible compounds was applied after reaction with bare nZVI and bimetallic 5% nickel nZVI (Ni-nZVI), Paper **V**. The assay was first applied using reduction products stemming from the reaction with bare nZVI particles, i.e. ammonium from nitrate reduction, aniline from nitrobenzene reduction, and phenol from p-halophenol dehalogenation (Figure 23A). Aniline production was extremely fast ($k = 17.9$ h$^{-1}$), ammonium production was observed ($k = 2.65$ h$^{-1}$), and phenol production was non-existent from any of the halophenols. This result was identical to that observed in Paper **V** when attempting to dehalogenate 4-chlorophenol with bare nZVI.

In Paper **V**, the addition of nickel to nZVI dramatically increased the reactivity of the particle (Figure 23B). By adding 5% Ni (wt:wt), the kinetics of Ni-nZVI were much faster for aniline ($k = 93.4$ h$^{-1}$) and ammonium ($k = 10.3$ h$^{-1}$), while phenol was then detected for the p-halophenols. Phenol production

rate constants for 4-iodophenol, 4-bromophenol, and 4-chlorophenol were 14.9, 10.1, and 5.72 h$^{-1}$, respectively. Addition of a secondary metal promotes iron corrosion and the higher standard redox potential of nickel develops a galvanic cell in which the corrosion is accelerated [128].
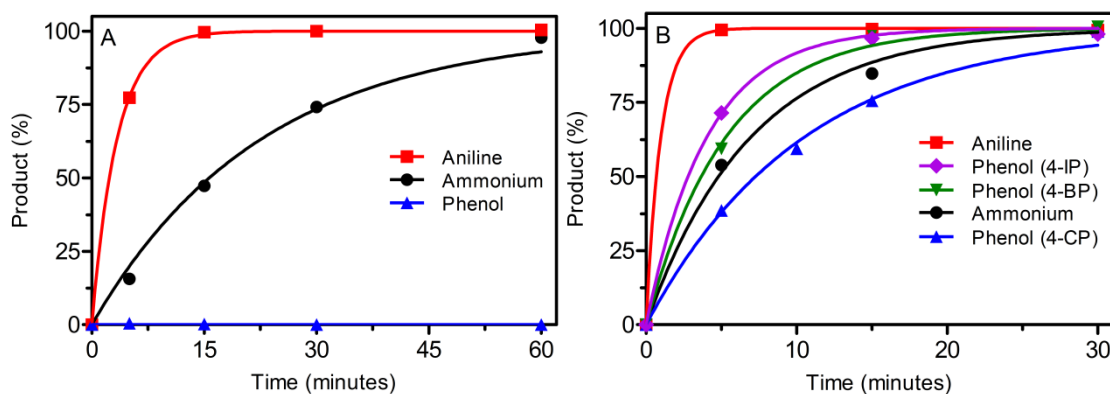


**Figure 23.** Generation of reaction products by reaction with bare nZVI (A) and bimetallic 5% Ni-nZVI (B). Note: that the iron concentration was constant at 2 g/L, and curves were fitted by pseudo first-order kinetics.

This dramatic difference in reactivity when nickel is added to nZVI is a result of the production of reactive hydrogen on the nickel surface, followed by dehalogenation and hydrogenation by the reactive hydrogen [130]. If not immediately apparent, the difference in dehalogenation of the p-halophenols was ordered according to position on the periodic table and the average bond enthalpies of the carbon-halogen bond. Average bond enthalpies of C-I, C-Br, and C-Cl are 240, 276, and 339 KJ/mol, respectively.

To emphasize its universal application and to determine the reactivity of an unknown nZVI sample, the colorimetric assay was employed using a commercially available product. Detailed in Paper **VI**, commercial nZVI was inconsequential towards producing any of the reduction products (i.e. ammonium, aniline, or phenol). However, when applying commercial Ni-nZVI (2 g/L), limited reactivity was achieved when reducing nitrate to ammonium and nitrobenzene to aniline, but no reactivity was achieved when applied to p-halophenols, even at a higher concentration of 10 g/L. The role of nickel, in this case, is most likely solely an accelerant of nZVI oxidation, rather than a producer of reactive hydrogen. Not surprisingly, it appears that commercial nZVI is much less reactive than lab-synthesized nZVI. Making the work and findings produced in Paper **III** all the more relevant to the real-world application of nZVI.

To summarize the graduated characterization results, nitrate and nitrobenzene can be applied with this colorimetric assay to assess the reduction reactivity of bare nZVI; while p-halophenols can be applied with this colorimetric assay to assess the catalytic reactivity of bimetallic nZVI, specifically Ni-nZVI.

## 4.2.3 Effect of secondary metal concentration

The preliminary assay in Paper **V** and the results thus far in Paper **VI** used a 5% nickel (wt:wt) concentration. This was done primarily to ensure there was an overabundance of the secondary metal to create the catalytic reaction. Although reactivity is paramount, other factors must be considered, such as the cost of the secondary metal and the possible release of the secondary metal into receiving waters. Therefore, a necessary facet of the assay to optimize is that of the secondary metal concentration.

Effects of nickel content with nZVI towards the suggested assay were determined by varying nickel concentrations from $0.01 - 5\%$ (Figure 24A). Concentrations higher than 5% were not considered, due to successful reaction kinetics previously achieved. Additionally, only 4-chlorophenol was tested, as it has been established to be the most difficult p-halophenol to dehalogenate. When applied, increasing the nickel content consequently increased the dehalogenation effect, up to a point. After a nickel concentration of 1%, the return in reactivity becomes very minimal (Figure 24B), meaning the Ni:Fe ratio is an important factor to consider when maximizing dehalogenation. It is surmised that as the nickel loading becomes too great, the contact area between the nickel and the iron decreases and results in a counterproductive relationship towards reactive hydrogen production, electron transport, catalytic sites, and galvanic cell formation. This is not unlike similar findings when using copper as a secondary metal with nZVI for dechlorination [140] or nitrophenol reduction [141].
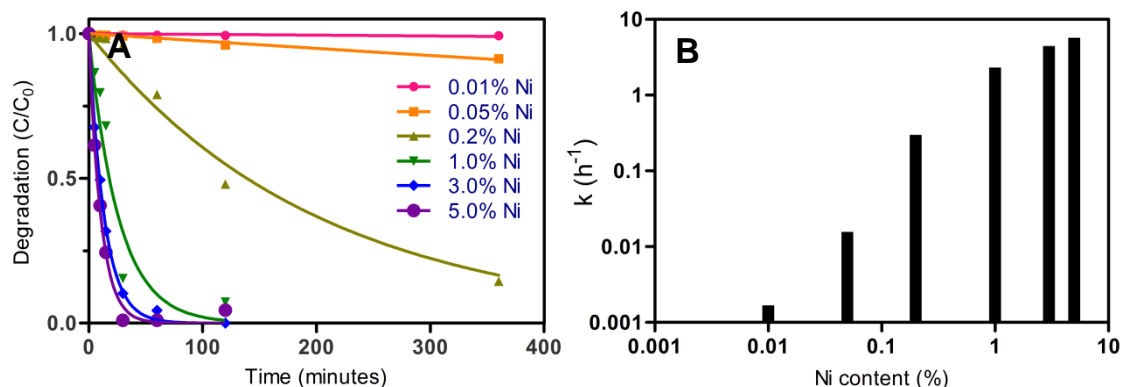
**Figure 24.** Effect of nickel content on 4-chlorophenol reduction by nZVI. Degradation of 4-chlorophenol, with respect to time (A) and derived rate constants by curve fitting, plotted over log10-scale (B). Note that the curves are fitted with pseudo first-order kinetics. Paper **VI**.

Given the combined data and optimizations found in both Paper **V** and Paper **VI**, an ultimate suggestion can be presented for the colorimetric assay procedure (Figure 25). The entirety of this includes first the preliminary batch test with a chosen nZVI material and its reaction with either nitrate, nitrobenzene, or a p-halophenol, followed by specific reagent addition depending on the analyte, and finally the colorimetric reaction that can be conducted in a 96-well microplate. Careful selection of bare nZVI or bimetallic nZVI, as well as the particular compound to be reduced, must be made.
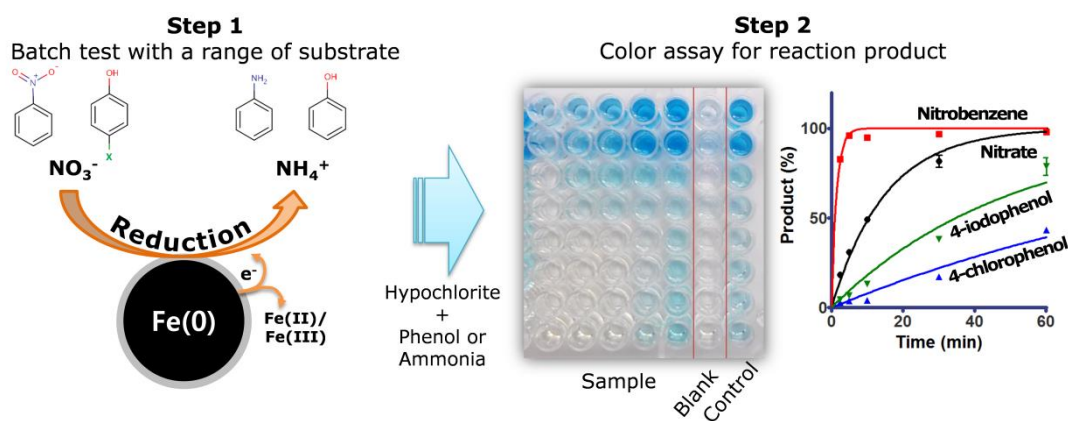


**Figure 25.** Schematic of the suggested reactivity assay procedure. Paper **VI**.

## 4.3 Color assay comparison with halogenated organic degradation

Paper **VI** provided an applicable colorimetric assay to analyze the reduction products of a variety of contaminants by nZVI and bimetallic Ni-nZVI. To validate the method even further, it was applied to treat a selection of typically difficult to dehalogenate compounds that are commonly found in water sources, trichloroethylene (TCE), 1,1,1-trichloroethane (TCA), and atrazine; Paper **VII**. This is especially important, as it is that treatment of many halogenated organics has been often mediocre at best [50,142]. Moreover, analysis of these compounds often requires length time-consuming analytics using sophisticated machinery, such as a purge-and-trap device coupled with gas chromatography – mass spectrometry (GC-MS). Therefore, applying the developed colorimetric assay as a precursory technique, to select if a nZVI material is a suitable candidate for treatment of such halogenated compounds, can potentially save valuable time and resources.

### 4.3.1 Termination of nZVI reactivity

Often times, especially when working in the field, measurements cannot immediately take place. This lag in the time from sample taking to sample measurement can potentially change the constituents present in a given sample, possibly from various chemical oxidation or reduction processes, or even from biological processes. Depending on the situation, one cannot be entirely certain that all affecting mechanisms are rendered inert, even if the sample is filtered for example. To make the analysis of nZVI reactivity more user-friendly, an appropriate technique to terminate the reactivity in the sample is ideal; allowing for analysis at the technician's convenience.

The first workload presented in Paper **VII** outlines the development of a nZVI reactivity termination regime. It is known, based on Paper **V** and Paper **VI**, that a concentration of 5% Ni with nZVI is more than enough to dehalogenate certain chlorinated organics, therefore all reactivity termination tests were conducted with this Ni:Fe ratio. Furthermore, a concentration of 300 µg/L of TCE was assessed, as that is slightly higher than reports that approximately 250 µg/L of TCE have been detected in Danish groundwater and are subsequently realistic concentrations found in the environment [143]. The initial attempt at terminating the reactivity of Ni-nZVI with TCE assumed that all that was necessary was to precipitate particles out of solution so that

the remaining supernatant was free of reactive iron. As zero-valent iron reduces different contaminants, itself becomes oxidized from contaminant reduction, water, and the dissolved oxygen in the water. In this process, ferrous ($Fe^{2+}$) is formed. Carbonate ($CO_3^{2-}$) is a well-known precipitant, and is commonly applied to ferrous iron for this purpose; the result is a rapidly settled green precipitate, which is outlined in Eqs. 13 and 14 (using water as the oxidizer) [144].

$$Fe^0 + 2H_2O \rightarrow Fe^{2+} + H_2 \uparrow + 2OH^- \qquad [13]$$
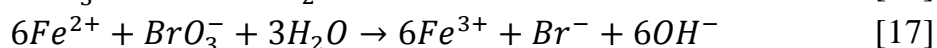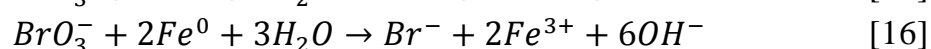$$Fe^{2+} + CO_3^{2-} \rightarrow FeCO_3(s) \qquad [14]$$
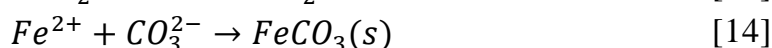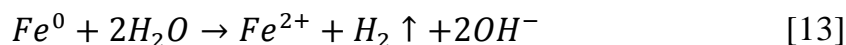
The assumption was that any ionic ferrous iron or remaining exposed $Fe^0$ would form $FeCO_3$ or $Fe(OH)_2$ as particulates or as a shell around nZVI that would act as a passivation layer [145]. However, when Ni-nZVI (2 g/L; 5%-Ni) was allowed to react with 300 µg/L of TCE solution for 30 minutes, it made nearly no difference whether or not there was an addition of $Na_2CO_3$ added. The most likely explanation is that although there are precipitates and oxide shells being formed, it is not fully passivating the nickel attached to the nZVI, allowing for electron transfer to continue to take place. So, it is apparent that only applying a precipitation and passivation mechanism towards the nZVI is not enough to terminate the reactivity sufficiently.

It is widely known that nitrate can react with nZVI and be reduced to ammonium [139]; and if the kinetics of reduction are compared when assessing nZVI reactivity towards nitrate [139] and 4-chlorophenol (Paper **V**), it is apparent that nitrate reduction is much faster than 4-chlorophenol reduction. Given that information, it is theorized that there would be preferential reactivity with nitrate over the dehalogenation of TCE. In this light, adding an excess of nitrate solution should consume all available/remaining reactive sites on the nZVI and terminate the reactivity, eliminating any subsequent reactivity with TCE. This theory was tested with an experimental design using Ni-nZVI to react with TCE for 30 minutes, with three different reagent schemes. The first, mixing TCE with Ni-nZVI, reacting for 30 minutes, and then adding a combination of $NaNO_3$ and $Na_2CO_3$; the second, mixing TCE with Ni-nZVI, $NaNO_3$, and $Na_2CO_3$, and then reacting for 30 minutes; and the third, only mixing TCE with $NaNO_3$ and $Na_2CO_3$ for 30 minutes. Expectedly, adding the nitrate after the reaction changed nothing and nearly all the TCE was removed, and not adding any Ni-nZVI did not remove any TCE. Whereas, the initial addition of nitrate inhibited roughly 50% of the reduction of TCE, albeit not completely (Figure 26A). While moderately effective,

adding nitrate to terminate the reactivity is not complete, and therefore not an appropriate technique for reactivity termination.

Efficient termination of the reaction using nitrate was unsuccessful; therefore a new technique had to be employed. Although not extensively studied, the reaction of bromate with nZVI has been performed and results indicate very fast reaction kinetics, with the proposed pathway detailed as follows in Eqs. 15-17 [146].

$$BrO_3^- + 3Fe^0 + 3H_2O \rightarrow Br^- + 3Fe^{2+} + 6OH^- \qquad [15]$$
$$BrO_3^- + 2Fe^0 + 3H_2O \rightarrow Br^- + 2Fe^{3+} + 6OH^- \qquad [16]$$
$$6Fe^{2+} + BrO_3^- + 3H_2O \rightarrow 6Fe^{3+} + Br^- + 6OH^- \qquad [17]$$
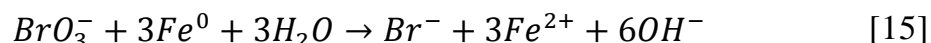
This concept was applied to improve upon the mediocre results obtained from the addition of nitrate. The same experimental design reacting Ni-nZVI with TCE used with nitrate was then tested with bromate, and the results were extremely positive. When using bromate to terminate the reaction, all of the initial TCE was detected after 30 minutes when adding it at the onset of the reaction period (Figure 26B).
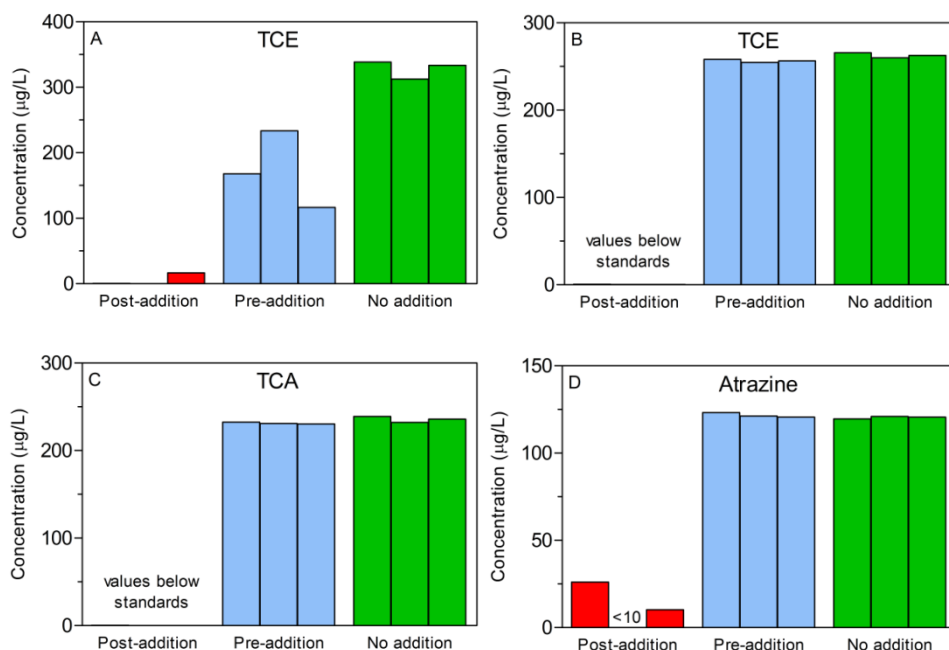


**Figure 26.** Using nitrate, reactivity termination of Ni-nZVI with TCE (A). Using bromate, reactivity termination of Ni-nZVI with TCE (B), TCA (C), and atrazine (D) (measurements in triplicate). Red bars: post-reaction addition of $NO_3/CO_3$ or $BrO_3/CO_3$; blue bars: pre-reaction addition; green bars: no addition. Paper **VII**.

Results were extremely successful with the bromate addition and the ideal outcome was achieved, where by with a simple reagent addition, one can

terminate the sample reactivity and have confidence that no matter when the ultimate analysis for reaction products is performed, it is indicative of the sample matrix at the time of sampling. With this determined, the procedure was subsequently applied to both TCA and atrazine (Figure 26C and 26D). Results for TCA and atrazine were nearly identical to that of TCE, with the exception that Ni-nZVI was not always able to fully degrade the initial atrazine concentration. It can be said with confidence that the work presented here in Paper **VII** has established, for the first time in reported literature, an appropriate method for terminating nZVI particle reactivity.

## 4.3.2 Dehalogenation of TCE, TCA, and atrazine

In Paper **VII**, the first aim to effectively terminate the reaction of nZVI particles was successful, making sample collection and analysis much more convenient for the researcher or technician. The second aim was to evaluate the dehalogenation of three chlorinated contaminants, TCE, TCA, and atrazine, and to establish reaction kinetics when varying the secondary metal content for comparison with the developed colorimetric assay (Paper **V** and Paper **VI**). This was done in a similar manner as performed in Paper **VI**, found in Section 4.2.3, by varying the nickel loading on nZVI and subsequently reacting the particles with each compound over time. Initial tests assessing reactivity termination were conducted with 5% Ni content to ensure complete degradation. So, for the kinetics modeling, different Ni-nZVIs were prepared with nickel contents of 0.1, 0.2, and 0.5%, as that was observed to be the middle range of dehalogenation for 4-chlorophenol (i.e. sufficient dehalogenation before kinetics become too rapid), Figure 27.
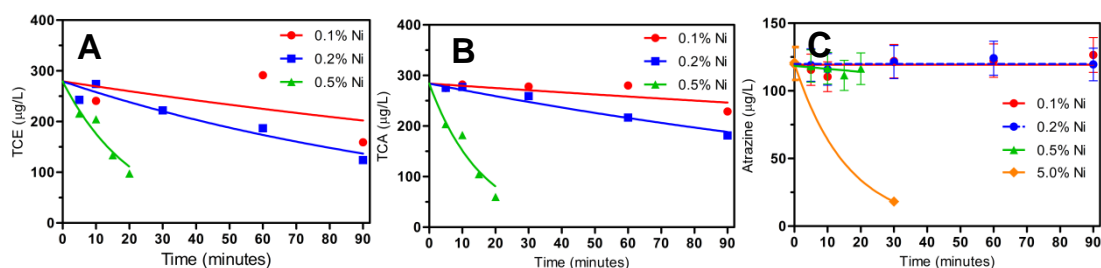


**Figure 27.** Effect of nickel content on TCE (A), TCA (B), and atrazine (C) reduction by nZVI with respect to time. Note that curves are fitted with pseudo first-order kinetics. Paper **VII**.

As expected, the higher concentrations of nickel increased the dehalogenation of each of the three compounds. However, it should be noted that atrazine degradation was very minimal with the three nickel concentrations; therefore,

a final test was performed with 5% nickel content, to estimate the kinetics. Not surprisingly, atrazine was much more difficult to degrade, as this difficulty in remediation correlates to past observed results. After calculating the rate constants using pseudo first-order kinetics, the values were compared with those obtained by similar concentrations of Ni-nZVI particles when dehalogenating 4-chlorophenol (Figure 24B). The comparison of which is outlined in Table 3.

**Table 3.** Effect of nickel content on TCE, TCA, atrazine, and 4-chlorophenol reduction by nZVI. Rate constants obtained by curve fitting using pseudo first-order kinetics. Paper **VII**.

| Nickel (%) | $k\ (h^{-1})$ | | | |
|---|---|---|---|---|
| | TCE | TCA | Atrazine | 4-chlorophenol |
| 0.05 | --- | --- | --- | 0.0157 |
| 0.10 | 0.0992 | 0.0946 | 0.0422 | --- |
| 0.20 | 0.417 | 0.274 | 0.060 | 0.1590 |
| 0.50 | 2.77 | 3.77 | 0.463 | --- |
| 1.00 | --- | --- | --- | 2.31 |

It is evident that the effect of nickel on the reduction capacity of nZVI towards various halogenated compounds is dynamic, which is not surprising in of itself. However, the important finding here is that there is a clear comparison between standard analytical techniques (i.e. GC-MS) and the developed colorimetric assay (Paper **V** and Paper **VI**). Rate constants, although different, are in the same general range of one another. And, it can be said that the developed assay is a very good indicator for dehalogenation by nZVI and that the assay can be used as a universal test for measuring reactivity potential for different nZVI materials.

# 5 Hybridized materials for robust water treatment operation

The first work package (Chapter 3) in this PhD project established new materials (i.e. MgAC and COPs) and synthesis procedures as effective routes for stabilizing the colloids and increasing the reactivity of nZVI. The second work package (Chapter 4) established a simple and efficient characterization procedure to evaluate the reactivity of nZVI based particles. Lastly, the third work package here in Chapter 5 and in Paper **VIII**, Paper **IX**, and Paper **X**, focused on broadening the use and applicability of nZVI by creating support materials that are robust enough to be effectively used on a large scale. This was done by utilizing activated carbon as the backbone material for nZVI immobilization. Activated carbon is the ideal backbone material for creating a hybridized treatment material containing nZVI, as it has long been the standard cheap material for contaminant adsorption in water treatment. It is actively employed in the removal of a wide variety of compounds, from pesticides [147] to pharmaceuticals and endocrine disruptors [148] to heavy metals [149] to inorganic ions [150], as well as many others.

## 5.1 One-pot synthesis of GAC-nZVI

There have been many cases of combining nZVI with granular activated carbon (GAC) reported in the past, using a variety of synthesis routes. These routes include methods like using wet impregnation where $Fe^{2+}$ is directly attached to GAC by soaking the GAC in a ferrous iron solution followed by chemical reduction (e.g. via $NaBH_4$) [151] or by iron attachment followed by thermal calcination and residual evaporation, and then chemical reduction [152]. And, during preparation of these composites, many factors can influence the outcome, such as the precursor iron salt used, different degrees of oxidation during nZVI formation, pH during synthesis, etc. But, the overall effects of these variables have not been intensively studied of summarized. The objective with this method is to investigate the effect of different synthesis conditions on GAC-nZVI properties and to suggest an optimal route for a convenient one-pot method. Although still in preparation, Paper **VIII** explores the optimization of GAC-nZVI preparation, as both a composite material itself, as well as a precursor to the eventual hybridized material proposed containing GAC, nZVI, and different COP materials.

Three different conditions were examined to prepare GAC loaded with nZVI: GAC1, iron impregnation by a $Fe(NO_3)_3$ mixing step followed by thermal treatment at 150 °C up to 300 °C, and $NaBH_4$ reduction; GAC2, iron impregnation by $FeSO_4$ soaking (pH = 3) followed directly by $NaBH_4$ reduction; and GAC3, the same as condition 2, but with the pH adjusted to 7. The first method using thermal treatment was capable of loading a large amount of total Fe onto the GAC matrix; however, following the reduction step using $NaBH_4$, it was very difficult to produce a significant quantity of ZVI in the matrix. Using the other two methods of soaking in a ferrous iron solution produced a lower total amount of iron; in this way, though, the amount of ZVI content drastically increased. In GAC2, due to the lower pH, there were less iron precipitates formed, which allowed for more ZVI to be produced. In GAC3, the pH was adjusted to neutral, and therefore saw more iron-hydroxides formed, resulting in less conducive conditions for forming ZVI. This is summarized in Figure 28.
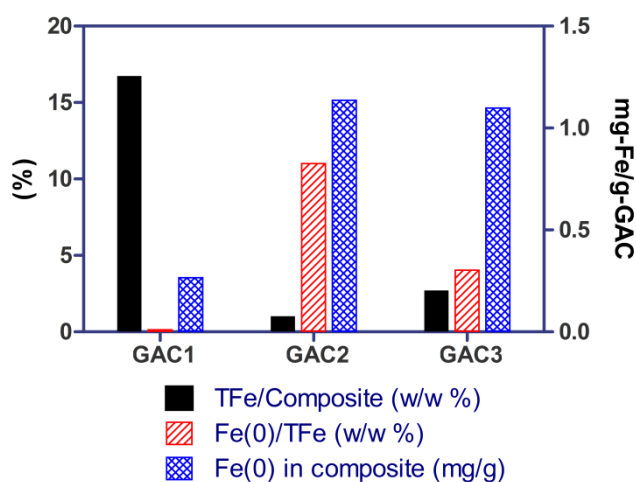


**Figure 28.** Total iron and elemental iron content in the GAC composites, prepared in different synthesis routes. Paper **VIII**.

Furthermore, optimizing conditions found that varying the reduction time using $NaBH_4$ changed the total ZVI content in the GAC. By increasing the reduction time up to two hours, the quantity of ZVI could be increased to as high 20%, compared to the results presented originally in Figure 28.

Finally, optimizing this process into a convenient one-pot method was obtained. By doing this, a washing step is eliminated that drastically increases the total iron content. The final one-pot method consists of: soaking of GAC with $FeSO_4$ and polyethylene glycol overnight without any pH adjustment (i.e. pH = 3), followed by the reduction of iron using $NaBH_4$ for two hours,

then washing with ethanol and drying in a vacuum oven. This way proves to be an efficient method for attaching nZVI onto/into GAC, maintaining a high percentage of ZVI in the process.

## 5.2  Chemical grafting of COPs to GAC

Grafting of COPs to the surface of activated carbon was performed in a step-wise manner that consisted of four major procedures (Figure 29). Inspiration for this procedure was derived from previous studies investigating the surface modification using thionyl chloride targeted at graphene [153] and carbon black [154], as well as amino-functionalization of carbon nanotubes [155]. The goal of the first step was to heavily oxidize the surface of the carbon in order to introduce carboxylic (-COOH) functional groups to the surface, upon which monomer and eventual polymer attachment could take place. In the second step, the goal was to convert the carboxylic group to an acyl chloride (-COCl), which is well known to be highly reactive with a wide variety of other functional groups. Once an acyl chloride group was achieved, mono-mer attachment was the goal, in the form of melamine. Melamine was cho-sen as it has three amine (-NH$_2$) groups, where the first can substitute for the acyl chloride and the remaining two are left free for further polymerization. Lastly, the final step was to form the polymer shell around the surface of the carbon particle, stemming from the melamine and branching out amorphous-ly. COP-19 was chosen as the polymer; as it was that there were previous positive results from the first work package using COP-19 (Section 3.2).

### 5.2.1 Development of grafting procedure

Three different activated carbons were tested to determine the most suitable candidate for polymer grafting, each with different amounts of impurities (i.e. variance from pure carbon). The first carbon tested was an ultra-pure brand carbon (AC-Norit®) that thermogravimetric analysis (TGA) revealed very few defects present (~ 6%), Table 4C. This proved to be an ineffective carbon for polymer grafting, as the lack of impurities made it difficult to break the car-bon bonds and subsequently change the surface chemistry enough for further grafting. The next carbon tested was a very crude carbon (AC-Sigma) with a high level of impurities and lack of structural integrity, resulting in an overall breakdown of the carbon structure and complete loss of surface area and pores during the grafting procedure. Ultimately, the most suitable carbon

was that of a moderately pristine and structurally sound carbon that still possessed a high surface area (943 m$^2$/g) with a diverse range of pore sizes. Once the carbon source was chosen, surface modification and polymer grafting could take place. Outlined in Figure 29, the settled upon series of reactions consisted of: 1. carbon oxidation in nitric acid at 100 °C (AC-Ox), 2. acyl chloride formation by thionyl chloride in dichloromethane (AC-Thio), 3. melamine grafting in a dimethyl sulfoxide solution (AC-Mel), and 4. COP growth [102,103] (AC-COP).
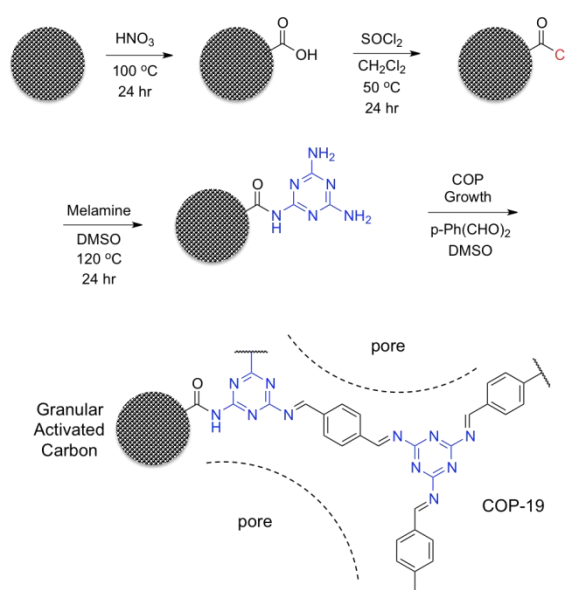


**Figure 29.** Step-wise evolution of the COP attachment to the surface of activated carbon (illustrated as large gray object, not-to-scale). Paper **IX**.

Vigorous washing with selected solvents was performed after each step, in order to eliminate residual species present, and ensure that all material present was chemically attached to the carbon material. However, after the second step where AC-Thio was produced, no washing or characterization as performed, as the acyl chloride is extremely reactive, even to air and moisture in the air. Therefore, AC-Thio was immediately purified and dried via rotary evaporation in a vacuum and then subjected to the next reaction step.

## 5.2.2 Properties of materials and grafting confirmation

Intensive characterization of the particles was undertaken throughout the entire grafting procedure, in order to confirm that the suggested mechanisms were taking place. Table 4 presents the characterization data from elemental

analysis (EA), X-ray photoelectron spectroscopy (XPS), and the TGA data mentioned previously. Chemical composition from EA matched nicely for each stage of the procedure, with an initial material of mostly carbon, acid oxidation brought about a substantial amount of oxygenated groups, followed by an increase in nitrogen and decrease in oxygen as the melamine substituted for some of the carboxylic functionalities, and ultimately with the COP grafted a substantial amount of nitrogen present from the COP itself. XPS data, which is purely a surface measurement (penetration depth of 5-10 nm), measured a significantly higher amount of nitrogen, which corresponds to a COP shell on the exterior of the particle. Further insight from the C1s and N1s scan of XPS elucidated a polymeric structure; where the C1s scan yielding peaks representing the C-N, C=O, and C bonds of the COP (Figure 30B), and the N1s scan yielding peaks representing aromatic N and N-H bonds (not shown).

**Table 4.** Elemental concentrations of carbon particles at each stage of the modification reactions, determined by elemental analysis (A) and XPS (B). Carbon vs. defect quantities, determined by TGA (C). Paper **IX**.

|  | C | N | O | H | Other |
|---|---|---|---|---|---|
| *A. Elemental Analysis (%)* | | | | | |
| AC | 82.40 | 0.58 | 6.50 | 1.67 | 8.85 |
| AC-Ox | 55.43 | 2.16 | 33.40 | 2.04 | 6.97 |
| AC-Mel | 61.90 | 7.57 | 19.48 | 4.23 | 6.82 |
| AC-COP | 55.85 | 17.52 | 12.43 | 2.65 | 11.54 |
| *B. X-ray photoelectron spectroscopy (%)* | | | | | |
| AC | 77.36 | 0.00 | 18.58 | --- | 4.06 |
| AC-COP | 57.28 | 32.80 | 6.36 | --- | 3.56 |
| *C. Thermogravimetric analysis (%)* | | | | | |
| AC-Norit® | 94 | --- | --- | --- | 6 |
| AC-Samchun | 88 | --- | --- | --- | 12 |
| AC-Sigma | 67 | --- | --- | --- | 33 |

A greater acumen is necessary though, to qualitatively confirm the existence of the exact chemical structure attached to the carbon particle. For this, FTIR was employed to detect the organic bonds of the material being produced. Figure 30A tracks the evolution through each step of the procedure, to confirm the existence of expected structures. The pure carbon (AC) exhibited no discernible peak data, AC-Ox has two major peaks formed, corresponding to C-O and C=O bonds of the carboxylic group. AC-Mel has two more peaks

appear for the N-H and C-N groups. And, AC-COP has a multitude of peaks appear that are identical to the peak pattern found in pure COP-19.
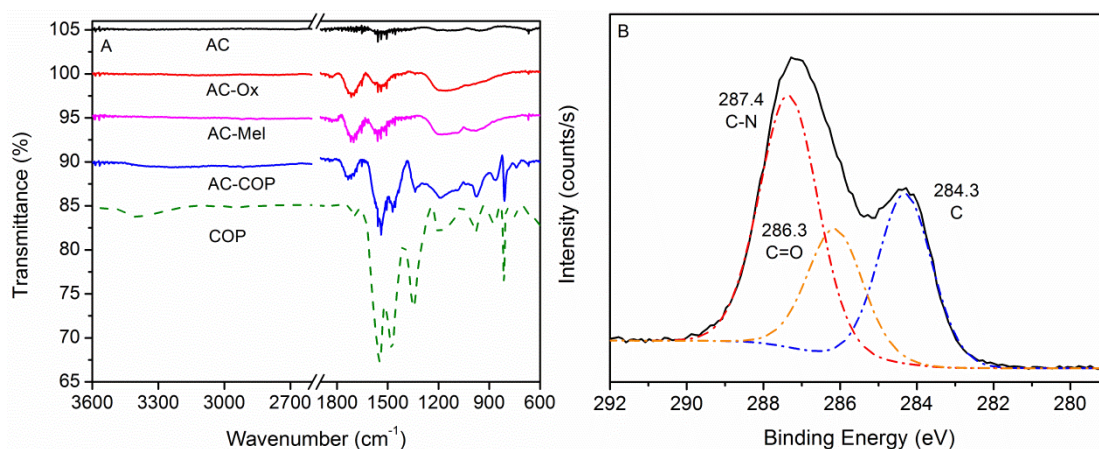


**Figure 30.** A) FTIR spectra AC (black), AC-Ox (red), AC-Mel (magenta), AC-COP (blue), and COP-19 (green); XPS C1s scan of AC-COP. Paper **IX**.

Lastly, visual confirmation was done using TEM, in order to visually see the effects of the grafting procedure and that the COP was forming in a shell-like fashion. Figure 31 presents images of AC-COP particles (A,B), and for comparison, an image of AC-Mel (C) and the bare COP-19. When looking at AC-COP, there are large carbon particles at the core, out-of-focus in the foreground; while there is an obvious shell of interwoven porous polymer chains bound to the outer edges of the carbon. Notably, the COP shell very closely resembles the morphology of bare COP-19. Furthermore, when compared to AC-Mel, the porous nature of the COP material is noticeable present and different in structure to the simple monomer structure that the melamine grafting exhibits.
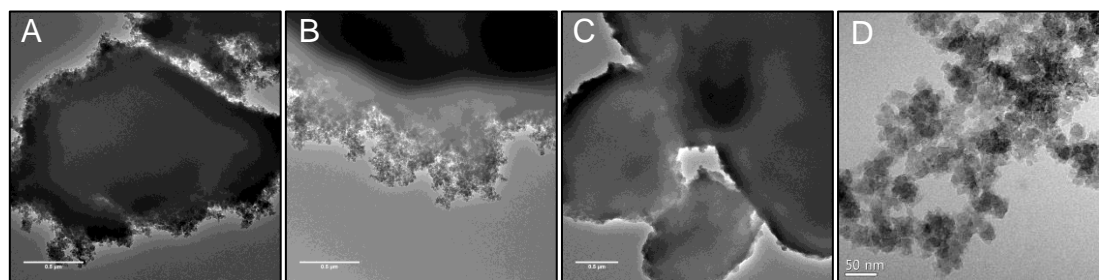


**Figure 31.** TEM images of AC-COP particles with an attached shell of COP material (A,B), AC-Mel particles with a grafted layer of melamine (C), and bare COP-19 (D). Paper **IX**.

With the grafting of COP to AC confirmed, final characterization was done by looking at pore structure of the different materials produced during the procedure. Using BET physisorption analysis, the pore structure can be observed at each stage of the grafting procedure (Figure 32).
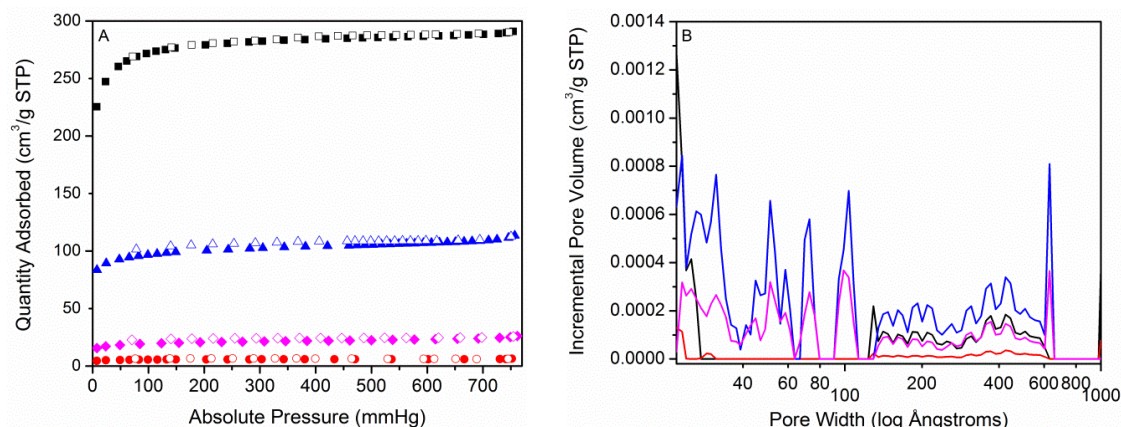


**Figure 32.** A) $N_2$ adsorption (filled)-desorption (empty) isotherms at 77 K; B) pore size/volume distribution by 2D-NLDFT (slit pores, $N_2$ carbon model) of AC (black), AC-Ox (red), AC-Mel (magenta), and AC-COP (blue). Paper **IX**.

Looking at each stage of the process, it is apparent that the pore structure is initially very large in the AC with a high capacity for gas uptake, and that the oxidation method is very aggressive, breaking down the pore structure almost entirely. The gas adsorbed pore size distribution becomes very minimal. However, subsequent monomer and COP attachment exhibit a reappearance of pore structure, to the point where the final AC-COP pore structure is very diverse with a nanoporous to microporous range of pore sizes. The final structure of AC-COP is much more similar to that of the bare COP material.

## 5.2.3 Water treatment for contaminant adsorption

Although the main goal of the first part of this final work package was merely to produce a hybridized composite of activated carbon with grafter porous polymers, initial experiments were performed to evaluate the efficacy of AC-COP for water contaminant adsorption. Based on previous success using COP-19 to adsorb the azo dye naphthol blue black (NBB) [104], it again was tested, along with cadmium, and iron for future application by impregnating nZVI into AC-COP material. AC-COP was tested in parallel with COP-19 and bare AC. Similar to previous results (Section 3.2.3), AC-COP completely removed NBB from solution (up to 23.6 mg-NBB/g), while the bare AC was fairly ineffective at NBB removal (5.6 mg-NBB/g) (Figure 33A). Both

AC-COP and AC have a porous structure, however, the most likely explanation is a combination of pore size diversity found in AC-COP and the phenomenon of pi-pi stacking mentioned in Section 3.2.3. When analyzing for cadmium adsorption, results were much lower (Figure 33B), AC-COP removed 5.6 mg-Cd/g. Of special interest though, is that AC-COP had the higher removal than both COP-19 and AC, resulting in a synergistic effect from the two precursory materials. Even so, these results were comparable to cadmium adsorption using carbon nanotubes [156]. As a preliminary test for future application with nZVI impregnation, iron adsorption was tested (Figure 33C). AC-COP did not adsorb as much iron (8.7 mg-Fe/g) as COP-19 (12.4 mg-Fe/g) or AC (11.5 mg-Fe/g), however an unexpected phenomenon appeared. That although the total iron adsorbed was less in AC-COP, it maintained and even slowly adsorbed more iron over a period of 72 hours. Contrastingly, COP-19 and AC adsorbed more initially, but saw a release of iron back into solution after 8 hours. Indicating that although iron adsorption was slightly less efficient, trapping and permanent impregnation of iron was taking place, which is ideal for water treatment applications.
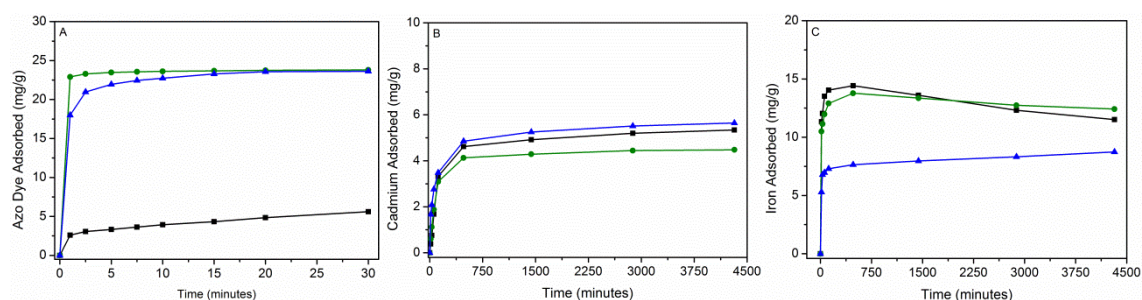


**Figure 33.** Adsorption isotherm of: A) azo dye naphthol blue black; B) cadmium; and C) iron adsorbed by AC-COP (blue), COP-19 (green), and AC (black). Material dosage: 0.5 g/L; initial pH: 6.5; $C_0$-azo dye: 40 µM; $C_0$-Cd: 10 mg/L; $C_0$-Fe: 10 mg/L. Paper **IX**.

## 5.3 Nanocomposites of GAC-COP with nZVI

Building on the successful fabrication of a novel hybrid material combing activated carbon and covalent organic polymer, and subsequent adsorption of iron with that material; this next phase of the work package aimed to first modify the material synthesis strategy to a less harsh and more environmentally friendly method, and to then impregnate the material with nZVI for water contaminant degradation. Stabilizing nZVI in this hybrid material not only isolates nZVI by physically caging it within the pores of the activated carbon and COP matrix (AC-COP), but also to further sequester nZVI into their own microcosms, as each granule can be considered its own island of a reac-

tion vessel, henceforth referred to as GAC-COP-Fe. GAC-COP-Fe was then ultimately tested for reactivity towards nitrobenzene and nitrate.

### 5.3.1 Optimization of COP grafting procedure

The previous method to graft COP to AC was an extremely harsh method requiring high concentrations of vigorous chemicals at high temperatures. Specifically, the previous acid oxidation method completely broke down the pore structure of the backbone activated carbon (Figure 32). A more ideal composite would retain the pore structure of the activated carbon with further enhancement via addition of pore structure from the COP material. Therefore, several attempts were made to change and weaken these harsh conditions, to make the method not only more environmentally friendly, but also safer for the chemist or lab technician. This optimized grafting procedure is outlined in Figure 34.
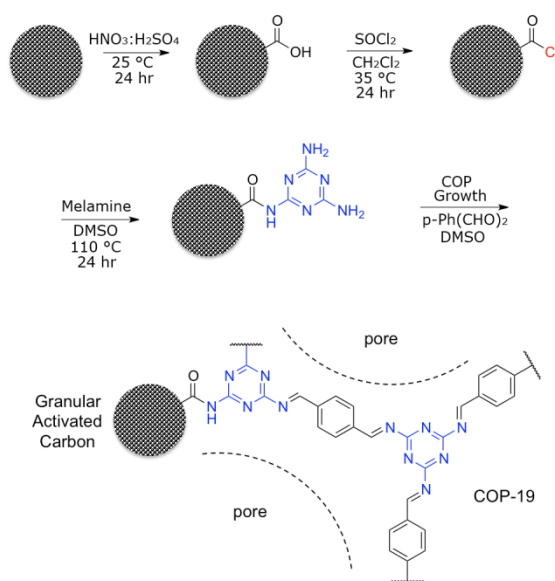


**Figure 34.** Schematic representation of the COP-19 grafting process to the GAC (illustrated as large gray object, not to scale). Paper **X**.

In the method described in Section 5.1.1 (Method-1), AC-Ox was achieved by boiling 60 % nitric acid at 100 °C; in the optimized method (Method-2), the same results were achieved by using a pseudo *aqua regia* with a 3:1 mixture of 30 % $HNO_3$ and 47 % $H_2SO_4$ at room temperature (i.e. 25 °C). AC-Thio was achieved in Method 1 using a 2:1 mixture of dichloromethane to thionyl chloride ($SOCl_2$) at 50 °C, while Method 2 reduced the extremely toxic $SOCl_2$ concentration to using a 4:1 dichloromethane ratio and lowered the

temperature to 35 °C.  The remaining steps to produce AC-Mel and AC-COP were not significantly different between Method 1 and 2.  The combination of chemical concentration and temperature reductions are a significant improvement in the "greening" of the overall process, as well as for safety purposes.

## 5.3.2 Properties of GAC-COP-Fe

Following COP grafting to GAC, iron impregnation and subsequent reduction to ZVI was performed using $NaBH_4$ (Eq. 2).  Much of the characterization data of GAC-COP-Fe, including FTIR, was nearly identical to that in Section 5.1.2 and therefore not presented.  However, XPS analysis is a very powerful tool to reveal insight into all elemental data, including organic and metallic species, analysis of which is presented in Table 5.  The composition of carbon with grafted polymer (GAC-COP) did not vary significantly with that obtained in the AC-COP (Section 5.1.2).  After iron impregnation (GAC-COP-Fe), XPS revealed confirmation that the iron was there in low percentages, as well as sodium that was an artifact from the nZVI reduction process using $NaBH_4$.

**Table 5.**  Surface atomic percentages of the different GAC materials, as determined by XPS.  Paper **X**.

|            | C    | O    | N    | Fe   | Na   |
|------------|------|------|------|------|------|
| GAC        | 92.0 | 8.0  | ---  | ---  | ---  |
| GAC-COP    | 61.0 | 6.4  | 32.6 | ---  | ---  |
| GAC-COP-Fe | 52.0 | 19.5 | 12.2 | 1.2  | 15.1 |

Further look into the C1s and N1s surface scans also yielded results quite similar to that detailed in Section 5.1.2; where the polymer structure was verified.  Analysis with XPS also allows for a unique tool to be employed that can reveal a composition profile in descending layers into the material being analyzed; by alternating consecutive ion etches and XPS analyses to reveal a depth profile of the material.  As illustrated in Figure 35, the C1s and Fe2p depth profile scans elucidate the gradual change in polymer structure on the surface to the carbon granule below and the change in iron speciation from the surface to the inner layers.  The trend in the C1s profile was as expected, as the top layer resembles the COP structure already observed and the bottom layer resembles the bare mostly carbon GAC surface.  Of particular interest is

the progressive build-up of the two major $Fe^0$ peaks and the slow diminishing of various other iron oxide peaks as more ion etches are performed. The identity of these various Fe2p peaks were confirmed by comparison with a previous study focusing on XPS analysis of ZVI [157]. Although surface oxidation is inevitable during sample preparation, it should be noted that the nanoporous structure of the COP material on the GAC surface is protecting the iron from the oxidation effects of the surrounding environment, allowing for increased reactivity and shelf-life of the ZVI. Not only did the speciation of iron change with increasing depth, the percentage of iron with respect to the other elements present changed; the top layer having approximately 1.2 % Fe and the bottom layer after ion etching having approximately 3.3 % Fe.
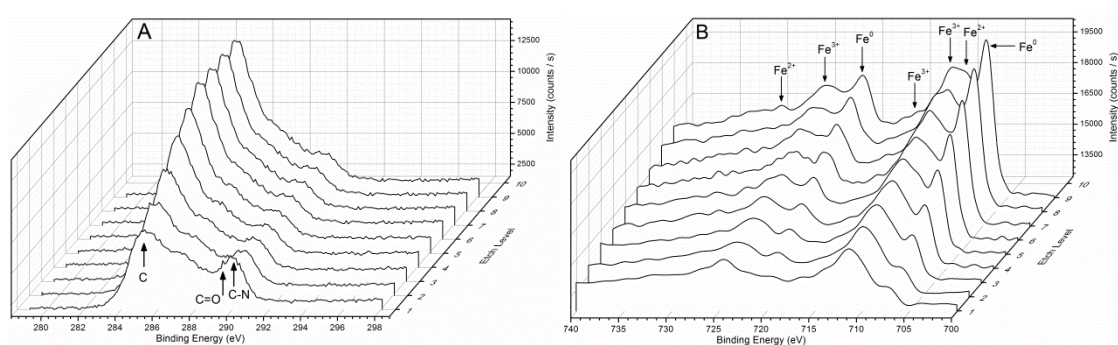


**Figure 35.** XPS analysis. Depth profile ion etched C1s scan for GAC-COP-Fe (A) and depth profile ion etched Fe2p scan for GAC-COP-Fe (B). Paper **X**.

Again, visual confirmation was needed to observe the development of the COP network and subsequent impregnation of nZVI. This was done using scanning electron microscopy (SEM), as the granules were too large for TEM analysis. Figure 36 presents images of the bare GAC, GAC-COP-Fe and an elemental mapping image, using energy dispersive X-ray spectroscopy (EDS), of the surface to identify iron found in the matrix. Bare GAC revealed a very typical structure of a porous carbon material typical to most activated carbons. While the GAC-COP-Fe image revealed a very obvious alteration of the granule surface, with the polymer shell surrounding the granule. Furthermore, when mapping the image with EDS, clusters and regions of iron are confirmed to be scattered, albeit randomly, throughout the granule surface. This lack of uniformity in iron impregnation is an inherent consequence of the procedure, due to the attractive tendencies nZVI towards other nZVI particles [56,58], and has been observed before when impregnating GAC with nZVI [158].

The total amount of iron found in the samples was determined by acid digestion, followed by analysis with AAS. Results for the amount of iron found in

the bare GAC impregnated with nZVI (GAC-Fe) were comparable to previously reported numbers from a study also attaching nZVI to GAC with similar size distributions [159]. However, the total iron content, as determined by AAS analysis, decreased when impregnating nZVI into the GAC-COP matrix (GAC-COP-Fe), from approximately 1.7 % to 0.9 %. This loss in total iron percentage can be explained due to the added mass of the COP shell grafted to the GAC surface, as well as the smaller pore sizes of the COP material inhibiting more mass transfer of iron into the composite matrix. However, from the analysis result of the $H_2$ production method on GAC-COP-Fe, it is clear that the COP material creates conditions where the nZVI is more protected from the surrounding environment, in terms of susceptibility to oxidation. Under controlled anaerobic conditions, to prevent any external oxidation, the zero-valent content of the GAC-Fe, as determined by $H_2$ production followed by GC analysis, was approximately 80.2 %, while the zero-valent content in the GAC-COP-Fe composites was nearly perfect, at approximately 98.8 %. Another study applying nZVI particles to dechlorinate trichloroethylene and using the same $H_2$ production method to determine reactive iron content found that freshly synthesized nZVI and commercially available nZVI contained 92 % and 52 % reactive iron, respectively [121]. Moreover, the fact that the reactive iron content increased when supported on GAC/COP is a major advantage, since more often than not, stabilizing nZVI onto a support material does not always bring beneficial effects to the reactive iron content [160]. This is a breakthrough in the applicability of nZVI for contaminant degradation, to be able to protect the nZVI from oxygen and other constituents on the surrounding environment, while still maintaining reactivity with the contaminant of concern. Full application of nZVI is largely dependent on combatting the negative effects of oxygen and complexing agents in the surrounding environment [50], and, the added benefits of creating oxidation-proof composites results in a material much better suited for real-world utilization.
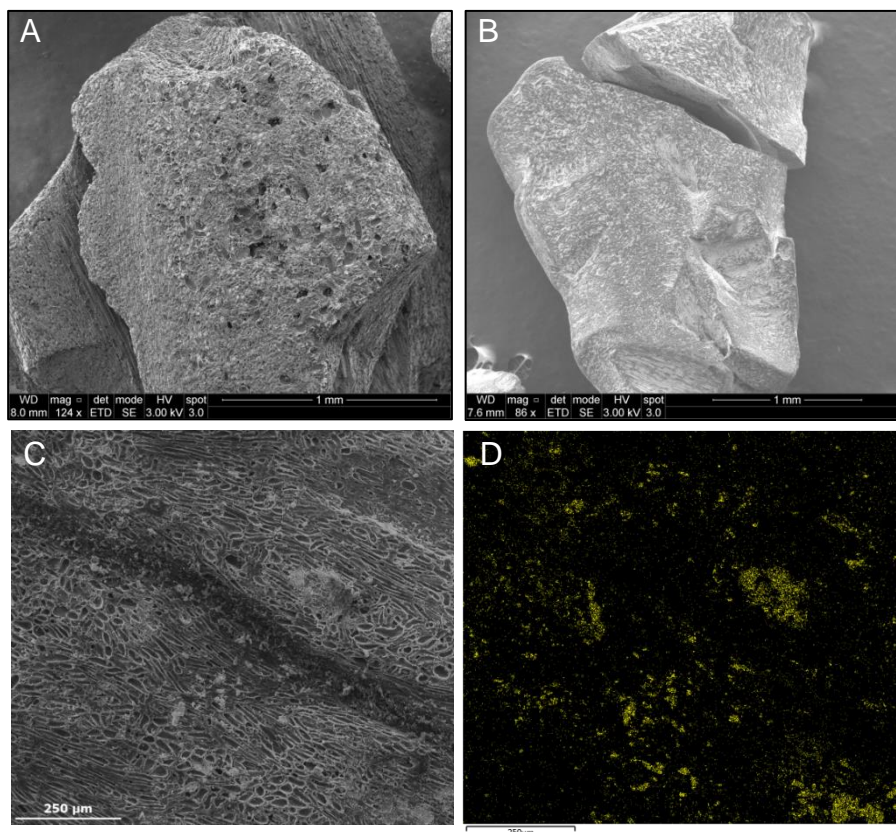
**Figure 36.** SEM imaging. Bare GAC (A); GAC-COP-Fe (B); GAC-COP-Fe at higher magnification (C); and SEM-EDS iron mapping of the image in C (D). Paper **X**.

### 5.3.3 Water treatment for contaminant degradation

Two common water contaminants were chosen as model compounds to test the ability of GAC-COP-Fe to degrade them, nitrobenzene and nitrate. Nitrobenzene was chosen because of its status as a contaminant of emerging concern [161] and that nZVI has previously been reported to degrade nitrobenzene to aniline [162]. Nitrate was chosen because it is recognized as a common source of contamination in groundwater [88] and that nZVI is well known to degrade nitrate to ammonium [89]. Assessment of the degradation was done by comparing the difference between bare GAC impregnated with nZVI (GAC-Fe) and GAC-COP-Fe. After four hours, the GAC-Fe proved to be capable of adsorbing 233 μM of aniline (46.7 % of original aniline concentration); while it was also able to produce at least 283 μM of aniline (56.6 % of original nitrobenzene concentration) before the adsorption mechanisms took over (Figure 37A). Concurrently, after four hours, the GAC-COP-Fe proved to be capable of adsorbing 471 μM of aniline (94.2 % of original aniline concentration); while it also was able to produce at least 318 μM of ani-

line (63.6 % of original nitrobenzene concentration) before the adsorption mechanisms took over (Figure 37B). Assuming the sum of the adsorbed aniline in the control test (Figure 37A,B; red lines) and the produced aniline in the reactivity test (Figure 37A,B; blue lines) is the total amount of degraded nitrobenzene, and using pseudo first-order kinetics, reaction curves were plotted and calculated rate constants were 0.0702 and 0.2212 $min^{-1}$ for GAC-Fe and GAC-COP-Fe, respectively (Figure 37C). It can also be inferred that once both lines converge, that the reaction of nitrobenzene to aniline is primarily over and the remaining operating mechanism is adsorption. GAC-COP-Fe exhibited not only higher total removal of nitrobenzene, but higher aniline adsorption, and faster reaction kinetics, outperforming similar materials using nZVI supported on carbon [162]. The faster reaction kinetics, especially in the first 15 minutes, are most likely due to the higher fraction of zero valent iron compared with the total iron. These tests also reveal an interesting occurrence, in that the COP grafted material exhibits an extremely larger capacity for nitrobenzene and aniline adsorption, which was described previously (Section 3.2.3) to be most likely due to the phenomenon of pi-pi stacking. Therefore, exact quantification of nitrobenzene becomes difficult, but we assume that the sum of produced aniline and adsorbed aniline can be the maximum amount of nitrobenzene reduction (Figure 37C). The synergistic effects of the adsorption capacity of the COP and the degradation capability of the nZVI make this a very effective material for environmental remediation.
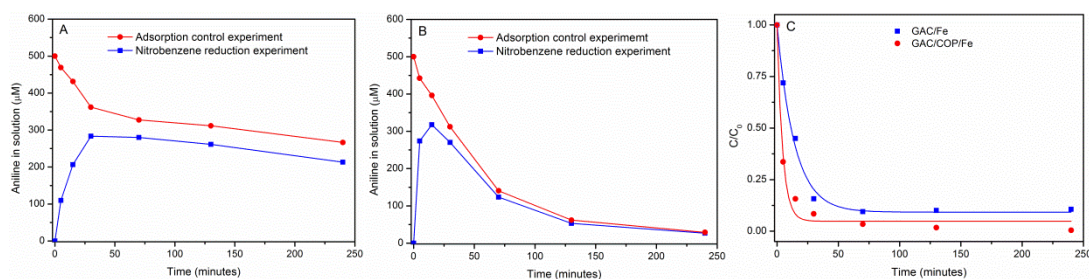


**Figure 37.** Nitrobenzene-reduction/aniline-adsorption batch tests. Aniline adsorption control experiment (red) and nitrobenzene reduction experiment (blue) by bare GAC-Fe (A); aniline adsorption control experiment (red) and nitrobenzene reduction experiment (blue) by GAC-COP-Fe (B); and reaction kinetics of bare GAC-Fe (blue, from A) and GAC-COP-Fe (red, from B) (C). Paper **X**.

As with the assessment with nitrobenzene, the effect that the COP shell has on the ability to degrade and remove nitrate was compared with GAC-Fe; there was again a control test performed on the ablility to adsorb ammonia by

each material. After four hours, the GAC-Fe proved to be capable of adsorbing 12.2 mg-N/L of ammonia (48.8 % of original ammonia concentration); while it also was able to produce 11.6 mg-N/L of ammonia (46.4 % of original nitrate concentration) (Figure 38A). Concurrently, after four hours, the GAC-COP-Fe proved to be capable of adsorbing 20.0 mg-N/L of ammonia (79.9 % of original ammonia concentration); while it also was able to produce at least 6.3 mg-N/L of ammonia (25.2 % of original nitrate concentration) before the adsorption mechanisms took over (Figure 38B). Assuming the sum of the adsorbed ammonia in the control test (Figure 38A,B; red lines) and the produced ammonia in the reactivity test (Figure 38A,B; blue lines) is the total amount of degraded nitrate, and using pseudo first-order kinetics, reaction curves were plotted and calculated rate constants were 0.04611 and 0.04541 $min^{-1}$ for GAC/Fe and GAC/COP/Fe, respectively (Figure 38C). It can also be inferred that once both lines converge, that the reaction of nitrate to ammonia is primarily over and the remaining operating mechanism is adsorption. Overall, the degradation and removal of contaminants was much better using GAC-COP-Fe, and furthermore, the degradation and removal by GAC-COP-Fe favors aromatic contaminants due to the effect of pi-pi stacking of the aromatic compound to the COP material.
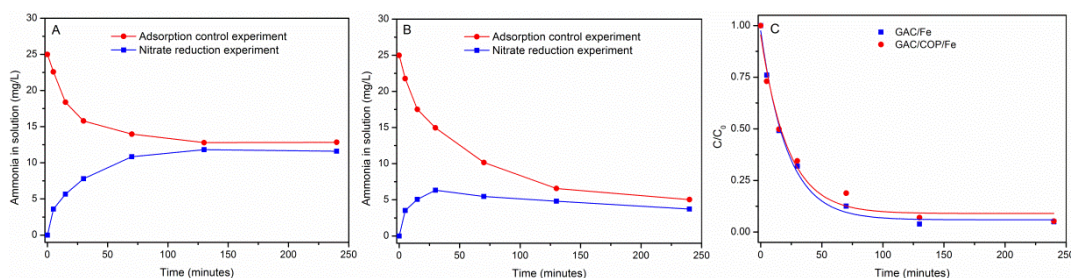


**Figure 38.** Nitrate-reduction/ammonia-adsorption batch tests. Ammonia adsorption control experiment (red) and nitrate reduction experiment (blue) by bare GAC-Fe (A); ammonia adsorption control experiment (red) and nitrate reduction experiment (blue) by GAC-COP-Fe (B); and reaction kinetics of bare GAC-Fe (blue, from A) and GAC-COP-Fe (red, from B) (C). Paper **X**.

In summary, Paper **X** optimized the COP grafting procedure discussed in Paper **IX**; so that the porous structure of the activated carbon was not destroyed, while still achieving proper COP attachment to the carbon surface. This nanocomposite hybridized material was then successfully impregnated with nZVI. Not only was the nZVI impregnated, but after analysis of the reactive iron content, it was determined that the percentage of $Fe^{0}$ out of the total iron was nearly 99%. Meaning this composite is very ideally suited to the impregnation of nZVI and for protection against the effects of oxidation on the

iron. This led to improved removal of two water contaminants, nitrobenzene and nitrate.

This work, discussed here in Paper **X,** is considered the culmination of the development of a hybridized nanocomposite material containing reactive iron. Different materials and procedures were explored to finalize on this combination of granular activated carbon with COP-19 and impregnated nZVI. Although requiring further optimization, this composite is paving the way for a new class of robust materials capable of treating, whether by adsorption or degradation, polluted water streams.

# 6 Conclusions and future outlook

Valuable insights and accomplishments were gained in each of the three work packages contained in the PhD project that should lead to more efficient use of reactive iron-containing nanomaterials for water treatment. These insights offer to both further the use of nZVI as a treatment material in water purification operations and provide a means for different laboratories to compare developed nZVIs against other nZVIs.

In the first work package, two new materials were utilized in combination with nZVI: a synthetic magnesium-aminoclay (MgAC) and a variety of covalent organic polymers (COPs). First, application of MgAC provided a means to substantially improve the colloidal stability of nZVI, provided a high enough weight ratio (i.e. 7.5:1) of MgAC:Fe was present. This ratio of MgAC:Fe increased the characteristic time and zeta potential, as well as decreased the particle size. A similar effect correlated to the reactivity, where the ideal range for nitrate reduction was approximately 7.5:1. Second, application of selected COPs proved to be efficient materials for trapping nZVI, on average approximately 10% by mass. They also dramatically increased the colloidal stability of nZVI, and in the case of COP-19, improved the stability to a de facto infinite level for all intents and purposes. On the other hand, the reactivity of the COP-nZVI composites was difficult to quantify due to the aggressive adsorption of the dye being degraded by the COPs. Further optimizing the COP-nZVI composites could prove to yield very productive results given the unique ability to trap iron and act as a powerful adsorbent.

In the second work package, development of a new method for adequately quantifying the reactivity of nZVI that can be applied universally to any synthesized product was performed. This method built on the shortcomings of various other common methods so that a simple, inexpensive, and user-friendly technique can be applied to nZVI. Initial work developed the colorimetric assay to quantify dehalogenation based on 4-chlorophenol reduction to phenol. This was then optimized to create a miniaturized version in the form of analysis using a 96-well microplate to expand sample count and decrease sample preparation time; then further optimized to broaden the range of reducible compounds capable of being analyzed. Ultimately, the effectiveness of the developed colorimetric assay was proven by comparing the reactivity of different nZVI materials using both the colorimetric assay and real-world contaminants like TCE, TCA, and atrazine. Although the kinetics

varied slightly, the correlation between the assay and the halogenated contaminants was apparent. Therefore, it was concluded that the developed assay has potential to be a universal reactivity assay when assessing nZVI materials.

In the third and final work package, the lessons learned in the first work package were applied to create a hybridized material that combines three different technologies into one robust treatment nano-composite material. The first material being granular activated carbon, a pseudo nanomaterial itself due to the micro and nanoporous properties it holds. The second material being the porous polymer networks of COPs, which possess unique adsorptive characteristics towards nZVI and many other compounds. And, lastly nZVI itself to utilize the reductive properties it holds towards contaminants. This composite of GAC-COP-nZVI was the ultimate produced material that proved to be efficient at both contaminant adsorption as well as degradation. It is this material that culminates the work done in this PhD project to create a brand new state-of-the-art material that both effective at water treatment and robust enough to be used on a large scale in water treatment applications.

Future work, however, must be done to see this material come to fruition in water treatment operations. First and foremost, the synthesis of GAC-COP-nZVI must be optimized even further to address issues such as the greening of the synthesis procedure and increasing the adsorptive and/or degradative properties. This can also include what was learned in the washing and storage investigations, to maintain and prolong the reactivity of the composite materials. Additionally, exploring the use of different polymers, chelating agents, or stabilizing agents with the composite can lead to even more diversity in the application of these materials. Lastly, applying the COP grafting procedure to various other carbon-based materials could lead to improved treatment abilities, material robustness, or final treatment system arrangements. Potential carbon materials to look into could be carbon nanotubes or carbon foam/felt products, for example.

# 7 References

[1]     L. Roberts, Science (80-. ). 333 (2011) 540 LP.

[2]     U.N. Water, World Water Day (2007) 1.

[3]     G. Prokop, M. Schamann, I. Edelgaard, A.R. Gentile, Management of Contaminated Sites in Western Europe, European Environment Agency, Copenhagen, Denmark, 2000.

[4]     E. Gazit, Chem. Soc. Rev. 36 (2007) 1263.

[5]     A. Bhatnagar, M. Sillanpää, Adv. Colloid Interface Sci. 152 (2009) 26.

[6]     D.W. Breck, Zeolite Molecular Sieves: Structure, Chemistry, and Use, 1st ed., John Wiley & Sons Publishing, New York, NY, USA, 1974.

[7]     L. Ding, Y. Zheng, Mater. Res. Bull. 42 (2007) 584.

[8]     B. Vogel, C. Schneider, E. Klemm, Catal. Letters 79 (2002) 107.

[9]     W. Song, V.H. Grassian, S.C. Larsen, Chem. Commun. (2005) 2951.

[10]    J. Theron, J.A. Walker, T.E. Cloete, Crit. Rev. Microbiol. 34 (2008) 43.

[11]    G. Itskos, A. Koutsianos, N. Koukouzas, C. Vasilatos, Int. J. Miner. Process. 139 (2015) 43.

[12]    E. Álvarez-Ayuso, A. García-Sánchez, X. Querol, Water Res. 37 (2003) 4855.

[13]    H. Yeritsyan, A. Sahakyan, V. Harutyunyan, S. Nikoghosyan, E. Hakhverdyan, N. Grigoryan, A. Hovhannisyan, V. Atoyan, Y. Keheyan, C. Rhodes, Sci. Rep. 3 (2013) 2900.

[14]    N. Savage, M.S. Diallo, J. Nanoparticle Res. 7 (2005) 331.

[15]    B. Pan, B. Xing, Environ. Sci. Technol. 42 (2008) 9005.

[16]    Y.-H. Li, J. Ding, Z. Luan, Z. Di, Y. Zhu, C. Xu, D. Wu, B. Wei, Carbon N. Y. 41 (2003) 2787.

[17]    G.P. Rao, C. Lu, F. Su, Sep. Purif. Technol. 58 (2007) 224.

[18]    S. Iijima, Nature 354 (1991) 56.

[19]    X. Liu, M. Wang, S. Zhang, B. Pan, J. Environ. Sci. 25 (2013) 1263.

[20]    J.A. Spadaro, T.J. Berger, S.D. Barranco, S.E. Chapin, R.O. Becker, Antimicrob. Agents Chemother. 6 (1974) 637.

[21]    S.Y. Liau, D.C. Read, W.J. Pugh, J.R. Furr, A.D. Russell, Lett. Appl. Microbiol. 25 (1997) 279.

[22]    Z.-M. Xiu, J. Ma, P.J.J. Alvarez, Environ. Sci. Technol. 45 (2011) 9003.

[23]    M. Rai, A. Yadav, A. Gade, Biotechnol. Adv. 27 (2009) 76.

[24]    P. Jain, T. Pradeep, Biotechnol. Bioeng. 90 (2005) 56.

[25]    Q. Li, S. Mahendra, D.Y. Lyon, L. Brunet, M. V Liga, D. Li, P.J.J. Alvarez, Water Res. 42 (2008) 4591.

[26]    I. Ojea-Jiménez, X. López, J. Arbiol, V. Puntes, ACS Nano 6 (2012) 2253.

[27]    Y.-L. Fang, J.T. Miller, N. Guo, K.N. Heck, P.J.J. Alvarez, M.S. Wong, Catal. Today 160 (2011) 96.

[28]    H. Qian, Z. Zhao, J.C. Velazquez, L.A. Pretzer, K.N. Heck, M.S. Wong, Nanoscale 6 (2014) 358.

[29]    M.E. Pena, G.P. Korfiatis, M. Patel, L. Lippincott, X. Meng, Water Res. 39 (2005) 2327.

[30]    H.G. Yang, C.H. Sun, S.Z. Qiao, J. Zou, G. Liu, S.C. Smith, H.M. Cheng, G.Q. Lu, Nature 453 (2008) 638.

[31]    Y. Kikuchi, K. Sunada, T. Iyoda, K. Hashimoto, A. Fujishima, J. Photochem. Photobiol. A Chem. 106 (1997) 51.

[32]    J. Joo, S.G. Kwon, T. Yu, M. Cho, J. Lee, J. Yoon, T. Hyeon, J. Phys. Chem. B 109 (2005) 15297.

[33]    T.A. Egerton, S.A.M. Kosa, P.A. Christensen, Phys. Chem. Chem. Phys. 8 (2006) 398.

[34]    M. Sökmen, F. Candan, Z. Sümer, J. Photochem. Photobiol. A Chem. 143 (2001) 241.

[35]    J. Sawai, J. Microbiol. Methods 54 (2003) 177.

[36]    L.K. Adams, D.Y. Lyon, P.J.J. Alvarez, Water Res. 40 (2006) 3527.

[37]    R. Brayner, R. Ferrari-Iliou, N. Brivois, S. Djediat, M.F. Benedetti, F. Fiévet, Nano Lett. 6 (2006) 866.

[38]    Z. Huang, X. Zheng, D. Yan, G. Yin, X. Liao, Y. Kang, Y. Yao, D. Huang, B. Hao, Langmuir 24 (2008) 4140.

[39]    P.K. Stoimenov, R.L. Klinger, G.L. Marchin, K.J. Klabunde, Langmuir 18 (2002) 6679.

[40]    K.J. Klabunde, J. Stark, O. Koper, C. Mohs, D.G. Park, S. Decker, Y. Jiang, I. Lagadic, D. Zhang, J. Phys. Chem. 100 (1996) 12142.

[41]    N. Sun, K.J. Klabunde, J. Am. Chem. Soc. 121 (1999) 5587.

[42]    D. Koeppenkastrop, E.H. De Carlo, Environ. Sci. Technol. 27 (1993) 1796.

[43]    C.T. Yavuz, J.T. Mayo, W.W. Yu, A. Prakash, J.C. Falkner, S. Yean, L. Cong, H.J. Shipley, A. Kan, M. Tomson, D. Natelson, V.L. Colvin, Science (80-. ). 314 (2006) 964.

[44]    M. Auffan, J. Rose, O. Proux, D. Borschneck, A. Masion, P. Chaurand, J.-L. Hazemann, C. Chaneac, J.-P. Jolivet, M.R. Wiesner, A. Van Geen, J.-Y. Bottero, Langmuir 24 (2008) 3215.

[45]    F. Fu, D.D. Dionysiou, H. Liu, J. Hazard. Mater. 267 (2014) 194.

[46]    X. Zhang, S. Lin, X.-Q. Lu, Z. Chen, Chem. Eng. J. 163 (2010) 243.

[47]    R. Thiruvenkatachari, S. Vigneswaran, R. Naidu, J. Ind. Eng. Chem. 14 (2008) 145.

[48]    P.G. Tratnyek, T.L. Johnson, M.M. Scherer, G.R. Eykholt, Gr. Water Monit.

Remediat. 17 (1997) 108.

[49]  S. Comba, A. Molfetta, R. Sethi, Water, Air, Soil Pollut. 215 (2010) 595.

[50]  R.A. Crane, T.B. Scott, J. Hazard. Mater. 211–212 (2012) 112.

[51]  B. Karn, T. Kuiken, M. Otto, Environ. Health Perspect. 117 (2009) 1823.

[52]  Y.-P. Sun, X. Li, J. Cao, W. Zhang, H.P. Wang, Adv. Colloid Interface Sci. 120 (2006) 47.

[53]  W. Zhang, J. Nanoparticle Res. 5 (2003) 323.

[54]  W. Zhang, D.W. Elliott, Remediat. J. 16 (2006) 7.

[55]  C.-B. Wang, W. Zhang, Environ. Sci. Technol. 31 (1997) 2154.

[56]  T. Phenrat, N. Saleh, K. Sirk, R.D. Tilton, G. V. Lowry, Environ. Sci. Technol. 41 (2006) 284.

[57]  B. Schrick, B.W. Hydutsky, J.L. Blough, T.E. Mallouk, Chem. Mater. 16 (2004) 2187.

[58]  F. He, D. Zhao, Environ. Sci. Technol. 39 (2005) 3314.

[59]  T. Tosco, M. Petrangeli Papini, C. Cruz Viggi, R. Sethi, J. Clean. Prod. 77 (2014) 10.

[60]  N. Saleh, K. Sirk, Y. Liu, T. Phenrat, B. Dufour, K. Matyjaszewski, R.D. Tilton, G. V. Lowry, Environ. Eng. Sci. 24 (2006) 45.

[61]  N. Saleh, H.-J. Kim, T. Phenrat, K. Matyjaszewski, R.D. Tilton, G. V Lowry, Environ. Sci. Technol. 42 (2008) 3349.

[62]  F. He, D. Zhao, Environ. Sci. Technol. 41 (2007) 6216.

[63]  H.-J. Kim, T. Phenrat, R.D. Tilton, G. V Lowry, Environ. Sci. Technol. 43 (2009) 3824.

[64]  H. Dong, I.M.C. Lo, Water Res. 47 (2013) 419.

[65]  A. Tiraferri, K.L. Chen, R. Sethi, M. Elimelech, J. Colloid Interface Sci. 324 (2008) 71.

[66]  K.K.R. Datta, M. Eswaramoorthy, C.N.R. Rao, J. Mater. Chem. 17 (2007) 613.

[67]  P. Chaturbedy, D. Jagadeesan, M. Eswaramoorthy, ACS Nano 4 (2010) 5921.

[68]  S. Mann, Nat Mater 8 (2009) 781.

[69]  J.L. Vickery, S. Thachepan, A.J. Patil, S. Mann, Mol. Biosyst. 5 (2009) 744.

[70]  S.C. Holmstrom, A.J. Patil, M. Butler, S. Mann, J. Mater. Chem. 17 (2007) 3894.

[71]  A.J. Patil, M. Li, E. Dujardin, S. Mann, Nano Lett. 7 (2007) 2660.

[72]  W. Farooq, Y.-C. Lee, J.-I. Han, C.H. Darpito, M. Choi, J.-W. Yang, Green Chem. 15 (2013) 749.

[73]  Y.-C. Lee, B. Kim, W. Farooq, J. Chung, J.-I. Han, H.-J. Shin, S.H. Jeong, J.-Y. Park, J.-S. Lee, Y.-K. Oh, Bioresour. Technol. 132 (2013) 440.

[74] Y.-C. Lee, Y.S. Huh, W. Farooq, J. Chung, J.-I. Han, H.-J. Shin, S.H. Jeong, J.-S. Lee, Y.-K. Oh, J.-Y. Park, Bioresour. Technol. 137 (2013) 74.

[75] Y.-C. Lee, Y.S. Huh, W. Farooq, J.-I. Han, Y.-K. Oh, J.-Y. Park, RSC Adv. 3 (2013) 12802.

[76] Y.-C. Lee, E.J. Kim, D.A. Ko, J.-W. Yang, J. Hazard. Mater. 196 (2011) 101.

[77] Y.-C. Lee, S.-J. Chang, M.-H. Choi, T.-J. Jeon, T. Ryu, Y.S. Huh, Appl. Catal. B Environ. 142–143 (2013) 494.

[78] Y.-C. Lee, E.J. Kim, J.-W. Yang, H.-J. Shin, J. Hazard. Mater. 192 (2011) 62.

[79] M.R. Mankbadi, M.A. Barakat, M.H. Ramadan, H.L. Woodcock, J.N. Kuhn, J. Phys. Chem. B 115 (2011) 13534.

[80] Y. Hwang, D.-G. Kim, H.-S. Shin, Appl. Catal. B Environ. 105 (2011) 144.

[81] Y.-C. Lee, C.-W. Kim, J.-Y. Lee, H.-J. Shin, J.-W. Yang, Desalin. Water Treat. 10 (2009) 33.

[82] J. Shin, Y.-C. Lee, Y. Ahn, J.-W. Yang, Desalin. Water Treat. 50 (2012) 102.

[83] Z. Ai, L. Lu, J. Li, L. Zhang, J. Qiu, M. Wu, J. Phys. Chem. C 111 (2007) 4087.

[84] Z. Ai, L. Lu, J. Li, L. Zhang, J. Qiu, M. Wu, J. Phys. Chem. C 111 (2007) 7430.

[85] S. Luo, P. Qin, J. Shao, L. Peng, Q. Zeng, J.-D. Gu, Chem. Eng. J. 223 (2013) 1.

[86] Y.-P. Sun, X.-Q. Li, W.-X. Zhang, H.P. Wang, Colloids Surfaces A Physicochem. Eng. Asp. 308 (2007) 60.

[87] T. Luo, Z. Ai, L. Zhang, J. Phys. Chem. C 112 (2008) 8675.

[88] J.F. Power, J.S. Schepers, Agric. Ecosyst. Environ. 26 (1989) 165.

[89] S.-S. Chen, H.-D. Hsu, C.-W. Li, J. Nanoparticle Res. 6 (2004) 639.

[90] M.J. Alowitz, M.M. Scherer, Environ. Sci. Technol. 36 (2002) 299.

[91] A. Ryu, S.-W. Jeong, A. Jang, H. Choi, Appl. Catal. B Environ. 105 (2011) 128.

[92] A.P. Côté, A.I. Benin, N.W. Ockwig, M. O'Keeffe, A.J. Matzger, O.M. Yaghi, Sci. 310 (2005) 1166.

[93] A. Thomas, Angew. Chem. Int. Ed. Engl. 49 (2010) 8328.

[94] Y.J. Choi, J.H. Choi, K.M. Choi, J.K. Kang, J. Mater. Chem. 21 (2011) 1073.

[95] B.M. Rambo, J.J. Lavigne, Chem. Mater. 19 (2007) 3732.

[96] W. Niu, C. O'Sullivan, B.M. Rambo, M.D. Smith, J.J. Lavigne, Chem. Commun. (2005) 4342.

[97] L.M. Lanni, R.W. Tilford, M. Bharathy, J.J. Lavigne, J. Am. Chem. Soc. 133 (2011) 13975.

[98] H.A. Patel, F. Karadas, A. Canlier, J. Park, E. Deniz, Y. Jung, M. Atilhan, C.T. Yavuz, J. Mater. Chem. 22 (2012) 8431.

[99] H.A. Patel, F. Karadas, J. Byun, J. Park, E. Deniz, A. Canlier, Y. Jung, M. Atilhan, C.T. Yavuz, Adv. Funct. Mater. 23 (2013) 2270.

[100]  H.A. Patel, S.H. Je, J. Park, Y. Jung, A. Coskun, C.T. Yavuz, Chemistry 20 (2014) 772.

[101]  H.A. Patel, M.S. Yavuz, C.T. Yavuz, RSC Adv. 4 (2014) 24320.

[102]  M.G. Schwab, B. Fassbender, H.W. Spiess, A. Thomas, X. Feng, K. Müllen, J. Am. Chem. Soc. 131 (2009) 7216.

[103]  H.A. Patel, C.T. Yavuz, Faraday Discuss. 183 (2015) 401.

[104]  P.D. Mines, J. Byun, Y. Hwang, H.A. Patel, H.R. Andersen, C.T. Yavuz, J. Mater. Chem. A 4 (2016) 632.

[105]  H. Zhu, Y. Jia, X. Wu, H. Wang, J. Hazard. Mater. 172 (2009) 1591.

[106]  J. Byun, H.A. Patel, D.J. Kim, C.H. Jung, J.Y. Park, J.W. Choi, C.T. Yavuz, J. Mater. Chem. A 3 (2015) 15489.

[107]  K. Yin, I.M.C. Lo, H. Dong, P. Rao, M.S.H. Mak, J. Hazard. Mater. 227–228 (2012) 118.

[108]  S.-H. Chang, S.-H. Chuang, H.-C. Li, H.-H. Liang, L.-C. Huang, J. Hazard. Mater. 166 (2009) 1279.

[109]  C. Nasr, K. Vinodgopal, S. Hotchandani, A.K. Chattopadhyay, P. V Kamat, Res. Chem. Intermed. 23 (1997) 219.

[110]  C. Nasr, K. Vinodgopal, L. Fisher, S. Hotchandani, A.K. Chattopadhyay, P. V Kamat, J. Phys. Chem. 100 (1996) 8436.

[111]  A. Troupis, E. Gkika, T. Triantis, A. Hiskia, E. Papaconstantinou, J. Photochem. Photobiol. A Chem. 188 (2007) 272.

[112]  S. Grimme, Angew. Chemie Int. Ed. 47 (2008) 3430.

[113]  B. Lippa, G. Pan, M. Corbett, C. Li, G.S. Kauffman, J. Pandit, S. Robinson, L. Wei, E. Kozina, E.S. Marr, G. Borzillo, E. Knauth, E.G. Barbacci-Tobin, P. Vincent, M. Troutman, D. Baker, F. Rajamohan, S. Kakar, T. Clark, J. Morris, Bioorg. Med. Chem. Lett. 18 (2008) 3359.

[114]  Y. Morisaki, Y. Chujo, Bull. Chem. Soc. Jpn. 82 (2009) 1070.

[115]  F.D. Lewis, P. Daublain, G.B. Delos Santos, W. Liu, A.M. Asatryan, S.A. Markarian, T. Fiebig, M. Raytchev, Q. Wang, J. Am. Chem. Soc. 128 (2006) 4792.

[116]  B.I. Kharisov, H. V Rasika Dias, O. V Kharissova, V. Manuel Jimenez-Perez, B. Olvera Perez, B. Munoz Flores, RSC Adv. 2 (2012) 9325.

[117]  Q. Wang, S. Lee, H. Choi, J. Phys. Chem. C 114 (2010) 2027.

[118]  B.-W. Zhu, T.-T. Lim, Environ. Sci. Technol. 41 (2007) 7523.

[119]  K.K.R. Datta, C. Kulkarni, M. Eswaramoorthy, Chem. Commun. 46 (2010) 616.

[120]  Y. Hwang, Y.-C. Lee, P.D. Mines, Y.S. Huh, H.R. Andersen, Appl. Catal. B Environ. 147 (2014) 748.

[121]  Y. Liu, S.A. Majetich, R.D. Tilton, D.S. Sholl, G. V Lowry, Environ. Sci. Technol. 39 (2005) 1338.

[122]  Y. Hwang, D. Kim, H.-S. Shin, Environ. Technol. 36 (2015) 1178.

[123]   Z. Shi, J.T. Nurmi, P.G. Tratnyek, Environ. Sci. Technol. 45 (2011) 1586.

[124]   E.J. Reardon, Environ. Sci. Technol. 39 (2005) 7311.

[125]   E.J. Reardon, R. Fagan, J.L. Vogan, A. Przepiora, Environ. Sci. Technol. 42 (2008) 2420.

[126]   Y. Liu, G. V. Lowry, Environ. Sci. Technol. 40 (2006) 6085.

[127]   V. Sarathy, P.G. Tratnyek, J.T. Nurmi, D.R. Baer, J.E. Amonette, C.L. Chun, R.L. Penn, E.J. Reardon, J. Phys. Chem. C 112 (2008) 2286.

[128]   K.-F. Chen, S. Li, W. Zhang, Chem. Eng. J. 170 (2011) 562.

[129]   S. Bae, W. Lee, Environ. Sci. Technol. 48 (2014) 2368.

[130]   W. Zhang, X. Quan, Z. Zhang, J. Environ. Sci. 19 (2007) 362.

[131]   Y. Li, Y. Zhang, J. Li, G. Sheng, X. Zheng, Chemosphere 92 (2013) 368.

[132]   P.L. Searle, Analyst 109 (1984) 549.

[133]   A. Afkhami, R. Norooz-Asl, J. Brazilian Chem. Soc.  19 (2008) 1546.

[134]   D.F. Boltz, J.A. Howell, Colorimetric Determination of Nonmetals, 2nd ed., Wiley, New York, NY, USA, 1978.

[135]   R.G. Harfmann, S.R. Crouch, Talanta 36 (1989) 261.

[136]   D. O'Carroll, B. Sleep, M. Krol, H. Boparai, C. Kocur, Adv. Water Resour. 51 (2013) 104.

[137]   D.M. Cwiertny, S.J. Bransfield, K.J.T. Livi, D.H. Fairbrother, A.L. Roberts, Environ. Sci. Technol. 40 (2006) 6837.

[138]   Y.H. Liou, S.-L. Lo, C.-J. Lin, W.H. Kuan, S.C. Weng, J. Hazard. Mater. 127 (2005) 102.

[139]   Y. Hwang, D.-G. Kim, H.-S. Shin, J. Hazard. Mater. 185 (2011) 1513.

[140]   R.J. Barnes, O. Riba, M.N. Gardner, T.B. Scott, S.A. Jackman, I.P. Thompson, Chemosphere 79 (2010) 448.

[141]   B. Lai, Y. Zhang, Z. Chen, P. Yang, Y. Zhou, J. Wang, Appl. Catal. B Environ. 144 (2014) 816.

[142]   F. He, D. Zhao, C. Paul, Water Res. 44 (2010) 2360.

[143]   U.S. McKnight, S.G. Funder, J.J. Rasmussen, M. Finkel, P.J. Binning, P.L. Bjerg, Ecol. Eng. 36 (2010) 1126.

[144]   P.D. Mackenzie, D.P. Horney, T.M. Sivavec, J. Hazard. Mater. 68 (1999) 1.

[145]   J.T. Nurmi, P.G. Tratnyek, Corros. Sci. 50 (2008) 144.

[146]   Q. Wang, S. Snyder, J. Kim, H. Choi, Environ. Sci. Technol. 43 (2009) 3292.

[147]   K.Y. Foo, B.H. Hameed, J. Hazard. Mater. 175 (2010) 1.

[148]   Z. Yu, S. Peldszus, P.M. Huck, Environ. Sci. Technol. 43 (2009) 1467.

[149]   M.O. Corapcioglu, C.P. Huang, Water Res. 21 (1987) 1031.

[150]   A. Bhatnagar, M. Sillanpää, Chem. Eng. J. 168 (2011) 493.

[151]   H. Choi, S. Agarwal, S.R. Al-Abed, Environ. Sci. Technol. 43 (2009) 488.

[152]   H. Choi, S.R. Al-Abed, S. Agarwal, D.D. Dionysiou, Chem. Mater. 20 (2008) 3649.

[153]   J.K. Wassei, K.C. Cha, V.C. Tung, Y. Yang, R.B. Kaner, J. Mater. Chem. 21 (2011) 3391.

[154]   H. He, M. Zhong, D. Konkolewicz, K. Yacatto, T. Rappold, G. Sugar, N.E. David, K. Matyjaszewski, J. Mater. Chem. A 1 (2013) 6810.

[155]   T. Ramanathan, F.T. Fisher, R.S. Ruoff, L.C. Brinson, Chem. Mater. 17 (2005) 1290.

[156]   Y.-H. Li, S. Wang, Z. Luan, J. Ding, C. Xu, D. Wu, Carbon N. Y. 41 (2003) 1057.

[157]   J.N. Fiedor, W.D. Bostick, R.J. Jarabek, J. Farrell, Environ. Sci. Technol. 32 (1998) 1466.

[158]   J. Xiao, Q. Yue, B. Gao, Y. Sun, J. Kong, Y. Gao, Q. Li, Y. Wang, Chem. Eng. J. 253 (2014) 63.

[159]   H.-H. Tseng, J.-G. Su, C. Liang, J. Hazard. Mater. 192 (2011) 500.

[160]   Y. Su, A.S. Adeleye, Y. Huang, X. Zhou, A.A. Keller, Y. Zhang, Sci. Rep. 6 (2016) 24358.

[161]   S.D. Richardson, Anal. Chem. 81 (2009) 4645.

[162]   X. Ling, J. Li, W. Zhu, Y. Zhu, X. Sun, J. Shen, W. Han, L. Wang, Chemosphere 87 (2012) 655.

# 8 Papers

**I**  Hwang Y., Lee Y.-C., **Mines P.D.**, Huh Y.S., Andersen H.R. (2014). Nanoscale zero-valent iron (nZVI) synthesis in a Mg-aminoclay solution exhibits increased stability and reactivity for reductive decontamination. *Applied Catalysis B: Environmental,* 147:748-755.

**II**  **Mines P.D.**, Byun J., Hwang Y., Patel H.A., Andersen H.R., Yavuz C.T. (2016). Nanoporous networks as effective stabilization matrices for nanoscale zero-valent iron and groundwater pollutant removal. *Journal of Materials Chemistry A,* 4:632-639.

**III**  Hwang Y., Lee Y.-C., **Mines P.D.**, Oh Y.-K., Seok Choi J., Andersen H.R. (2014). Investigation of washing and storage strategy on aging of Mg-aminoclay (MgAC) coated nanoscale zero-valent iron (nZVI) particles. *Chemical Engineering Science*, 119:310-317.

**IV**  Uthuppu B., **Mines P.D.**, Fjordbøge A.S., Broholm M.M., Jakobsen M.H., Andersen H.R., Hwang Y. (2016). Appropriate washing and storage strategy to prolong life-time of nanoscale zero-valent iron using sodium borohydride solution. *Manuscript.*

**V**  Hwang Y., **Mines P.D.**, Jakobsen M.H., Andersen H.R. (2015), Simple colorimetric assay for dehalogenation reactivity of nanoscale zero-valent iron using 4-chlorophenol. *Applied Catalysis B: Environmental,* 166:18-24.

**VI**  Hwang Y., Salatas A., **Mines P.D.**, Jakobsen M.H., Andersen H.R. (2016), Graduated characterization method using a multi-well microplate for reducing reactivity of nanoscale zero valent iron materials. *Applied Catalysis B: Environmental,* 181:314-320.

**VII** **Mines P.D.**, Hansen K.M.S., Droumpali A., Lee W., Andersen H.R., Hwang Y. (2016). Trichloroethylene dehalogenation comparison with 4-chlorophenol reduction color assay by bimetallic zero-valent Fe/Ni particles. *Manuscript.*

**VIII** **Mines P.D.**, Andersen H.R., Hwang Y. (2016). One-pot synthesis of nanoscale zero-valent iron immobilized granular activated carbon (GAC/nZVI) and appropriate methods for characterizing reducing reactivity. *Manuscript.*

**IX** **Mines P.D.**, Thirion D., Uthuppu B., Hwang Y., Jakobsen M.H., Andersen H.R., Yavuz C.T. (2016). Covalent organic polymer functionalization of activated carbon surfaces through acyl chloride for environmental clean-up. *Under Review – Chemical Engineering Journal.*

**X** **Mines P.D.**, Uthuppu B., Thirion D., Jakobsen M.H., Yavuz C.T., Andersen H.R., Hwang Y. (2016). Granular activated carbon with grafted nanoporous polymer enhances nanoscale zero-valent iron impregnation and water contaminant removal. *Submitted – Journal of Hazardous Materials.*

## TEXT FOR WWW-VERSION (without papers)

In this online version of the thesis, **Paper I-X** are not included but can be obtained from electronic article databases e.g. via www.orbit.dtu.dk or on request from.

DTU Environment
Technical University of Denmark
Miljoevej, Building 113
2800 Kgs. Lyngby
Denmark

info@env.dtu.dk.